

For Reference

NOT TO BE TAKEN FROM THIS ROOM

For Reference

NOT TO BE TAKEN FROM THIS ROOM

Ex LIBRIS
UNIVERSITATIS
ALBERTAEASIS



THE UNIVERSITY OF ALBERTA

SEPARATION OF MAGNETIC SUBSTORM FIELDS
FOR MANTLE CONDUCTIVITY STUDIES
IN THE WESTERN UNITED STATES

by



DOUGLAS WILLIAM OLDENBURG

A THESIS
SUBMITTED TO THE FACULTY OF GRADUATE STUDIES
IN PARTIAL FULFILMENT OF THE REQUIREMENTS FOR THE DEGREE
OF MASTER OF SCIENCE

DEPARTMENT OF PHYSICS

EDMONTON, ALBERTA

FALL, 1969

UNIVERSITY OF ALBERTA
FACULTY OF GRADUATE STUDIES

The undersigned certify that they have read, and recommend
to the Faculty of Graduate Studies for acceptance, a thesis
entitled SEPARATION OF MAGNETIC SUBSTORM FIELDS FOR MANTLE CONDUCTIVITY
STUDIES IN THE WESTERN UNITED STATES submitted by Douglas William
Oldenburg in partial fulfilment of the requirements for the degree of
Master of Science.

TABLE OF CONTENTS

	<u>Page</u>
ABSTRACT	1
INTRODUCTION	3
CHAPTER I ELECTROMAGNETIC INDUCTION	12
1.1 "Flat Earth" Model with Uniform Conductivity	13
1.2 Effect of Dimensions of the Source Field	19
CHAPTER II HISTORY AND DERIVATION OF THE SEPARATION INTEGRALS	26
2.1 History	26
2.2 Derivation of Separation Integrals	32
2.3 Separation in Polar Coordinates	39
2.4 Separation Formulae in the Frequency Domain	41
CHAPTER III DATA, MAPPING AND COMPUTATION PROCEDURES	44
3.1 The Array	44
3.2 Variometer	45
3.3 Records	48
3.4 Spectral Analysis	49
3.5 Interpolation	51
3.6 Extrapolation	53
3.7 Computation	54
CHAPTER IV SEPARATED FIELDS	56
4.1 Time Domain	56
4.2 Scale length of the External Field	73

TABLE OF CONTENTS (CONT'D.)

		<u>Page</u>
CHAPTER IV (cont'd.)		
4.3	Separated Magnetic Components in the Time Domain	76
4.4	Separation in the Geomagnetic Coordinate System	82
4.5	Analysis of Errors	83
4.6	Separated Fields in the Period Domain	94
4.7	Phase Variation of External Fields	102
CHAPTER V MODEL STUDIES		
5.1	Isolation and Normalization of Anomalous Fields	107
5.2	Types of Anomalies	116
5.3	Conductivity Models	126
5.4	Conductivity	128
CHAPTER VI MORPHOLOGY OF THE SUBSTORM		
		131

ABSTRACT

A geomagnetic disturbance was recorded on September 1, 1967, by forty-two three component variometers in a two-dimensional array in the mid-western United States. The observed magnetic field perturbations on the surface of the earth are the vector sum of an external part, which consists of magnetic perturbations arising from sources in the ionosphere; and an internal part, resulting from electromagnetically induced currents within the earth. The primary objective of this thesis is to show that a valid three-dimensional separation of the observed magnetic field, or its Fourier transform, into internal and external parts is possible by the evaluation of surface integrals of the magnetic components. The separation of the magnetic field components has been made at four times in the time domain and at two periods in the frequency domain. Interpolation of horizontal components between stations was assisted by application of the condition $\partial X / \partial y = \partial Y / \partial x$, that is, the recorded field satisfies the existence of a potential. Extrapolation outside the array did not appear to be an insuperable problem, and valid separations appeared possible at internal stations of the array. Modelling of internal current distributions to satisfy the results of the separated internal field was briefly considered, while the characteristics

of the separated external field were compared with those predicted from a substorm current model.

ACKNOWLEDGEMENTS

I am grateful to my supervisor Dr. D. I. Gough and also to Dr. H. Porath, Southwest Center for Advanced Studies, Dallas, Texas for guiding me in my research. I would like to thank Dr. G. Rostoker for his very helpful discussions concerning characteristics of polar magnetic substorms. I am also grateful to my wife for her tireless efforts in drafting my diagrams and to my typist Mrs. M. Lybacki

INTRODUCTION

The earth's magnetic field varies over a wide range of periods, extending from a few seconds (micropulsations) to thousands of years (secular variation). This time varying field electromagnetically induces secondary currents within the earth. If the magnetic permeability is assumed to be unity, then the range of depths of these induced currents varies inversely as the product of the conductivity of the material in the earth and the frequency of the inducing field. Geomagnetic bays and storms, associated with intense currents flowing mainly in the auroral zone, have periods from fifteen minutes to a number of hours, and thus give rise to secondary currents in the Earth's upper mantle.

The variational field measured at the surface of the earth is the vector sum of the external field (magnetic field associated with current systems in the ionosphere) and the internal field (the magnetic field associated with the induced secondary currents). The interpretation of geomagnetic depth sounding data requires the separation of this recorded field into its constituent internal and external parts. The external field may then be correlated with the proposed types of ionospheric currents causing the

variational magnetic field, while the internal field may be related directly to the induced currents. By fitting the response of various models to this internal field it is then possible to obtain a model of the conductivity structure within the upper mantle.

The conductivity, σ , of surface rocks may be quite large ($\sim 10^{-12}$ e.m.u) since the pores and cracks of such rocks are filled with electrolyte. The conductivity then decreases ($\sim 10^{-14} - 10^{-16}$ e.m.u) with depth since increasing pressure results in the closure of such cracks and pores. The total conductivity is a sum of the conductivities due to impurity, intrinsic and ionic semi-conduction, each of which have the form $\sigma = \sigma_0 e^{-E/T}$ (Bullard, 1967). Impurity semi-conduction is important only near the surface. Ionic semi-conduction may be of importance only in the region of relatively low pressure (depth of 100-200 km), for at greater depths the pressure is so great that the crystal lattices will not permit ionic movement. Intrinsic semi-conduction is probably dominant at depths greater than 100-200 km. If the conductivity at depth can be found from magnetic depth sounding, and the mechanism of conduction is known at this depth, then a value of the temperature may be obtained. Thus σ may be used as a relative thermometer since an increase in σ may be correlated with an increase in

temperature. This step depends ultimately on experimental measurements of the σ -T relations for ultrabasic rocks. While some results exist, the uncertainties in composition of the upper mantle, especially its iron content, make it impossible to deduce temperatures within limits less than 200 or 300°C (Hamilton 1965).

There are two types of problems in which the recording of magnetic variations may give useful information about the earth's interior: (i) global and (ii) local problems. The former utilizes magnetic variations recorded over the entire surface of the earth in order to find σ as a function of the radius of the earth only. The results depend upon expanding the observed field in a series of spherical harmonics and finding internal and external parts of these harmonics by a method used by Gauss (Chapman and Bartels, 1940).

In the area of global problems, Chapman (1919) analysed the diurnal variation field and found that the world wide average of the ratio of internal to external parts was consistent with a uniform core of conductivity $\sigma = 3.6 \times 10^{-13} \text{ e.m.u.}$, surrounded by a nonconducting outer shell with a thickness of 250 km. Chapman and Whitehead (1922) showed that the effect of the highly conducting oceans is large and introduces an uncertainty in the estimate

of σ . In seeking a consistent explanation of the ratio of internal to external parts for daily variations, Sq; and the storm-time variations, Dst, Lahiri and Price (1939) developed two models such that any real conductivity distribution was expected to lie within the limits set by these two models. The d-model, which corresponded to the slowest permissible rate of increase of σ with depth, consisted of a thin shell of integrated conductivity 2×10^{-6} e.m.u x cm. surrounding a conductor in which σ varied as $r^{-3/7}$ (r is distance from center of the earth). The conducting outer shell represented the integrated effect of the influence of the oceans and highly conducting strata near the earth's surface. The e-model consisted of an outer conducting shell ($\sigma = 5 \times 10^{-6}$ e.m.u x cm.) overlying a 700 km. thick non-conducting region, and a core within this having a conductivity greater than 10^{-11} e.m.u. In the e-model the currents do not penetrate appreciably beyond the highly conducting inner core (i.e. a depth of 700 km or about one-tenth of the earth's radius), while in the d-model even the currents associated with the long periods of Dst and Sq penetrate only to a depth of about 1200 km (or about one-fifth of the earth's radius). By using longer period variations, i.e. the 27-day recurrence or six-monthly variations, it may be possible to find σ at greater depths. Maximum depths of penetration of currents caused by variational fields used

in magnetic depth sounding is, however, between 700 and 1200 km.

There is much evidence suggesting that σ is not only a function of radius, but also has lateral variations. For local problems we neglect the sphericity of the earth and assume it to be the surface of a semi-infinite conductor. One then looks for lateral variations of σ on a scale which was smoothed out in the treatment of the global problem. The geomagnetic variations observed near local structures can be considered to consist of a normal and anomalous part. The normal part contains only fields of scale-length large compared with the structure, and is not separable by an array of instruments suitable for study of the structure; while the anomalous field is in general composed of an inhomogeneous external part and an internal anomalous part, and can be separated if observed over an area which contains the structure. Since the external magnetic fields are relatively smooth at geomagnetic mid-latitudes, large differences in the characteristics of magnetic components recorded at stations close together (~100 km.) must have an internal origin. These variations, occurring most prominently in the Z-component, can, after separation of the magnetic field, be related to anomalous induced currents caused by an undulation or lateral

discontinuity of a surface of constant σ (and by inference also an isotherm having the same shape as the σ -surface). From potential theory, it is shown in this thesis that a valid separation of the magnetic field may be completed by evaluation of surface integrals if the three magnetic components are known over an area with linear dimensions of comparable size to the extent of the anomalous field.

Local anomalies may be subdivided into two groups; intra-continental anomalies and continental edge anomalies. Continental edge anomalies have been studied in Australia by Parkinson (1964), along the California coast by Schmucker (1964), and in British Columbia by Lambert and Caner (1965). These anomalies, whose effects can be noticed up to a few hundred kilometers inland from the continental edge, are associated with induced currents in the upper mantle and in the highly conducting ocean. These currents flow parallel to the continental edge and are induced by external fields normal to the edge.

Intracontinental anomalies, associated with lateral variations of σ beneath the continents, have been studied in North Germany by Schmucker (1959) and Wiese (1965), at Alert and Mould Bay in the Canadian Arctic archipelago by Whitham, (1962, 1963) in Brith Columbia by Caner (1966), in Japan by Rikitake, and in the south-western

United States by Schumucker (1964).

Geomagnetic depth sounding in the south-western United States was originally carried out by Schumucker (1960-64). Operating an east-west line of Askania variometers from Tucson, Arizona to Sweetwater, Texas, he found that small Z-variations typical of Tucson ended about 400 km. east of there between Las Cruces and Cornudas, where the Z-amplitude of bays and storms increased about three-fold relative to Tucson. The transition from low Z, indicative of a highly conducting mantle, to high Z occurred in the region where the Basin and Range Province borders the Great Plains. The Z-variation remained intense as far east as Sweetwater, Texas. The close resemblance of the Z and D traces suggested a north-south striking conductivity structure parallel to the Rocky Mountain front in New Mexico. Schumucker postulated a step in a highly conducting stratum going from a depth of 160 km. beneath the Basin and Range, to a depth of 320 km. beneath the Great Plains. Temporary observatory stations to the north of Schumucker's line, established during IGY, supported his conclusion. Stations to the west of the margin (Leadville, Colorado; Espanola, New Mexico) observed $Z/D = 0.05$, while stations to the east of the margin (Burlington, Colorado; Beloit, Kansas; and Carrollton, Missouri) observed increased Z-variation,

$Z/D \sim 0.20$.

Looking for the northward continuation of Schmucker's Texas anomaly, Gough and Reitzel in 1966 operated eight test variometers along the Arkansas and Gunnison Rivers in Colorado. Recording a magnetic bay disturbance at Cimmaron and six stations further west, they found that Z-variations increased by a factor of two from west to east; the transition occurring near Salida which is near the boundary between the Southern Rockies and Great Plains. Again it was found that Z resembled D.

Caner, Canon, and Livingstone (1965) installed an east-west line of variometers from Horse Springs, New Mexico, to Sayre, Oklahoma. This profile was situated between Schmucker's and that of Gough and Reitzel. Small Z-variations were found at all stations except the eastern most station, Sayre, which was near the Texas-Oklahoma border about 500 km. east of the mountain front. An accumulation of results thus suggest that if all the anomalous stations found by Schmucker, Caner et al, Gough and Reitzel, and those operated during the IGY, are associated with one conductivity anomaly, then this anomaly must strike north-east from the eastern margin of the Rocky Mountains on Schmucker's line, into the Great Plains to Sayre, and then swing back toward the Rockies in

central Colorado. We shall see that a result of the work here reported is to show that the upper-mantle conductive structure in fact follows the Southern Rockies. Caner et al. were in fact misled by the effect of a deep sedimentary basin of highly-conducting material in the crust.

The major disadvantage of previous studies was that only a small number of variometers (four to eight) were used at one time. The interpretation of results then depended on the assumptions of the uniformity of the external field at mid-latitude stations and the choosing of a "normal" station as a standard reference. Although Siebert and Kurtz (1957) developed two-dimensional formulae to separate the three-dimensional field along special straight profiles, this separation works effectively only when these profiles are perpendicular to a two dimensional anomaly. It was the purpose of the design of an inexpensive variometer by Gough and Reitzel (1967), which could be built in large numbers, to attempt separation of fields recorded simultaneously over an anomalous area. In the 1967 field season, an array of forty-two variometers was installed in the mid-western United States in order to delineate more accurately this conductivity feature in the upper mantle.

CHAPTER I

ELECTROMAGNETIC INDUCTION

Although this thesis is to deal mainly with the separation of the magnetic field into parts of internal and external origin, this chapter is concerned with the theory of electromagnetic induction. The full electromagnetic theory for conducting bodies having non-planar boundaries has been solved only for some special cases; e.g. cylinder or sphere. The assumption of infinite conductivity is usually made for bodies having more complicated boundaries. Induction in a conducting half-space with a plane boundary ("flat-earth" model) is treated here since it shows some important properties of induction in the Earth; in particular that the horizontal inducing fields outside this half-space are increased by the induced fields, while the vertical field is reduced. Although the induction process is considered in terms of a harmonic inducing field, this is not physically unrealistic since any magnetic disturbance may be decomposed into harmonic fields with certain amplitudes and phases. It is also shown that penetration of the time-varying field into the half-space depends not only upon the conductivity of the medium and the period of the inducing field (skin effect), but also upon the linear dimensions of the inducing field.

The theory of induction as presented here is due mainly to A.T. Price, (1950, 1962).

1.1 "Flat Earth" Model with Uniform Conductivity

As shown in the appendix, Maxwell's equations reduce to

$$\begin{array}{lll}
 \nabla_x E = - \frac{\partial B}{\partial t} & \text{outside the} & \nabla_x E = - \frac{\partial B}{\partial t} & \text{inside the} \\
 & \text{conductor} & \nabla_x H = 4\pi J & \text{conductor} \\
 \nabla \cdot B = 0 & (z < 0) & \nabla \cdot B = 0 & (z > 0) \\
 \nabla \cdot D = 0 & & \nabla \cdot D = 0 & \\
 & & J = \sigma E &
 \end{array}$$

Let the surface of the conductor be the $z=0$ plane with z positive down. Maxwell's equations become

$$\nabla^2 E = 0 \quad z < 0 \quad \text{Laplace's equation} \quad (1.1)$$

$$\nabla^2 E = 4\pi\sigma(z)\mu^0 E \quad z > 0 \quad \text{Diffusion or induction} \quad (1.2) \\ \text{equation}$$

Since $\sigma = \sigma(z)$ only, the currents flow parallel to the surface of the conductor and therefore $E_z = 0$ within the conductor.

Since $\nabla \cdot J = 0$ in the conductor, then

$$\sigma \left(\frac{\partial E_x}{\partial x} + \frac{\partial E_y}{\partial y} + \frac{\partial E_z}{\partial z} \right) + E_z \frac{\partial \sigma}{\partial z} = 0$$

and therefore

$$\frac{\partial E_x}{\partial x} + \frac{\partial E_y}{\partial y} = 0. \quad (1.3)$$

Let the electric field be of the form

$$\vec{E}(x, y, z, t) = \vec{Z}(z, t) \vec{F}(x, y) \quad (1.4)$$

Equation (1.3) becomes

$$\frac{\partial \vec{F}}{\partial x} = -\frac{\partial \vec{F}}{\partial y} \quad \text{or} \quad \vec{F}(x, y) = \left(\frac{\partial P}{\partial y}, -\frac{\partial P}{\partial x}, 0 \right) \quad (1.5)$$

i.e. the electric field is derivable from a scalar potential $P(x, y)$. Substituting (1.4) into (1.2) and separating the variables, we have

$$\frac{1}{F} \left\{ \frac{\partial^2 F}{\partial x^2} + \frac{\partial^2 F}{\partial y^2} \right\} = \frac{1}{Z} \left\{ 4\pi\sigma\mu \frac{\partial Z}{\partial t} - \frac{\partial^2 Z}{\partial z^2} \right\} = -v^2$$

where v^2 is a constant of separation. If (1.5) is then used, the vector equation for $\vec{F}(x, y)$ reduces to a scalar equation for P . The equations to be solved for $z > 0$ are

$$\frac{\partial^2 P}{\partial x^2} + \frac{\partial^2 P}{\partial y^2} + v^2 P = 0 \quad (1.6)$$

and

$$\frac{\partial^2 Z}{\partial z^2} = \left\{ v^2 + 4\pi\mu\sigma \frac{\partial}{\partial t} \right\} Z \quad (1.7)$$

Equation (1.6) also holds for $z < 0$. Since the tangential components of \vec{E} and \vec{H} are continuous, the constant of separation for $z < 0$ must be the same as that for $z > 0$. For $z < 0$ the Z equation is simply

$$\frac{\partial^2 Z}{\partial z^2} = \nu^2 Z$$

which has the solution

$$Z(z, t) = C(t)e^{-\nu z} + D(t)e^{\nu z} \quad (1.8)$$

Applying equations (1.4) and (1.5) to $\nabla \times E = -\frac{\partial B}{\partial t} = -\mu H$ and completing the curl operation we obtain

$$-\mu H^0 = \left(\frac{\partial Z}{\partial z} \frac{\partial P}{\partial x}, \frac{\partial Z}{\partial z} \frac{\partial P}{\partial y}, \nu^2 P Z \right) \quad (1.9)$$

This equation holds for both $z < 0$ and $z > 0$. The boundary conditions on \vec{E} and \vec{H} reduce to

$$(i) \quad \frac{\partial Z}{\partial z} (0^-, t) = \frac{\partial Z}{\partial z} (0^+, t) \quad \text{tangential component of } \vec{H} \text{ is continuous across the boundary}$$

$$(ii) \quad Z(0^-, t) = Z(0^+, t) \quad \text{normal component of } \vec{B} \text{ is continuous}$$

The solution for \vec{E} inside the conductor is greatly simplified if in equation (1.7) we let σ be a constant and assume a time varying field of the type $e^{i\omega t}$.

Equation (1.7) then becomes

$$\frac{\partial^2 Z}{\partial t^2} = \theta^2 Z \quad \text{where} \quad \theta^2 = \nu^2 + i4\pi\mu\omega\sigma$$

This has a solution $Z = ae^{-\theta z} + be^{+\theta z}$. As $z \rightarrow \infty$ (i.e. deep in the conductor) the electric field must be zero. Therefore $b=0$. Hence

$$Z(z, t) = (Ce^{-\nu z} + De^{\nu z})e^{i\omega t} \quad z < 0$$

$$Z(z, t) = ae^{-\theta z}e^{i\omega t} \quad z > 0$$

Applying the boundary conditions (1.10) we have

$$a = C + D$$

$$-\frac{\partial a}{\nu} = -C + D$$

or

$$a = \frac{2\nu C}{\theta + \nu} \quad D = \left(\frac{\nu - \theta}{\nu + \theta}\right)C \quad (1.11)$$

Since $\nabla \times H = 0$ (for $z < 0$) the external field may be written in terms of the gradient of a potential Ω ,

$$H = -\nabla \Omega$$

$$\text{where } \Omega = \{A \exp(-\nu z) + B \exp(\nu z)\}P(x, y, \nu)e^{i\omega t} \quad (1.12)$$

Here the term $A \exp(-\nu z)$ represents the contribution to the potential of the currents in the ionosphere, while the term $B \exp(\nu z)$ is the contribution outside the conductor of the induced currents within the conductor. The modulus of B/A is the ratio of the amplitude of the induced magnetic field to that of the inducing field, while the argument of B/A gives the phase difference between these two fields. By combining equations (1.8) and (1.9) and using the harmonic time dependence, the expression for the external field becomes

$$H = \frac{-\nu}{i\mu\omega} [(-Ce^{-\nu z} + De^{\nu z})(\frac{\partial P}{\partial z}, \frac{\partial P}{\partial y}), \nu P(Ce^{-\nu z} + De^{\nu z})] e^{i\omega t} \quad (1.13)$$

or alternately written in terms of a gradient of a potential,

$$H = \frac{-\nu}{i\mu\omega} \nabla [(-Ce^{-\nu z} + De^{\nu z})P(x, y)] e^{i\omega t} \quad (1.14)$$

Comparing (1.12) and (1.13) we obtain

$$C = -\frac{i\mu\omega}{\nu} A \quad D = \frac{i\mu\omega}{\nu} B \quad (1.15)$$

With these definitions for C and D in equation (1.11)

$$a = -\frac{2i\mu\omega}{\theta+\nu} A \quad B = \left(\frac{\theta-\nu}{\theta+\nu}\right) A \quad (1.16)$$

We now have an expression for the induced field measured

in the conductor and the effect of these fields outside in terms of the potential of the inducing field. Equation (1.16) shows that the inducing field will produce an image field inside the conductor with a strength less than or equal to that of the original inducing field. How the magnetic components are affected at the surface of the earth can be shown by looking at the fields at $z = 0$. Substituting (1.16) into (1.13) and letting $z = 0$ the field at the surface becomes

$$H = -\{(A+B)\left(\frac{\partial P}{\partial x}, \frac{\partial P}{\partial y}\right), \nu P(-A+B)\}e^{i\omega t}, \quad (1.17)$$

whereas the inducing field was

$$H = -[A \frac{\partial P}{\partial x}, A \frac{\partial P}{\partial y}, \nu AP]$$

Thus it can be seen that at the surface the induced horizontal components add to the inducing field, while the induced vertical component opposes the inducing field. If $\theta \gg \nu$ i.e. the product of conductivity of the half space by the frequency is very large, then $B \rightarrow A$ and the resultant magnetic field is

$$H = -[2A \frac{\partial P}{\partial x}, 2A \frac{\partial P}{\partial y}, 0] \quad (1.18)$$

The horizontal components are then doubled while the

vertical component is cancelled out.

1.2 Effect of Dimensions of the Source Field

The reciprocal of the parameter, ν , used in the "flat earth" model is a measure of the horizontal scale of the source field ($\lambda = 2\pi/\nu$, where λ is the wavelength or scale length of the field). Since the inducing currents originate in the ionosphere, the values of λ are constrained to lie between two bounds. The maximum value possible for λ is the circumference of the earth, while the minimum value (arising from local fields) is about four times the height to the E-layer (about 100 km), the lowest level at which the currents may exist (Price, 1962). The values of ν of interest then lie between

$$1.6 \times 10^{-9} \text{ cm}^{-1} \leq \nu \leq 1.6 \times 10^{-7} \text{ cm}^{-1}$$

If we consider the uniform half-space and an external potential of the form

$$\Omega_e = -A \exp(\nu z + i\omega t) P(x, y)$$

then the current density at a depth z can easily be found from $\vec{J} = \sigma \vec{E}$

$$\vec{J} = -\frac{2\sigma i\omega}{\theta + \nu} \exp(-\theta z + i\omega t) \left(\frac{\partial P}{\partial y}, -\frac{\partial P}{\partial x}, 0 \right) \quad (1.19)$$

$$\theta^2 = \nu^2 + i4\pi\sigma\omega \quad (1.20)$$

$$\theta = \frac{1}{\sqrt{2}} [\{(\gamma^4 + v^4)^{\frac{1}{2}} + v^2\}^{\frac{1}{2}} + i\{(\gamma^4 + v^4)^{\frac{1}{2}} - v^2\}^{\frac{1}{2}}] \quad (1.21)$$

where

$$\gamma^2 = 4\pi\sigma\omega$$

The real part of θ describes the attenuation of the current with depth, while the imaginary part specifies a phase. If $v = 0$, that is, the wavelength of the inducing field is infinite, then $\text{Re}\theta = 2\sqrt{\pi\sigma\omega}$ and the attenuation reduces to the ordinary skin depth formula. From (1.21) it can be seen that the attenuation of current with depth is significantly affected by the scale of the inducing field when $v \sim 2\sqrt{\pi\sigma\omega}$.

In the "non-conducting" layers below the surface the conductivity $\sigma \sim 10^{-15}$ e.m.u. If v is taken as 10^{-8} cm $^{-1}$ (which may be a typical value for a bay in the mid-latitudes) and the period of the inducing field as 60 minutes, then $2\sqrt{\pi\sigma\omega} = 0.46 \times 10^{-8}$. Hence the attenuation of currents is highly affected by the scale length of the field. For the more highly conducting mantle $\sigma \sim 10^{-12}$ e.m.u. and $2\sqrt{\pi\sigma\omega} = 1.47 \times 10^{-7}$, which is almost an order of magnitude higher than v . Therefore, at greater depths and higher conductivity, the ordinary skin depth formula should be a good approximation.

For the "flat-earth" model the ratio of the induced to inducing fields (measured on the surface) was given by

$$\frac{B}{A} = \frac{\theta-v}{\theta+v} \quad (1.22)$$

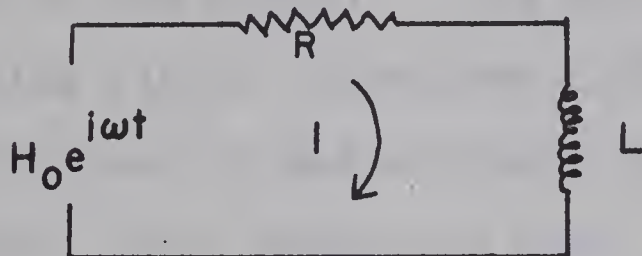
From (1.21) we see that if $\gamma^2 \ll v^2$ then $\theta \approx v$ and there will be no induction. If $\gamma^2 \gg v^2$ then $\theta = \frac{\gamma(1+i)}{\sqrt{2}}$, resulting in a doubling of the horizontal field and the extinguishing of the vertical field. The following table (Matsushita p.289) illustrates how the induction is affected as the ratio $\beta = 4\pi\sigma\omega/v^2$ is allowed to vary.

β	0.01	0.25	1.0	4.0	25	100	∞
Mod(B/A)	0.0025	0.065	0.22	0.48	0.75	0.87	1.00
Arg(B/A)	90°	77°	66°	39°	16°	8°	0°

From the table, it can be seen that induction becomes important only when $\beta \geq 1$. When $\beta = 1$, the horizontal fields are each increased by 22% while the vertical field is decreased by the same percentage. $\beta \geq 100$ represents almost complete induction. As β takes on higher values (corresponding to an increasing σ) the phase difference between the induced and inducing field decreases. For a good conductor this phase difference is small showing that the induced field follows the inducing field rather

than the time derivative of it.

The phase differences between the induced and inducing fields suggest that induction within the "flat-earth" model is analogous to induction in an LR circuit by an incident variational magnetic field.



The external (or inducing) potential is given by

$$V = (i\omega) (\text{const.}) H_0 e^{i\omega t}$$

For the LR circuit the current, I , for any inducing potential V , is given by

$$I = \frac{V(R - i\omega L)}{R^2 + (\omega L)^2}$$

Since $\vec{V} \times \vec{H} = \vec{J}$ we have that

$$H_{\text{in}} e^{i\omega t} = (\text{const.}) I_{\text{in}}$$

$$\text{and therefore } H_{\text{in}} = \frac{\text{const.}}{R^2 + (\omega L)^2} H_0 (\omega L + iR)$$

The phase difference between the inducing and induced fields is given by $\tan^{-1} (R/\omega L)$. For a resistive circuit, ($R \gg \omega L$), the internal field leads the external field by 90° .

If $\omega L \gg R$, that is, self-induction is dominant, the phase difference approaches zero.

Table (1.1) shows that the minimum value of σ , required to make $\text{mod}(B/A)$ attain certain values, is critically dependent on the period T and on the parameter v of the inducing field. Schmucker (1964) stated that v for geomagnetic bays at midlatitudes should be $0.4 \times 10^{-8} \text{ cm}^{-1}$, while Price (1962) suggested that $v = 10^{-8} \text{ cm}^{-1}$ is a representative value for most geomagnetic fluctuations. For the magnetic event analysed in this thesis, it has been found (Chapter IV) that $\lambda = 7,500$ to $10,000$ km. give probable values of v . Values from Table (1.1) of interest are then $\lambda = 7500$ km. and $T = 1$ hr. In order for the induction to become significant ($\text{mod } B/A = 0.22$) σ must be $\sim 3.2 \times 10^{-15} \text{ e.m.u.}$ Thus significant induction will occur in the saturated sediments, in the highly conducting mantle, and possibly in normal crustal rocks ($\sigma \sim 10^{-14} - 10^{-16}$). If induction is nearly complete ($\text{mod } B/A = 0.87$), then only the highly conducting sediments and mantle give large contributions to the induction, while the intermediate low conductivity region is effectively transparent.

A more realistic model of the earth may be the plane layered case used in magnetotellurics. If the three

TABLE (1.1)

Scale length

λ (km)	ν (cm $^{-1}$)	T (hrs.)	σ	Required for	mod(B/A) =
			0.065	0.22	0.87
1,000	6.28×10^{-8}	0.25	1.1×10^{-14}	4.5×10^{-14}	4.5×10^{-12}
		0.50	2.2×10^{-14}	9.0×10^{-14}	9.0×10^{-12}
		1.0	4.5×10^{-14}	1.8×10^{-13}	1.8×10^{-11}
		2.0	9.0×10^{-14}	3.6×10^{-13}	3.6×10^{-11}
		4.0	1.8×10^{-13}	7.2×10^{-13}	7.2×10^{-11}
5,000	1.25×10^{-8}	0.25	4.5×10^{-16}	1.8×10^{-15}	1.8×10^{-13}
		0.50	8.9×10^{-16}	3.6×10^{-15}	3.6×10^{-13}
		1.0	1.8×10^{-15}	7.2×10^{-15}	7.2×10^{-13}
		2.0	3.6×10^{-15}	1.4×10^{-14}	1.4×10^{-12}
		4.0	7.2×10^{-15}	2.8×10^{-14}	2.8×10^{-12}
7,500	0.838×10^{-8}	0.25	2.0×10^{-16}	8.1×10^{-16}	8.1×10^{-14}
		0.50	4.0×10^{-16}	1.6×10^{-15}	1.6×10^{-13}
		1.0	8.1×10^{-16}	3.2×10^{-15}	3.2×10^{-13}
		2.0	1.6×10^{-15}	6.5×10^{-15}	6.5×10^{-13}
		4.0	3.2×10^{-15}	1.3×10^{-14}	1.3×10^{-12}
10,000	0.628×10^{-8}	0.25	1.1×10^{-16}	4.5×10^{-16}	4.5×10^{-14}
		0.50	2.2×10^{-16}	9.0×10^{-16}	9.0×10^{-14}
		1.0	4.5×10^{-16}	1.8×10^{-15}	1.8×10^{-13}
		2.0	9.0×10^{-16}	3.6×10^{-15}	3.6×10^{-13}
		4.0	1.8×10^{-15}	7.2×10^{-15}	7.2×10^{-13}
15,000	0.417×10^{-8}	0.25	5.0×10^{-17}	2.0×10^{-16}	2.0×10^{-14}
		0.5	1.0×10^{-16}	4.0×10^{-16}	4.0×10^{-14}
		1.0	2.0×10^{-16}	8.0×10^{-16}	8.0×10^{-14}
		2.0	4.0×10^{-16}	1.6×10^{-15}	1.6×10^{-13}
		4.0	8.0×10^{-16}	3.2×10^{-15}	3.2×10^{-13}

magnetic components are known, the ratios H_z/H_x , H_z/H_y may be analysed to determine apparent resistivities. An interpretation of plane layered media can be made by comparing the apparent resistivity curves with characteristic model curves computed for magnetotelluric work (Cagniard, 1953). However, the analysis of plane layers was not undertaken in this thesis since the separated fields clearly showed anomalous lateral variations in the conductivity structure.

Geomagnetic depth sounding provides good resolution of lateral conductivity variations since additional horizontal and vertical fields are induced by the horizontal component perpendicular to the strike of the conductor. For example, currents parallel to a north-south striking conductivity structure will be induced by an eastward variational field. These currents give rise to an anomalous internal Z component (and also an anomalous internal Y), compared with the normal internal Z induced by the external vertical fields in the absence of lateral conductivity changes.

CHAPTER II

HISTORY AND DERIVATION OF THE SEPARATION INTEGRALS

2.1 History

Separation of the magnetic field into internal and external parts was originally made by Gauss (1839), and later by Chapman and Whitehead, Lahiri and Price, and others (Chapman and Bartels 1940). This method requires the fitting of a global magnetic field by a number of spherical harmonics, and then finding what portions of each harmonic result from external and internal sources. The final results are then world-wide averages of the internal and external ratios for each harmonic. For a sphere having magnetic fields on its surface derivable from a scalar potential V , the most general harmonic representation of V is of the form

$$V = a \sum_{n=0}^{\infty} \sum_{m=0}^n P_n^m(\cos\theta) \left[\left\{ c_n^m \left(\frac{r}{a} \right)^n + (1-c_n^m) \left(\frac{a}{r} \right)^{n+1} \right\} A_n^m \cos m\phi + \left\{ s_n^m \left(\frac{r}{a} \right)^n + (1-s_n^m) \left(\frac{a}{r} \right)^{n+1} \right\} B_n^m \sin m\phi \right] \quad (2.1)$$

a = radius of the earth

r = distance from the center of the earth

c_n^m and s_n^m are numbers between zero and one representing fractions of the harmonics $\cos m\phi$ and $\sin m\phi$ which are due to matter outside the sphere.

If the radial gradient $Z = \frac{\partial V}{\partial r}$ is known, then Z (vertical field measured at the surface) can be expanded in a Fourier series similar to (2.1)

$$\left. \frac{\partial V}{\partial r} \right|_{r=a} = \sum_{n=0}^{\infty} \sum_{m=0}^n P_n^m(\cos \theta) (\alpha_n^m \cos m\phi + \beta_n^m \sin m\phi) \quad (2.2)$$

If (2.1) is differentiated with respect to r , and r is set equal to a , then this expression may be compared with (2.2), to give values for the coefficients c_n^m and s_n^m . Since the potential V is not measured directly, the coefficients A_n^m and B_n^m are found from the northward (X) and eastward (Y) field components

$$Y_{r=a} = \left(\frac{-1}{r \sin \theta} \frac{\partial V}{\partial \phi} \right)_{r=a} = \frac{1}{\sin \theta} \sum_{n=0}^{\infty} \sum_{m=0}^n P_n^m (mA_n^m \sin m\phi - mB_n^m \cos m\phi) \quad (2.3)$$

$$X_{r=a} = \left(\frac{1}{r} \frac{\partial V}{\partial \theta} \right)_{r=a} = \sum_{n=0}^{\infty} \sum_{m=0}^n \frac{dP_n^m}{d\theta} \{ A_n^m \cos m\phi + B_n^m \sin m\phi \} \quad (2.4)$$

The coefficients are most easily derived from Y , but a comparison of those derived from (2.3) and (2.4) provides a check on the accuracy of the analysis.

It is not possible, however, to apply this type of analysis to local fields since there are neither enough

observatories, nor are they situated in the most ideal locations, to derive the large number of harmonics required to determine the potential accurately over a limited area.

Siebert and Kertz (1957) attempted to separate the local magnetic field in an area over the North-German anomaly by analysis of a magnetic bay recorded at fourteen stations. After a two-dimensional approximation of the three-dimensional field, the separation into internal and external parts was completed by means of an integral operator.

If X, Y, Z are the measured magnetic field components, and the magnetic potential satisfies Laplace's equation, then

$$\frac{\partial X}{\partial x} + \frac{\partial Y}{\partial y} + \frac{\partial Z}{\partial z} = 0 \quad (2.5)$$

The potential may be made to satisfy a two-dimensional equation under the transformation

$$(x, y, z) \rightarrow (u, v, z) \quad \text{and} \quad (X, Y, Z) \rightarrow (U, V, Z)$$

where the uv -system is obtained by rotating the xy -system through an angle ψ . Then $\frac{\partial U}{\partial u} + \frac{\partial Z}{\partial z} = 0$ along a profile chosen such that the horizontal field has no gradient at right angles to this profile, so that

$$\frac{\partial V}{\partial v} = 0 \quad (2.6)$$

A quadratic equation in $\tan \psi$ (or $\operatorname{ctn} \psi$) is obtained from (2.6).

$$\tan \psi = - \frac{1}{2(\frac{\partial X}{\partial x})} \left\{ \frac{\partial X}{\partial y} + \frac{\partial Y}{\partial x} \pm \sqrt{\left(\frac{\partial X}{\partial y} + \frac{\partial Y}{\partial x} \right)^2 - 4 \frac{\partial X}{\partial x} \frac{\partial Y}{\partial y}} \right\} . \quad (2.7)$$

Equation (2.7) may be solved in terms of the quantities:

$\frac{\partial X}{\partial y}$, $\frac{\partial Y}{\partial x}$, $\frac{\partial Y}{\partial y}$, $\frac{\partial X}{\partial x}$, which are values found by drawing lines of $X = \text{const.}$ and $Y = \text{const.}$ for the observed fields and then measuring the gradients of the magnetic components at selected points. The two values of ψ found from (2.7) may be plotted on a map. Although in most cases a curved path is required to join points along which u has the same direction, there may exist certain "selected profiles" in which this path is a straight line. The observations along this profile may be made an explicit function of u , such that the fields along this line may be separated by applying Kertz's two-dimensional integral operator K .

$$Kf(u) = \frac{1}{\pi} \int_{-\infty}^{\infty} \frac{f(u')}{u-u'} du' . \quad (2.8)$$

Then

$$U_E = KZ_E \quad U_I = -KZ_I$$

$$Z_E = -KU_E \quad Z_I = KU_I$$

where the subscripts E and I stand for external and internal respectively. Since $U = U_E + U_I$ and $Z = Z_E + Z_I$ we have

$$\begin{aligned} U_E &= \frac{1}{2}(U+KZ) & U_I &= \frac{1}{2}(U-KZ) \\ Z_E &= \frac{1}{2}(Z-KU) & Z_I &= \frac{1}{2}(Z+KU) \end{aligned} \quad (2.9)$$

and the field is completely separated. In actual practice the integral in equation (2.8) was changed to a sum

$$Kf(u_m) = -\frac{1}{\pi} \left[\sum_{n=-N}^N (1-\delta_{nm}) \frac{f(u_n)}{(n-m)} + 2af'(u_m) \right] \quad (2.10)$$

where

$$m = -N, -N+1, \dots, 0, 1, 2, \dots, N$$

δ_{nm} = kronecker delta function

The term $f'(u_m)$ is the derivative of the function and represents the contribution to the sum when $n = m$. The sum (2.10) is then computed for $2N+1$ equidistant points.

In the above analysis it has been assumed that the horizontal field has no gradient in the v-direction. In many cases this condition is too strict to allow a valid interpretation of the separated fields. The derivation of integral formulae, similar to (2.9) but appropriate to separate the three-dimensional field, is required.

The first application of the use of surface integrals to separate a three-dimensional magnetic field was made by Price and Wilkins (1963) in the analysis of the Sq field of 1932-3. The horizontal components of the Sq field for the earth were interpolated by adjusting these fields to fulfill the condition that the line integral of magnetic force around any closed contour on the surface was equal to zero. (i.e. the condition for a potential field). Values of the field were then found at the points of intersection of every 10° of latitude and 15° of longitude. By arbitrarily choosing the value of the potential at one point, the potential at all other points was easily evaluated. A surface integral, derived by Vestine (1941), was then used to compute the difference between the internal and external parts of the potential at any point A on the surface

$$(V_e - V_i)_A = V_o + \frac{1}{2\pi} \int_S \left\{ \frac{1}{r} \frac{\partial}{\partial n} (V - V_o) - (V - V_o) \frac{\partial}{\partial n} \left(\frac{1}{r} \right) \right\} ds \quad (2.11)$$

V_o = arbitrary constant

n = normal to the surface

r = distance from point A to the surface element ds

S = any closed surface

$V = V_e + V_i$ = total potential

If the surface S is a sphere, (2.11) reduces to

$$(V_e - V_i)_A = \int_S \frac{V + 2aZ}{4\pi a R} ds \quad (2.12)$$

Z = inward normal component of force

a = radius of the sphere

The integral in (2.12) may then be evaluated by methods suggested by Vestine and used by Taylor and Davids (1944).

2.2 Derivation of Separation Integrals

The approach of Price and Wilkins is easily adapted to separation analysis of local fields. The starting relation for the derivation of the surface integrals is again given by Vestine's formula giving the difference between internal and external parts of the potential

$$\begin{aligned} 2\pi(V_e - V_i)_A &= \int_S \left(\frac{1}{r} \frac{\partial V}{\partial n} - V \frac{\partial}{\partial n} \left(\frac{1}{r} \right) \right) ds \\ &= \int_S \left(\frac{1}{r} \frac{\partial V}{\partial n} + \frac{V}{r^2} \frac{\partial r}{\partial n} \right) ds \end{aligned} \quad (2.13)$$

When dealing with local fields the sphericity of the earth is neglected, which effectively means that S is regarded as a sphere with infinite radius. In the following material the coordinate system: x -positive north, y -positive east, and z -positive down, is used. Let $(x_A, y_A, 0)$ be the point at which the fields are to be separated, then

$$r^2 = (x_A - x)^2 + (y_A - y)^2 \quad \text{and} \quad \frac{\partial}{\partial n} = - \frac{\partial}{\partial z}$$

On the surface S , $\partial r / \partial n = 0$, thus (2.13) reduces to

$$2\pi(V_e - V_i) = \int_S \frac{1}{r} \frac{\partial V}{\partial n} ds. \quad (2.14)$$

The magnetic field is represented by

$$(X, Y, Z) = -\left(\frac{\partial V}{\partial x}, \frac{\partial V}{\partial y}, \frac{\partial V}{\partial z}\right).$$

Since the magnetic field components are found from the gradient of the potential, the differentiation of (2.14) will yield relations between the internal and external parts of each of the magnetic components. Equation (2.14) is of the type

$$F(x_A, y_A) = \int_S G(x_A, y_A; x, y, z) dx dy$$

If the point A is displaced slightly in the x -direction, then the effect of the integral upon F is given by explicit differentiation with respect to x_A .

Differentiating (2.14) explicitly w.r.t. x_A , we obtain

$$-\frac{\partial}{\partial x_A} [2\pi(V_e - V_i)_A] = 2\pi(X_e - X_i)_A = -\frac{\partial}{\partial x_A} \int_S \frac{1}{r} \frac{\partial V}{\partial n} ds$$

Recognizing that V is a function of x and y only, and that $\frac{\partial V}{\partial n} = -\frac{\partial V}{\partial z} = Z$ we have

$$2\pi(X_{e^{-X_i}})_A = \int_S \frac{(x_A - x)}{r^3} Z \, ds . \quad (2.15)$$

Similarly by differentiating (2.14) with respect to y_A , (or directly from symmetry considerations)

$$2\pi(Y_{e^{-Y_i}})_A = \int_S \frac{(y_A - y)}{r^3} Z \, ds . \quad (2.16)$$

Since the surface S is regarded as a plane, $\partial/\partial z_A = \partial/\partial z$. Differentiating the left side of (2.14) w.r.t. z_A and the right w.r.t. z , we have

$$2\pi(Z_{e^{-Z_i}})_A = - \int_S \frac{1}{r} \frac{\partial}{\partial z} \left(\frac{\partial V}{\partial n} \right) \, ds . \quad (2.17)$$

Since the potential satisfies Laplace's equation at the surface (2.17) becomes

$$2\pi(Z_{e^{-Z_i}})_A = - \int_S \frac{1}{r} \left(\frac{\partial^2 V}{\partial x^2} + \frac{\partial^2 V}{\partial y^2} \right) \, ds$$

Integrating by parts we obtain

$$2\pi(Z_{e^{-Z_i}})_A = - \int_S \left(\frac{(x_A - x)X + (y_A - y)Y}{r^3} \right) \, ds . \quad (2.18)$$

If the coordinate system is translated, so that the origin coincides with the point A , then equations (2.15), (2.16),

and (2.18) become

$$(X_e - X_i)_o = - \frac{1}{2\pi} \int_S \frac{xZ}{r^3} ds , \quad (2.19)$$

$$(Y_e - Y_i)_o = - \frac{1}{2\pi} \int_S \frac{yZ}{r^3} ds , \quad (2.20)$$

$$(Z_e - Z_i)_o = \frac{1}{2\pi} \int_S \frac{xX + yY}{r^3} ds . \quad (2.21)$$

When these equations are respectively combined with $X = X_e + X_i$, $Y = Y_e + Y_i$ and $Z = Z_e + Z_i$ a complete separation of each of the magnetic components into internal and external parts is obtained.

The variables of position in the integrand all have the form $\int \frac{x dx dy}{r^3}$ (2.22)

In cartesian coordinates the segmental area, $dx dy$, may be chosen to be a square of side $2a$. Then r is the distance from the origin to the center of this square. At the origin, where dx , dy , x and y are all identically zero, (2.22) reduces to the form $0/0$ (i.e. the value is indeterminate). From physical reasoning the contribution of a square of side $2a$ centered on the origin must be finite, and this contribution can be found in the following manner. Consider equation (2.19).

$$2\pi(X_e - X_i)_{2a} = - \int_{-a}^a \int_{-a}^a \frac{xZ}{r^3} = - \int_{-a}^a \int_{-a}^a \frac{xZ(x, y) dx dy}{(x^2 + y^2)^{3/2}}$$

Since the magnetic fields at mid-latitudes are smoothly varying, then within a small distance about the origin the field component may be expanded in a Taylor series involving only a constant plus the first derivative terms. Expanding $Z(x, y)$ in a Taylor series

$$Z(x, y) = Z_0 + x \left. \frac{\partial Z}{\partial x} \right|_0 + y \left. \frac{\partial Z}{\partial y} \right|_0 \quad (2.23)$$

and integrating by parts, we obtain

$$2\pi(X_e - X_i)_{2a} = - 2a \left. \frac{\partial Z}{\partial x} \right|_0 \ln \left(\frac{\sqrt{2}+1}{\sqrt{2}-1} \right) \quad (2.24)$$

A similar relation is obtained for the Y component.

$$2\pi(Y_e - Y_i)_{2a} = - 2a \left. \frac{\partial Z}{\partial y} \right|_0 \ln \left(\frac{\sqrt{2}+1}{\sqrt{2}-1} \right) \quad (2.25)$$

For the Z component, by expanding X and Y in Taylor series similar to (2.23), we obtain

$$2\pi(Z_e - Z_i)_{2a} = 2a \left(\left. \frac{\partial X}{\partial x} \right|_0 + \left. \frac{\partial Y}{\partial y} \right|_0 \right) \ln \left(\frac{\sqrt{2}+1}{\sqrt{2}-1} \right) \quad (2.26)$$

The separation formulae (2.19 - 2.21) have been derived by others using different methods. Hartmann (1963)

treated the separation of the fields as a problem in potential theory and obtained the required formulae by using Green's functions of the first and second kind. Weaver (1963) obtained both the two- and three- dimensional formulae by taking the two-dimensional Fourier transform of Laplace's equation for the potential, and then applying the Faltung Theorem.

There are several points of interest with regard to the integral separation formulae. These formulae require knowledge of the field over an infinite plane. However, the plane is only an approximation to the earth's surface over a certain region, and the variational magnetic field is known over only a portion of this plane. Some extrapolation of the observed fields beyond the area must be attempted. While the extrapolated values will inevitably include errors, these will be smaller than the errors involved in assuming zero or some other constant value for the field outside the area of observation. The effect of the field in an area element of given size varies as $1/r^2$ and so converges fairly rapidly. (Numerical examples are quoted in Chapter IV.) It is of course this relatively rapid convergence which makes even approximate separation feasible with a limited area of observation.

In equation (2.19), for $x = 0$ and any distribution of values of Z , the only value of y giving a non-zero contribution to the integral is $y = 0$. If Z is of the same sign for the whole array, then contributions to the integral from the area $x > 0$ (north of the point where separation is to be made) are of opposite sign to those from $x < 0$. The contributions to the integral thus depend upon the asymmetry of the Z -component about the $x = 0$ line. Therefore, if Z is a constant over the array, or if Z is an even function with respect to the $x = 0$ line, then $(X_e - X_i) = 0$. Similarly in equation (2.20) and (2.21) it is the asymmetry of the Z -component and the X and Y components respectively which give finite contributions to the surface integrals. The evaluation of the integrals (2.19-2.21) thus require summation over an area symmetrical about the point of separation.

In geomagnetic depth sounding we are concerned with four types of magnetic field variations:

1. normal external field
2. anomalous external field
3. normal internal field
4. anomalous internal field.

In mid-latitudes, far away from the equatorial electrojet and current sources in the auroral zone, the effect of the anomalous external field is small. The inducing field is then the smoothly varying normal field. The normal internal field results from the highly conducting "core" of the earth, and exhibits induction properties of the "flat-earth" model of Chapter I, while the anomalous internal field arises from lateral discontinuities in a highly conducting stratum.

Smoothly varying fields, having spatial wavelengths much larger than the dimensions of our array, e.g. normal internal and external fields, cannot be separated by the formulae (2.19 - 2.21). Therefore it is the dimensions of the array that dictate which fields are separable "anomalous" and which are inseparable "normal" fields.

2.3 Separation in Polar Coordinates

Although the surface integrations were computed in cartesian coordinates, it is possible to interpolate a cartesian grid of values of the field in such a way as to allow one to carry out the integration in polar coordinates. The polar grid, consisting of a series of annular rings with increasing radii, is moved over the array and a value for the difference between the external

and internal parts of a magnetic field component is obtained for a small circle at the center of the grid. Integration in polar coordinates has the advantage of automatically extending the area of integration by the same amount in each direction (i.e. a symmetric grid), and more importantly it enables one to see the contribution of each ring as one proceeds from the origin. It is therefore possible to see directly at what rate the integral converges.

Equations (2.19) to (2.21) in polar coordinates (r, θ) become

$$(X_e - X_i)_o = - \frac{1}{2\pi} \int_S \frac{Z(r, \theta) \sin \theta}{r} dr d\theta \quad (2.27)$$

$$(Y_e - Y_i)_o = - \frac{1}{2\pi} \int_S \frac{Z(r, \theta) \cos \theta}{r} dr d\theta \quad (2.28)$$

$$(Z_e - Z_i)_o = \frac{1}{2\pi} \int_S \frac{X(r, \theta) \sin \theta + Y(r, \theta) \cos \theta}{r} dr d\theta \quad (2.29)$$

As $r \rightarrow 0$ the above integrals are indeterminate. The exact contribution of a circle of radius "a" about the center may be found by the method used in cartesian coordinates.

Expand $Z(r, \theta)$ in a Taylor series about the origin:

$$Z(r, \theta) = Z_o + x \left. \frac{\partial Z}{\partial x} \right|_o + y \left. \frac{\partial Z}{\partial y} \right|_o = Z_o + r \sin \theta \left. \frac{\partial Z}{\partial x} \right|_o + r \cos \theta \left. \frac{\partial Z}{\partial y} \right|_o$$

Substituting this into (2.27) we obtain

$$(X_e - X_i)_a = - \frac{1}{2\pi} \int_0^a \int_0^{2\pi} (Z_o + r \sin\theta \frac{\partial Z}{\partial x} \bigg|_o + r \cos\theta \frac{\partial Z}{\partial y} \bigg|_o) \frac{\sin\theta}{r} dr d\theta$$

Therefore

$$(X_e - X_i)_a = - \frac{1}{2\pi} \int_0^a \int_0^{2\pi} \sin^2\theta \frac{\partial Z}{\partial x} \bigg|_o dr d\theta = - \frac{a}{2} \frac{\partial Z}{\partial x} \bigg|_o$$

(2.30)

Similarly the contributions of a circle of radius "a" about the origin to (2.28) and (2.29) are

$$(Y_e - Y_i)_a = - \frac{a}{2} \frac{\partial Z}{\partial y} \bigg|_o \quad (2.31)$$

$$(Z_e - Z_i)_a = \frac{a}{2} \left(\frac{\partial X}{\partial x} \bigg|_o + \frac{\partial Y}{\partial y} \bigg|_o \right) \quad (2.32)$$

2.4 Separation Formulae in the Frequency Domain

Whereas instantaneous values of the magnetic field in the time domain were separated into internal and external parts, the frequency domain requires the separation of sine and cosine transform coefficients at a particular period. For purposes of explanation, consider the application of (2.17) to separation in the frequency domain.

$$(X_e(t) - X_i(t))_o = - \frac{1}{2\pi} \int_S \frac{x}{r^3} Z(x, y, t) ds \quad (2.33)$$

The full Fourier transform of this equation cannot be used since the transform of each of the components X and Z involves two quantities; an amplitude and a phase. However, the sine (or cosine) transform of (2.33) will yield a single number, which is the amplitude of a sine (or cosine) wave at a particular frequency. The physical meaning of using such transforms is that the analysis of a magnetic component at all stations in the array occurs at the same phase.

Letting $(\bar{\cdot})$ denote either the sine or cosine transform, and noting that the integrals of space and time may be interchanged, (2.33) becomes

$$(\bar{X}_e - \bar{X}_i)_o = - \frac{1}{2\pi} \int_S \frac{x}{r^3} \bar{Z}(x, y) ds \quad (2.34)$$

At a particular period, the amplitudes of the sine and cosine transforms may be treated in exactly the same manner as the amplitudes of the actual components in the time domain, and hence the surface integral in (2.34) may be evaluated by methods suggested earlier. Since $X(t) = X_e(t) + X_i(t)$ then

$$\bar{X} = \bar{X}_e + \bar{X}_i \quad (2.35)$$

Equations (2.34) and (2.35) can be combined to find the separated components, \bar{X}_e and \bar{X}_i .

If (\bar{F}) and $(\bar{\bar{F}})$ respectively represent the sine and cosine transforms of the magnetic component F (i.e. $F = X_e, X_i, Y_e$, etc.) then these two transforms may be recombined into an amplitude and phase.

$$\text{AMPLITUDE} = \sqrt{\bar{F}^2 + \bar{\bar{F}}^2}$$

$$\text{PHASE} = \tan^{-1} \left(\frac{\bar{\bar{F}}}{\bar{F}} \right)$$

CHAPTER III

DATA, MAPPING AND COMPUTATION PROCEDURES

3.1 The Array

An array of forty-two magnetic variometers was installed in the midwestern United States in the summer of 1967. Twenty-one of these instruments were operated by the University of Alberta, while the remaining instruments were installed and operated by the Southwest Center for Advanced Studies in Dallas, Texas. The array covered an area of approximately 700 x 1200 km. between latitudes 36° and 42°N and longitudes 102° to 116° W, and was located to explore further the anomaly found by Reitzel and Gough in 1966 (Gough and Reitzel 1969) which they associated with the boundary between the Southern Rockies and the Great Plains, and to investigate the possibility that this anomaly was the northward continuation of the Texas anomaly found by Schmucker (1964). The array was placed also to show any possible upper-mantle conductive structure associated with the Wasatch Front and fault belt, and stations were concentrated across Utah and across the East Front to study these two questions. The instruments were arranged along four east-west profiles crossing the Southern Rockies and Colorado Plateau, and extending well into the Great Plains and the

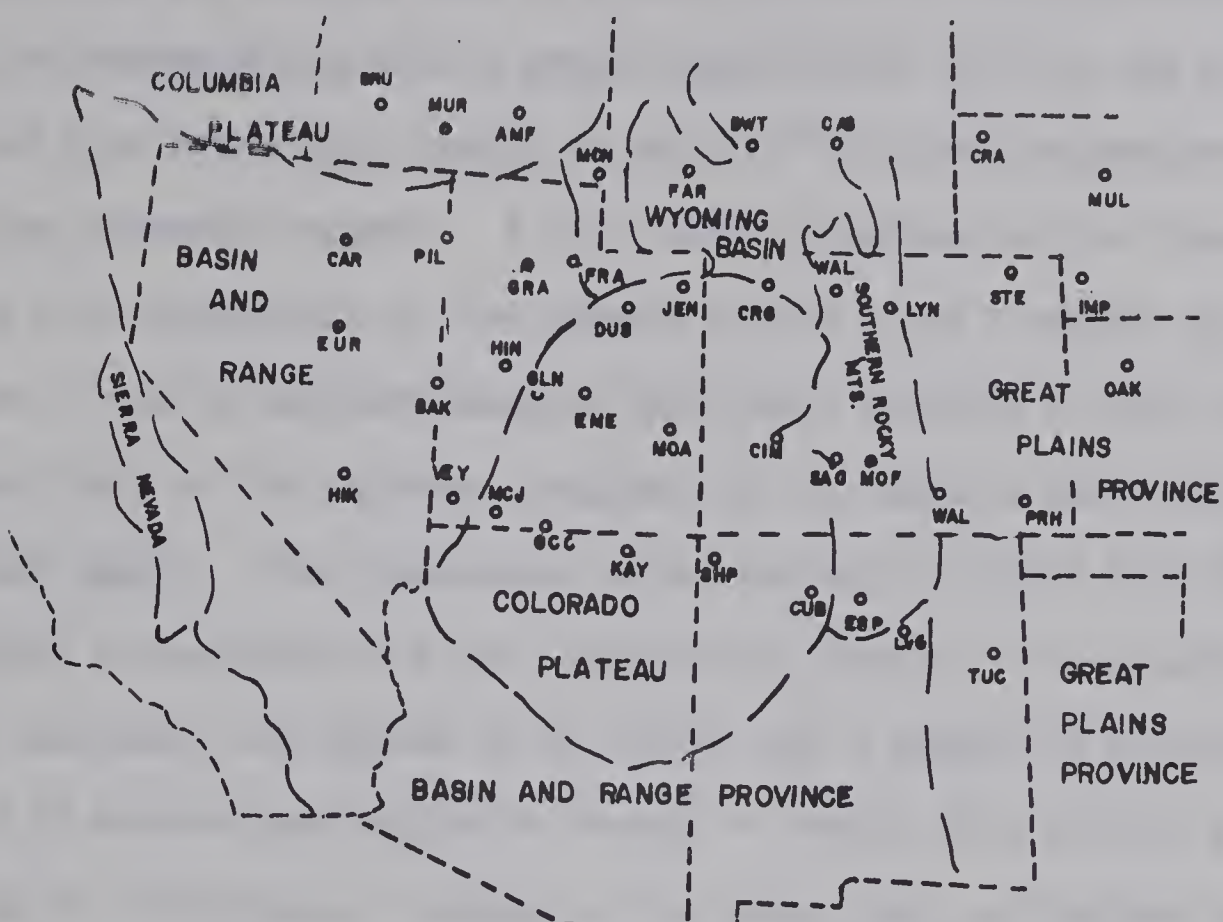
Basin and Range Provinces. The spacing between lines was about 150 km. while that between stations in each line averaged 120 km. Such distances between recording stations were chosen since the study was designed only to delineate large scale features in the conductivity structure of the upper mantle. Fig.(3.1) presents two maps of the central and southern part of the United States showing the array for 1967 plus the line profile of: Schmucker (1964), Caner, Cannon and Livingston (1965), Gough and Reitzel (1966), and stations operated during the IGY. The geological provinces are also indicated.

3.2. Variometer

In order to operate a large array of variometers, it is essential that these instruments be relatively inexpensive so that they may be purchased and operated on a limited research budget. Such a variometer was designed and built by Gough and Reitzel (1967). The instrument is of classical design, having the three magnets (H,D,Z) suspended on taut torsion wires. Variations in the torque due to a magnetic field component causes each magnet to move through small angles, and the angular positions of these magnets are recorded photographically at intervals of ten seconds. The traces of the magnetic components were recorded as rectangular spots of light on 35 mm. film.

The most serious problem, that of obtaining thermal stability, was solved mainly by encasing the variometer in a five-foot long

LOCATION OF 1967 ARRAY



LOCATION OF PREVIOUS STUDIES

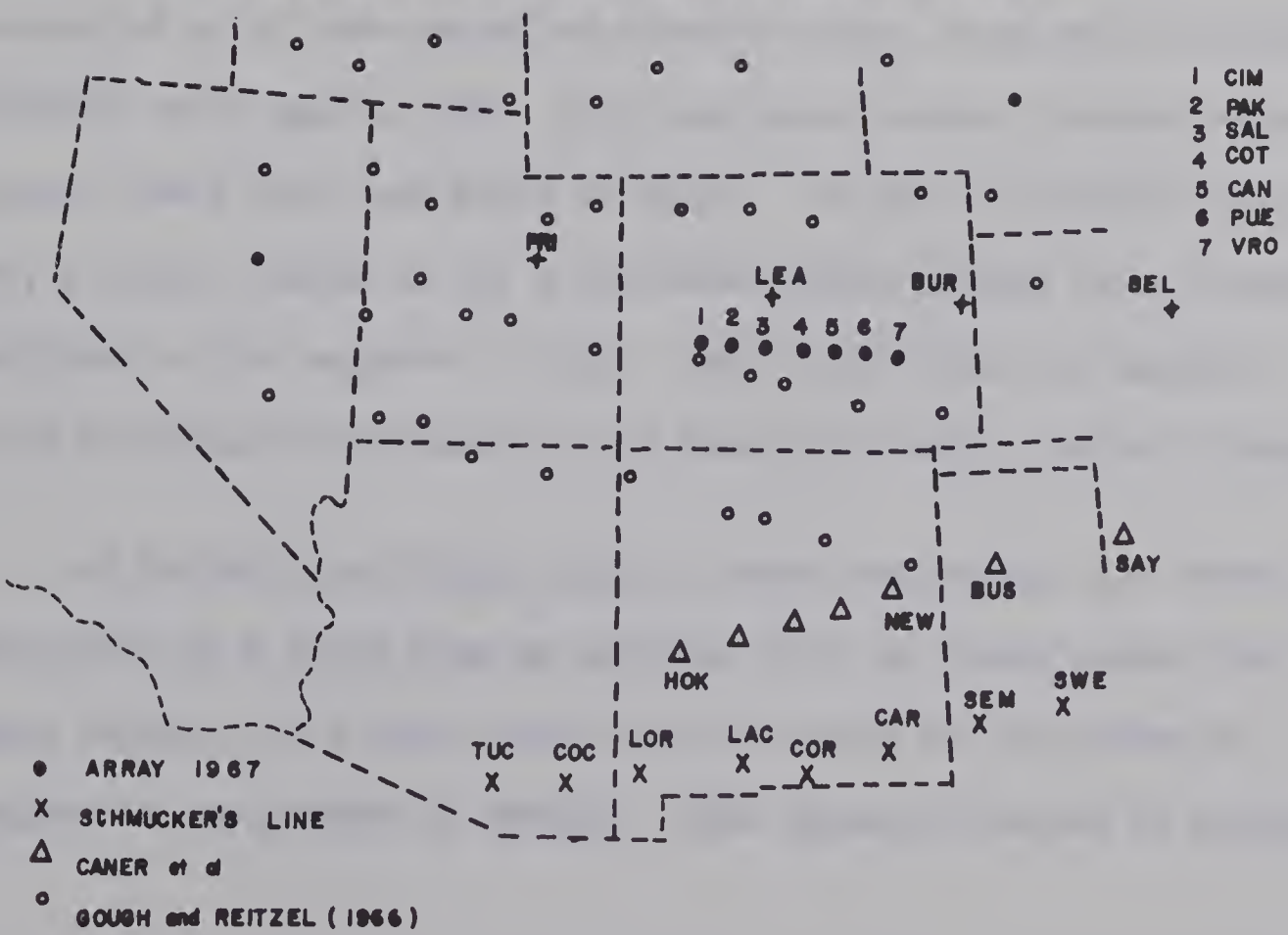


Fig. 3.1

aluminum tube and burying this in a vertical hole. This provided such effective thermostating that a weekly variation of 30°C at the surface resulted in a temperature change of only 0.1°C at the temperature-sensitive suspended magnets. A first order compensation for these small changes with temperature of the moments of the H and Z magnets was obtained by use of auxiliary magnets which were adjusted at some temperature to cancel half of the relevant component of the earth's main field at the suspended magnet. The instruments were levelled to within 0.1° in order to prevent contamination of one component by another. The sensitivity of the instrument was quoted to be better than 1 gamma and the sampling rate of 10 seconds gave reliable records of events with periods greater than one or two minutes. Because of the steep drop, at periods below 20 seconds, of the energy in magnetic variation events, the danger of aliasing was small with a sampling interval of 10 seconds. Timing was controlled by a fork-controlled electric timer (Accutron by Bulova) periodically rated against WWV. The timer gave contact closures every 10 seconds, every hour, and every 24 hours. At each 10 second contact closure, a light, turned on for a pre-determined exposure time, recorded the positions of the magnets on film. Small coils near the magnets were used to deflect the traces at the hourly and daily contact closures.

At periodic servicing visits to each variometer, the traces were deflected by a field from an external coil, at times known from WWV radio signals. The field from this coil could be calculated at each magnet to one percent or better. This operation served to determine

the sensitivities of the three suspended magnets and to give absolute time at an hour mark of the Accutron timer. From two such visits a linear approximation to the rate of drift of the Accutron could be determined.

An independent check of relative time between the instruments of the array and also a check on the assumption that the rate of drift of the Accutron was linear, was inferred by correlation of geomagnetic micropulsations which should occur simultaneously (within a minute or so) over the whole array (Rostoker, 1968). Such micropulsations as Pi 2's, with periods of 40 to 150 seconds, were clearly visible on the horizontal traces at all stations. This additional timing check should mean that the maximum error in timing was no more than one minute, and in most cases considerably less.

3.3 Records

This thesis is concerned with an analysis of the magnetic variations of a magnetic substorm occurring from 0500 to 0830 UT. on September 1, 1967. This event was selected because of the large amplitudes of the magnetic variations, and because the substorm was recorded by the array with nearly 95% efficiency. Enlarged electrostatic prints of the recording film, displaying the magnetic variations, were edited, and commercially digitized at one minute intervals.

Evaluation of the surface integrals requires that the magnetic components be plotted on a rectangular grid. The transferring of the stations from a sphere to a plane was first done by plotting the stations on an equal-area map. At any point on this map the z-direction was then normal to the plane, while the x- and y-directions were those of the longitudes and latitudes at that point. With this projection, however, the meridians were not parallel, so transformation to a rectangular grid was required. A north-south reference line was drawn through the center of the array, and at each station the angle η , between a line parallel to this reference line, and the meridian indicating true geographic north was found. Since Z was normal to the map and orthogonal to X and Y, it was invariant, and hence no correction for Z was required. Let XP and YP denote field values on a rectangular grid parallel to the reference line. The transformations to correct X to XP , and Y to YP are:

$$XP = X \cos \eta - Y \sin \eta$$

$$YP = X \sin \eta + Y \cos \eta$$

Although in the evaluation of the separation integrals the magnetic components XP , YP , Z were used, in the following work these components will be written as X, Y, Z.

3.4. Spectral Analysis

In the frequency domain a Fourier analysis, employing the Cooley-Tukey method, was made on the digitized data by using the RHARM program in the IBM SSR Package. Given $2N$ real numbers

$X_0, X_1, X_2 \dots X_{2N-1}$, this subroutine computes Fourier sine and cosine coefficients $a_0, a_1, b_1, a_2, b_2 \dots a_{N-1}, b_{N-1}, a_N$ in the equation

$$X_j = \frac{1}{2} a_0 + \sum_{k=1}^{N-1} \left(a_k \cos\left(\frac{\pi \cdot j \cdot k}{N}\right) + b_k \sin\left(\frac{\pi \cdot j \cdot k}{N}\right) \right) + \frac{1}{2} a_N (-1)^j \quad (3.1)$$

where

$$j = 0, 1, 2 \dots 2N-1$$

Before being subjected to Fourier analysis a linear trend was removed from each time series. Also, the first and last 5% of the data were smoothed by multiplying these data by coefficients of the sine function from 0 to $\pi/2$. This smoothing ensured that there were no sudden jumps at the beginning or end of the time series introducing fictitious high frequency components.

The fast Fourier algorithm operates most efficiently when the number of points in the time series is an integral power of 2. Since the data consisted of 211 points, zeros were added to bring this to 256. To increase the number of spectral estimates, it was necessary to add more zeros. The physical justification for this was that only the field variations during the analysed event were of interest so the variational field both before and after this event should be zero. This means that the substorm was regarded as a transient and any field changes before and after it were regarded as separate events.

To find the effect of adding zeros an analysis was undertaken in which the length of the work vector M (number of real data points N, plus the number of zeros added) took values 256, 512, 1024, and 2048.

All frequencies found in the Fourier analysis when $M = 256$ were found for each succeeding value of M ; however, in each case the values of the sine and cosine coefficients were attenuated by a different, but constant, value. For the coefficients to have values in gammas, it was found that each coefficient must be multiplied by a factor N/M . It was then found that the sine or cosine coefficient at a particular frequency was the same for all values of M . While additional estimates secured by increasing M must become less reliable, the spectra for values $M = 256$ to the maximum value $M = 2048$ remained smooth. For the present analysis $M = 2048$ was used.

3.5. Interpolation

To contour the maps of the magnetic field components X , Y , or Z (or their sine or cosine Fourier transform), the values of the magnetic field between the stations must be found by interpolation. Although a linear interpolation may first be used, for a field derived from a scalar potential we have an additional constraint which can be applied to the horizontal field.

The magnetic field $\vec{H} = (X, Y, Z)$, measured on the surface of the earth, is curl-free, i.e. $\vec{\nabla} \times \vec{H} = 0$

Therefore

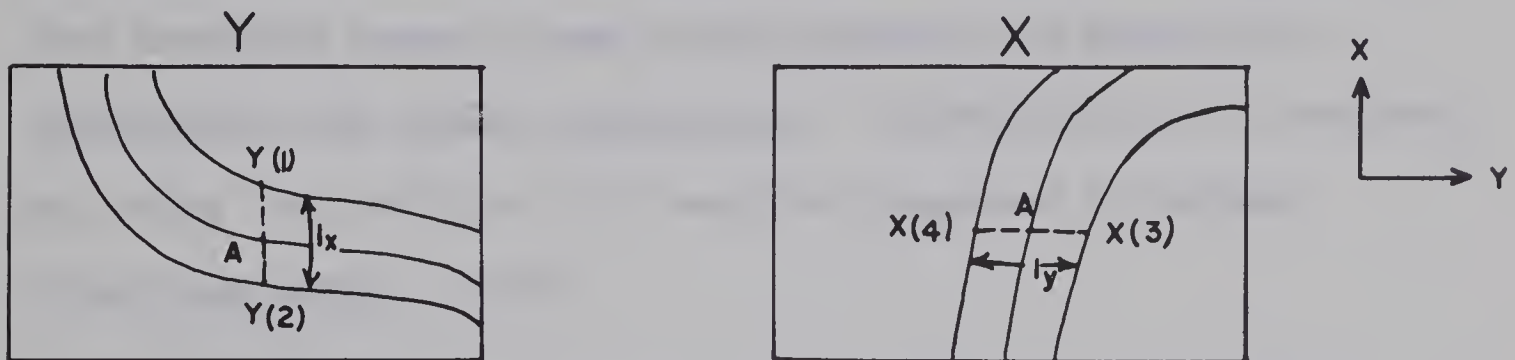
$$\hat{i}\left(\frac{\partial Z}{\partial y} - \frac{\partial Y}{\partial z}\right) + \hat{j}\left(\frac{\partial X}{\partial z} - \frac{\partial Z}{\partial x}\right) + \hat{k}\left(\frac{\partial Y}{\partial x} - \frac{\partial X}{\partial y}\right) = 0 \quad (3.2)$$

For (3.2) to hold, each term must be identically zero.

Since our observations were made on the xy -plane, we have no knowledge of $\partial/\partial z$, hence only the \mathbb{R} term provides a useable constraint, which is

$$\frac{\partial Y}{\partial x} = \frac{\partial X}{\partial y} \quad (3.3)$$

If maps of X and Y have been contoured, these contours may be physically adjusted to fulfill this curl-free condition.



$$\frac{\partial Y}{\partial x} = \lim_{\delta \rightarrow 0} \frac{Y(x+\delta) - Y(x-\delta)}{2\delta} \approx \frac{Y(1) - Y(2)}{l_x}$$

and similarly

$$\frac{\partial X}{\partial y} \approx \frac{X(4) - X(3)}{l_y}$$

l_x = distance in the x direction between $Y(1)$ and $Y(2)$

l_y = distance in the y direction between $X(4)$ and $X(3)$

The curl-free condition implies

$$\frac{Y(1)-Y(2)}{lx} = \frac{X(4)-X(3)}{ly} \quad (3.4)$$

If the contour intervals of the maps are equal, then the numerators in (3.4) are the same, hence $lx = ly$ for all points on the map. This condition was used by superposing the X and Y maps, and was most successfully applied when the gradient of X in the y-direction (and therefore the gradient of Y in the x-direction) was large. If $\partial X / \partial y$ and $\partial Y / \partial x$ were very small, then the curl-free condition became a near trivial equality and gave little improvement over linear interpolation. Interpolation on a contoured map using the condition (3.3) was first suggested by Reitzel (Gough and Reitzel, 1969).

As no condition similar to (3.3) can be applied to the Z field, maps of Z must be contoured by linear interpolation modified by the avoidance of sharp corners and abrupt changes of gradient.

3.6. Extrapolation

Some extrapolation of the magnetic field was necessary to obtain a better estimate of the values of the surface integrals at points within the array. The extrapolation of the X and Y fields was aided by application of the curl-free condition already discussed. Although the field so extrapolated was not unique, and inevitably contains errors, it was felt that smooth continuation of

the contours, determined by measured values inside the array, plus the restraint of the condition $\frac{\partial X}{\partial y} = \frac{\partial Y}{\partial x}$, gave a better estimate of the integrals than the assumption that the field outside the array was a constant or zero. Extrapolation was carried to 300 km. outside the array. Although the extrapolated fields at larger distances from the array were unreliable, the error in the integral remained small, since the effect of a surface element varies as $1/r^2$ (where r is the distance from the point of separation to the surface element). The Z field was extrapolated only by smoothly extending the existing contours outward from the array.

3.7. Computation

The surface integrals may be evaluated if the average values of X , Y , Z , $\partial X/\partial x$, $\partial Y/\partial y$, $\partial Z/\partial x$ and $\partial Z/\partial y$ are known for each square in a symmetric grid, centered at the point of separation and used as a "summation window". The effects of using windows of different sizes, i.e. squares of sides 700, 900, and 1100 km., was compared, and variation of values of the separated components was found not to be appreciable, being only about 1 or 2% near the edge of the array.

A program was written to compute the surface integrals by moving a square grid about the map. The value of the difference between the internal and external part of each magnetic component was thus found for a square at the center of this "window". In

attempting separation at a point near an edge of the array, extrapolated parts of the contour map contribute much of the integral while some parts of the array area had to be excluded. Considerable errors from these edge effects will affect separations near the limits of the array.

CHAPTER IV

SEPARATED FIELDS

4.1. Time Domain

The magnetic variations of the H, D, and Z components for the substorm of September 1, 1967 are shown in Fig.(4.1). Although Chapter VI discusses the morphology of this substorm, there are a number of details of the magnetograms which can be mentioned here.

An anomalous station may be regarded as one at which the characteristics of a magnetic component are greatly different from the characteristics of the same component at nearby stations. Since the Z component is highly affected by conductivity distributions beneath the surface, it is this component which most easily distinguishes an anomalous station. It can be seen that the stations MUL and CRW, and IMP and STE on lines 1 and 2 respectively are anomalous. These stations represent the East Front anomaly, while the stations MON, DUC and FRA, EME and SLN, and MCJ are associated with the Wasatch Front.

The characteristics of the H and D traces change relatively smoothly from east to west on all lines, with the exception of D at CRW which has a very large amplitude. It can be seen from Fig.(4.1) that all of the Z magnetograms from the anomalous stations mentioned above, resemble the D magnetograms. This indicates that

SEPTEMBER 1, 1967

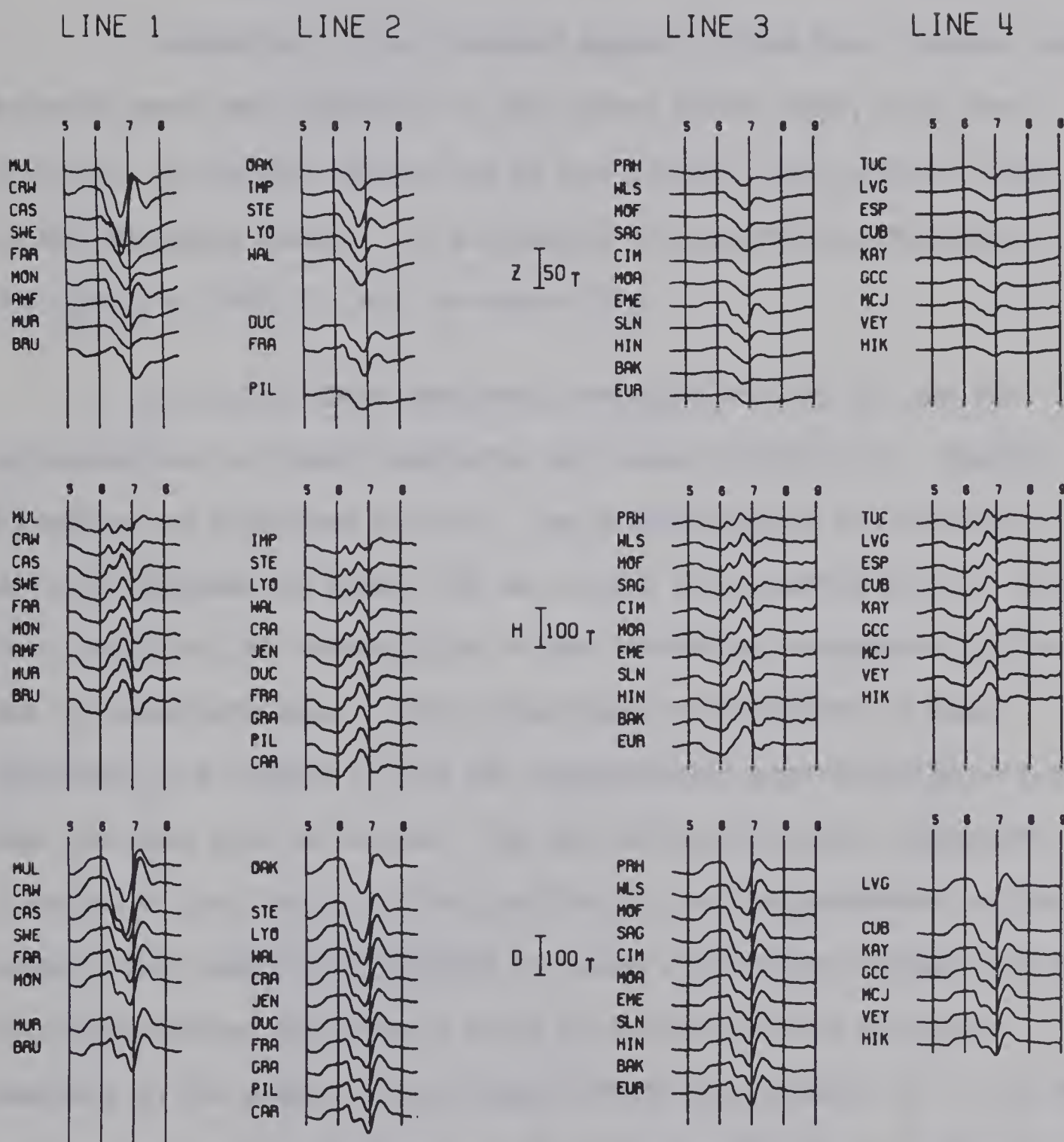


Fig. 4.1

both the Wasatch Front and the East Front anomalies are approximately north-south features. However, in order to make a quantitative study of these anomalies, a separation analysis must be carried out.

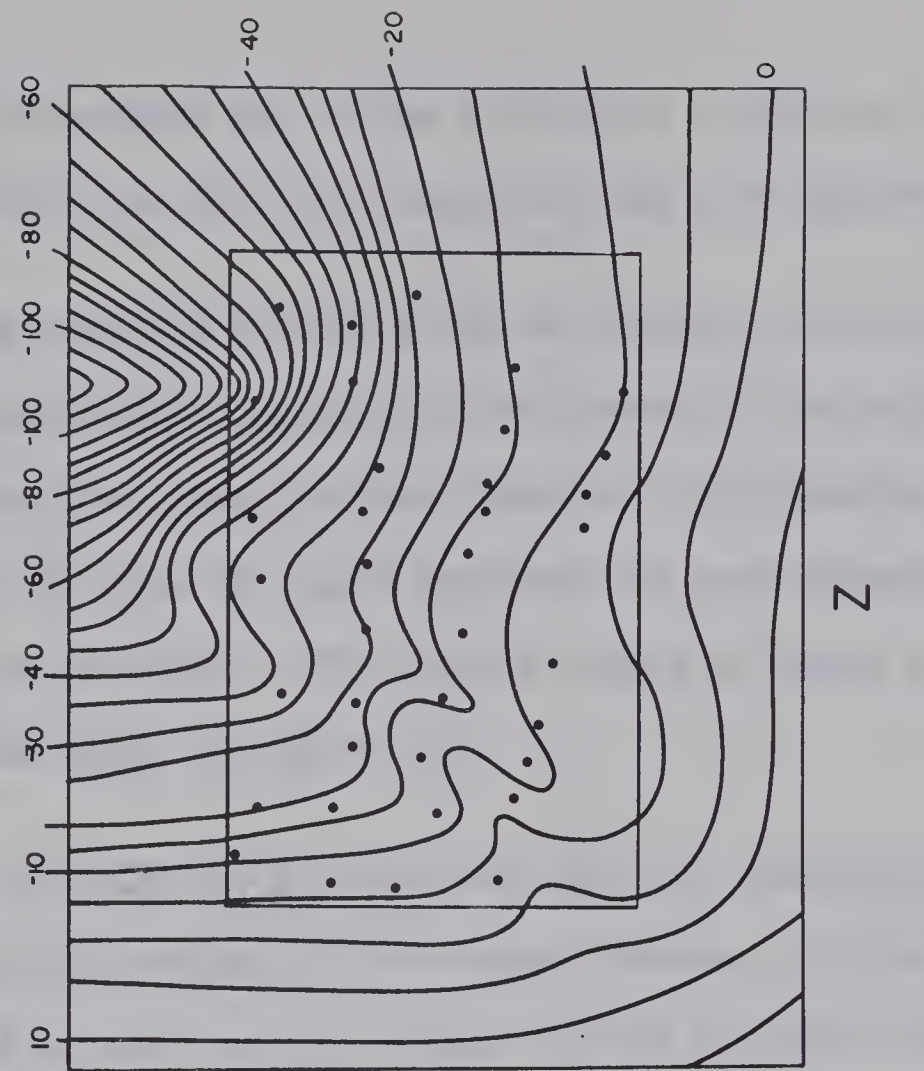
Separation of the observed magnetic field into internal and external parts was completed at four times (0630, 0645, 0700, and 0715 UT.) in the time domain and at two periods (30.1 and 60.2 min.) in the frequency domain. To illustrate the separation procedure, the fields at 0645 UT. will be shown first.

The total field components measured at 0645 UT. and the extrapolations of these components are shown in Fig.(4.2). Station locations are indicated by dots. The extrapolations were carried out to a distance of almost 300 km. beyond the observed fields. The curl-free condition has been applied to the horizontal components by the use of superposed maps. Since these maps are contoured in equal intervals, the lengths of the two perpendicular arrows should be the same for each pair of arrows. The map of the horizontal components illustrates that the curl-free condition is well approximated on the eastern side where the gradients are large, and hence outside this region the extrapolation was greatly aided by the use of this condition. However, in the region of the Wasatch Front the gradient of Y in the x -direction, and the gradient of X in the y -direction, are both very small. Thus although the condition $\partial X / \partial y = \partial Y / \partial x$ is satisfied, it can be seen that it does not help in the extrapolation of the horizontal fields. The

SUBSTORM SEPT 1, 1967

OBSERVED AND EXTRAPOLATED FIELDS AT 06:45 U.T.

CONTOUR INTERVAL = 5 GAMMAS



X {
Y }

AFTER CURL-FREE ADJUSTMENT

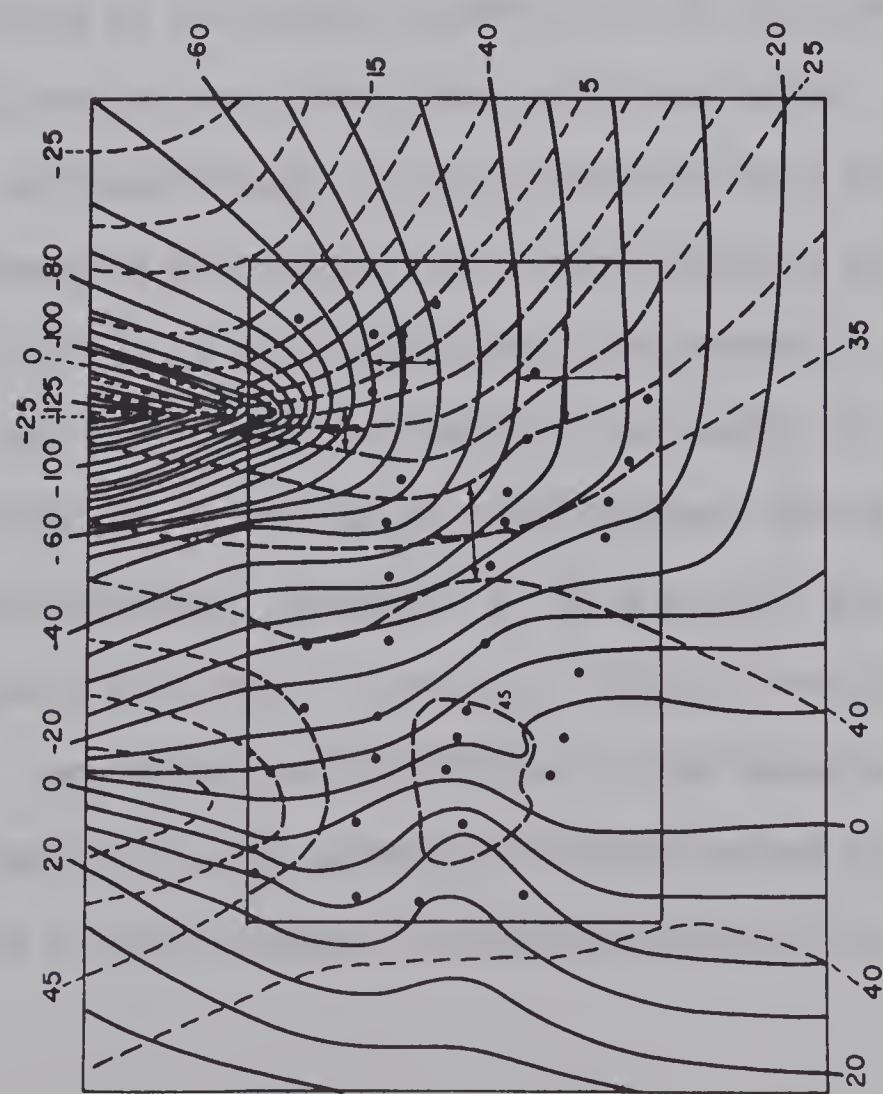


Fig. 4.2

arrows on the superposed map of the horizontal components indicate the success with which the curl-free condition has been applied.

The separation procedure may be thought of as providing a value of each separated component at the center of the square at which the separation integrals were computed. By assuming a linear interpolation, the grid of values obtained for each separated component may be contoured. The contoured maps of these six components of the field are shown in Fig.(4.3).

The external field shows many expected characteristics. In Chapter VI a possible model of the source currents is discussed, but for the present we need only note that for the external field we expect no large gradients or large changes of gradient, since concentrated parts of the source current will be at least a distance of several map-lengths away from stations in our array. We also expect Z to be negative and X to be positive over the array. Y may be of either sign but should become more positive from east to west. From Fig.(4.3) it can be seen that the external Z is negative, quite smooth, and has a positive gradient from north to south. The east-west gradient of Z may be an "edge" effect caused by inaccurate extrapolation. External Y is also very smooth, especially when compared with the total Y or Y_I fields. The line corresponding to $Y_E = 0$ may or may not be related to the demarcation line mentioned in Chapter VI, for although relative values of separated components have a high accuracy, the absolute value is not significant

SUBSTORM SEPT. 1, 1967

CONTOUR INTERVALS 2.5 GAMMAS

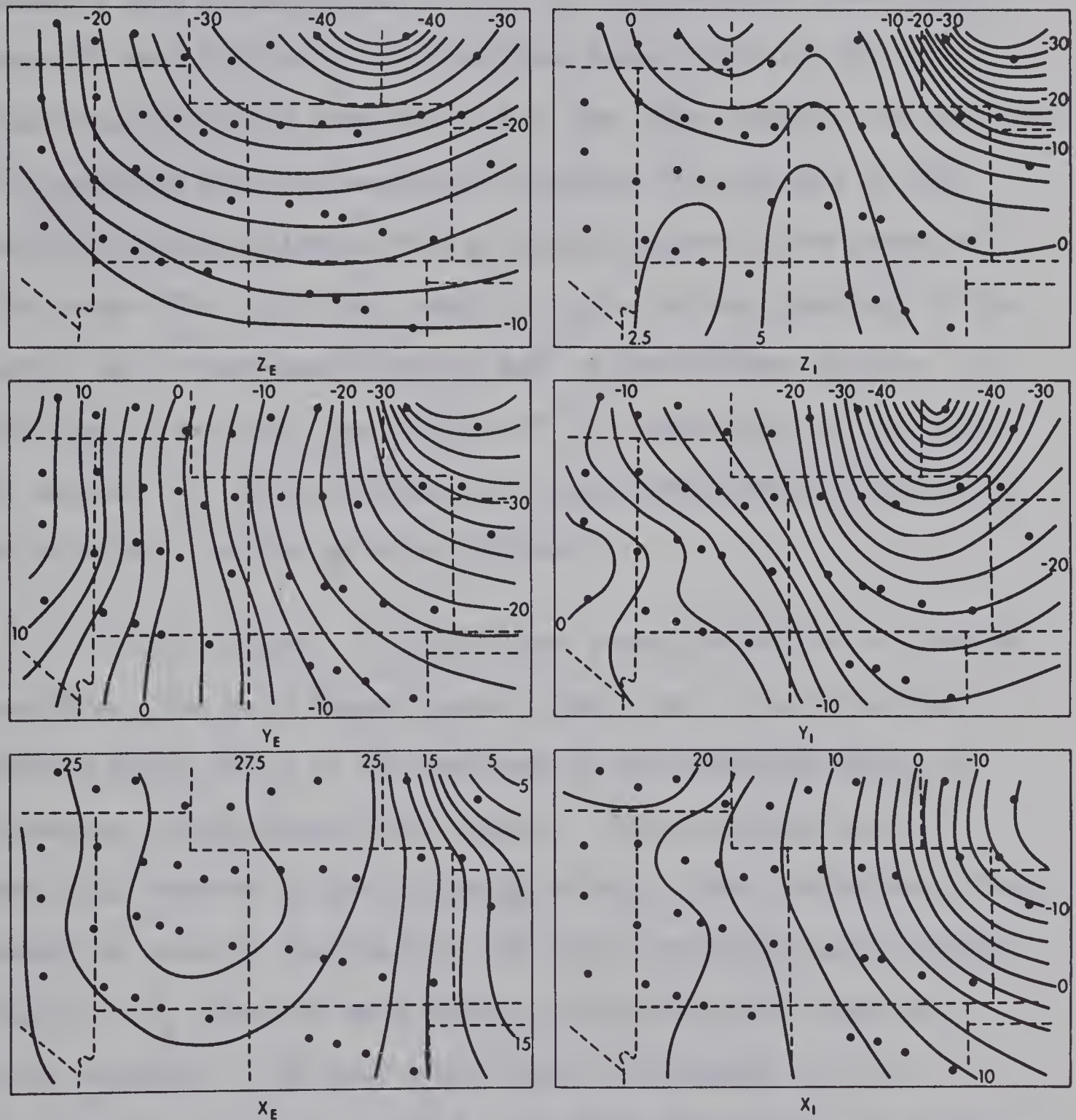


Fig. 4.3

for a reason discussed in Section 4.5.

A comparison of the internal and external maps for Y suggests some contamination of Y_I in Y_E near CRW. The fields near CRW were difficult to extrapolate since the array did not completely cover the area affected by the large anomaly. It is therefore expected that the separation procedure in this part of the map will be less reliable than at a point closer to the center of the array. The X_E field, which is quite uniform over most of the array, has an east-west gradient east of the Southern Rockies. It can also be seen that the minimum of Y_E corresponds to the region of maximum X_E , which is reasonable since the external field should be relatively uniform at mid-latitudes.

The internal Z field shows anomalies related to internal currents. The small anomaly seen on the total Z map over the Wasatch Front (Fig.4.2) has been lost in the smoothing effect of averaging the components over squares. This averaging can be partially overcome by the following method. Since the external field should be smoothly varying over the array, an interpolated smoothed value of Z_E found at each station may be subtracted from the total measured Z to give a new value for internal Z . (i.e. $Z_I = Z - Z_E$). New values of Z_I at 0645 found by this method are shown in Fig.(4.4). The Wasatch Front anomaly now is seen as a general negative maximum with a small positive maximum, due to the values of Z at the stations HIN and SLN, superposed upon this. For

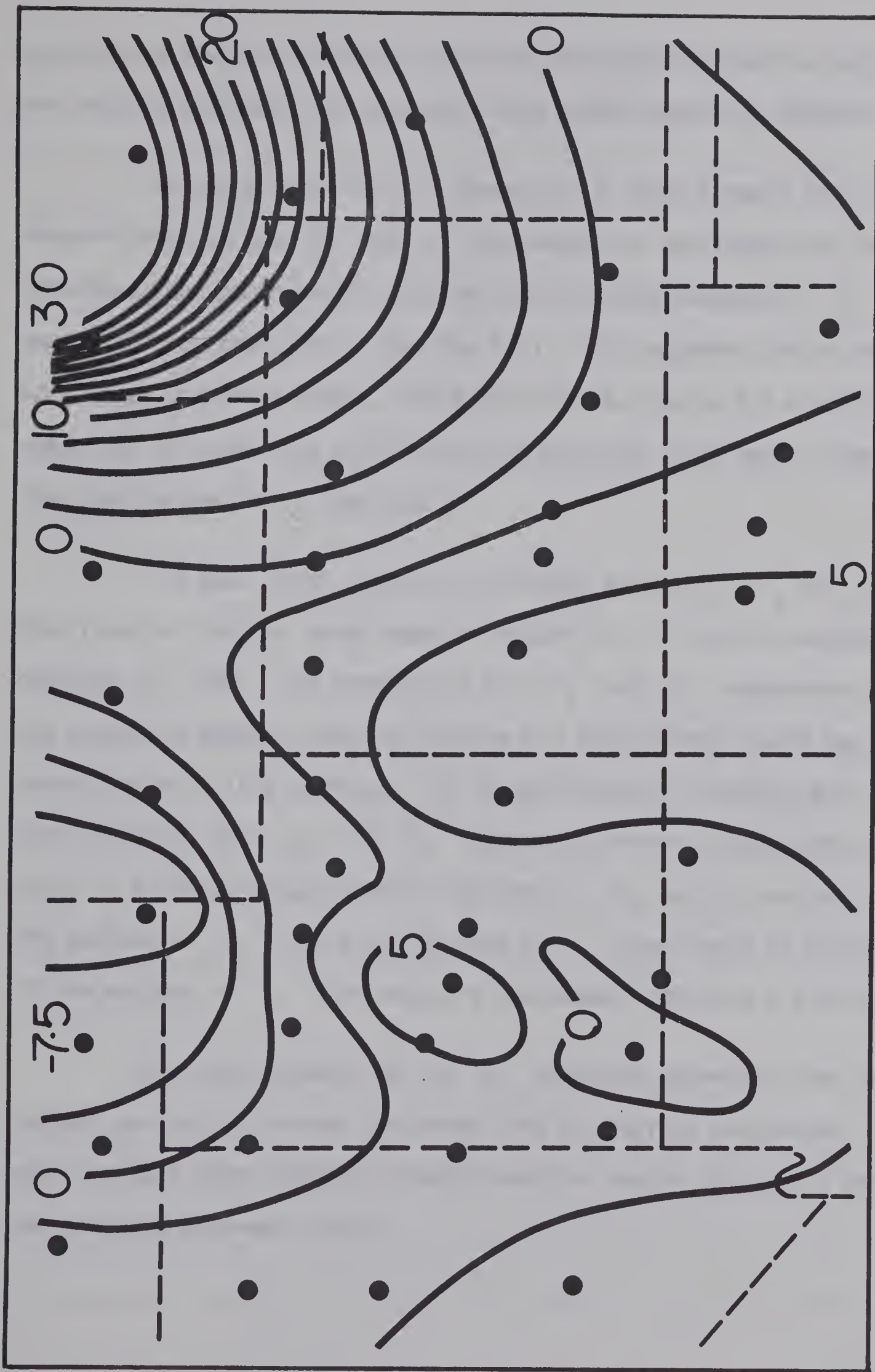


Fig. 4.4

qualitative studies, however, the above technique will not be employed, and will be used only in connection with model studies in Chapter VI.

We can account for the absence of a large anomaly over the Wasatch Front in the Z_I and Y_I components by realizing that the structure runs north-south, and that the inducing component, Y_E , is nearly zero in this area. (See Fig. 4.1). This suggests the existence of a large induction effect, since the internal fields for a good conductor of large size will follow the inducing field rather than the time derivative of that field.

The East Front anomaly is strongly evident in Y_I and Z_I . This results from the large negative values of D over the eastern stations at 0645. The symmetry of the Z_I and Y_I components over the anomalies suggest that the sources for the internal field may be associated with line currents. If we qualitatively consider such line currents, then Z_I and Y_I indicate a current flowing from north to south directly under the maximum of Y_I and to the west of the maximum of Z_I . Since the maximum of Y_I does occur to the west of the maximum of Z_I both maps are consistent with such a line current.

The small anomaly in the X_I component appearing over the eastern portion of the map indicates that the current associated with the East Front anomaly probably does not strike true north but has a slight east-west trend.

Since the surface of the earth is in a nonconducting zone below the ionosphere and above the conducting interior of the earth, the external and internal fields must each be curl-free on this surface. Therefore:

$$\vec{\nabla} \times \vec{H}_E = 0$$

$$\vec{\nabla} \times \vec{H}_I = 0 \quad (4.1)$$

where H_E and H_I represent the total external and internal fields respectively. The conditions

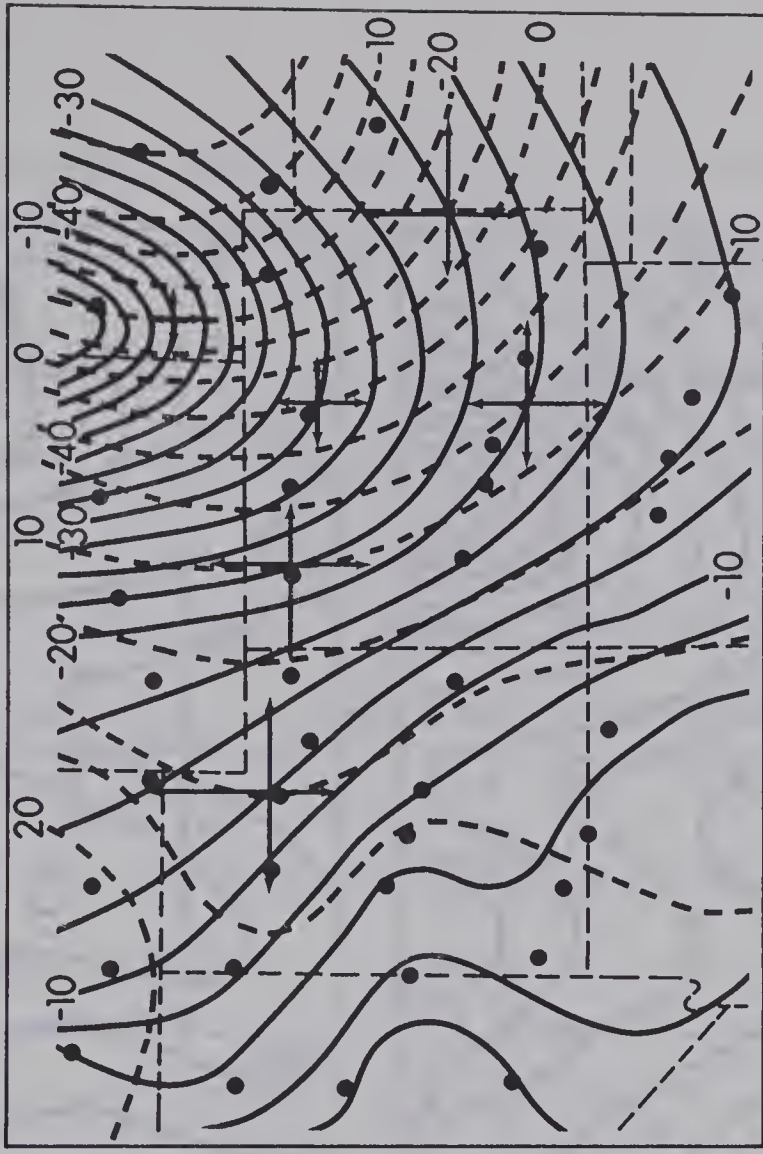
$$\frac{\partial X_E}{\partial y} = \frac{\partial Y_E}{\partial x} \quad \text{and} \quad \frac{\partial X_I}{\partial y} = \frac{\partial Y_I}{\partial x} \quad (4.2)$$

can be used as a check on the validity of the separated horizontal components. The superposed maps of the horizontal fields are shown in Fig.(4.5). These fields were contoured by linear interpolation and no attempt was made to adjust these fields to comply with conditions (4.2). It is evident that the curl-free conditions are well approximated, especially over the East Front region where the gradients are quite large.

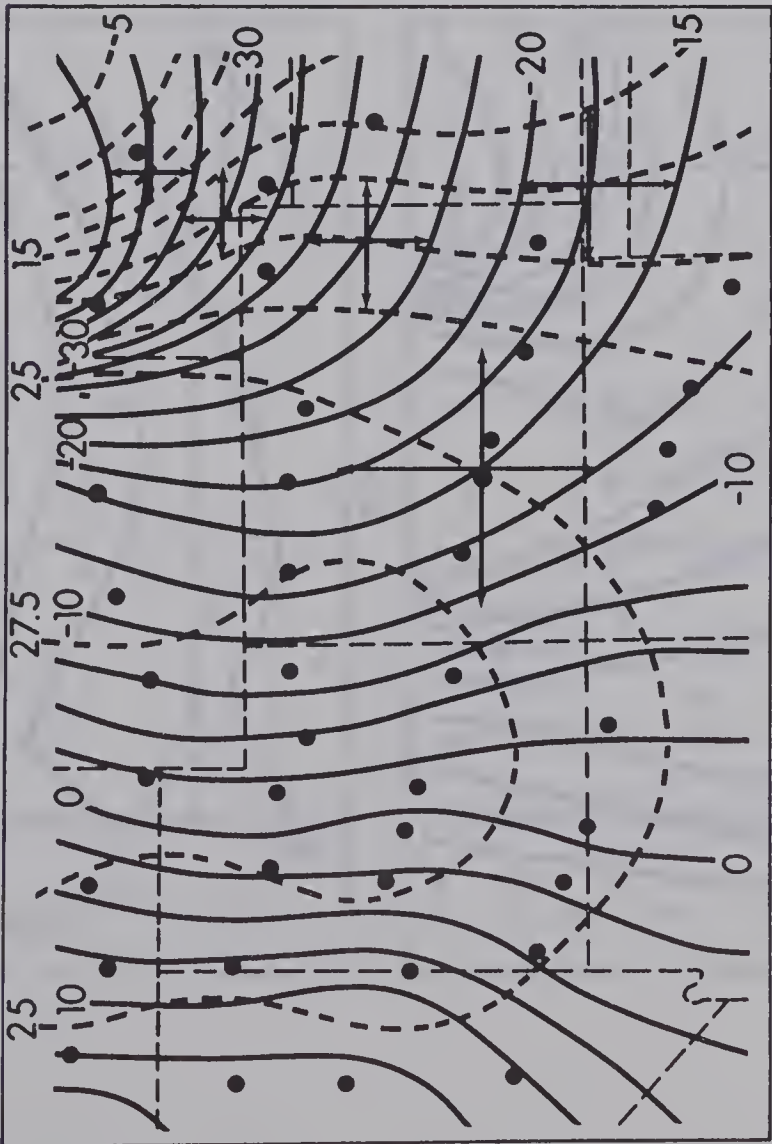
The internal and external maps for the separated Y and Z components at 0630 UT are shown in Fig.(4.6). The X_E and X_I components showed no features of interest and hence have been omitted. The characteristics of the external maps are very similar to the corresponding maps at 0645, except that they are less smooth about the

SEPARATED HORIZONTAL COMPONENTS: 06.45 U.T.
EXTERNAL AND INTERNAL FIELDS ARE CURL-FREE

CONTOUR INTERVAL 2.5 GAMMAS



X_I - - -
 Y_I ~



X_E - - -
 Y_E ~

Fig. 4.5

SEPARATED FIELD COMPONENTS AT 06.30 U.T.

CONTOUR INTERVAL 2.5 GAMMAS

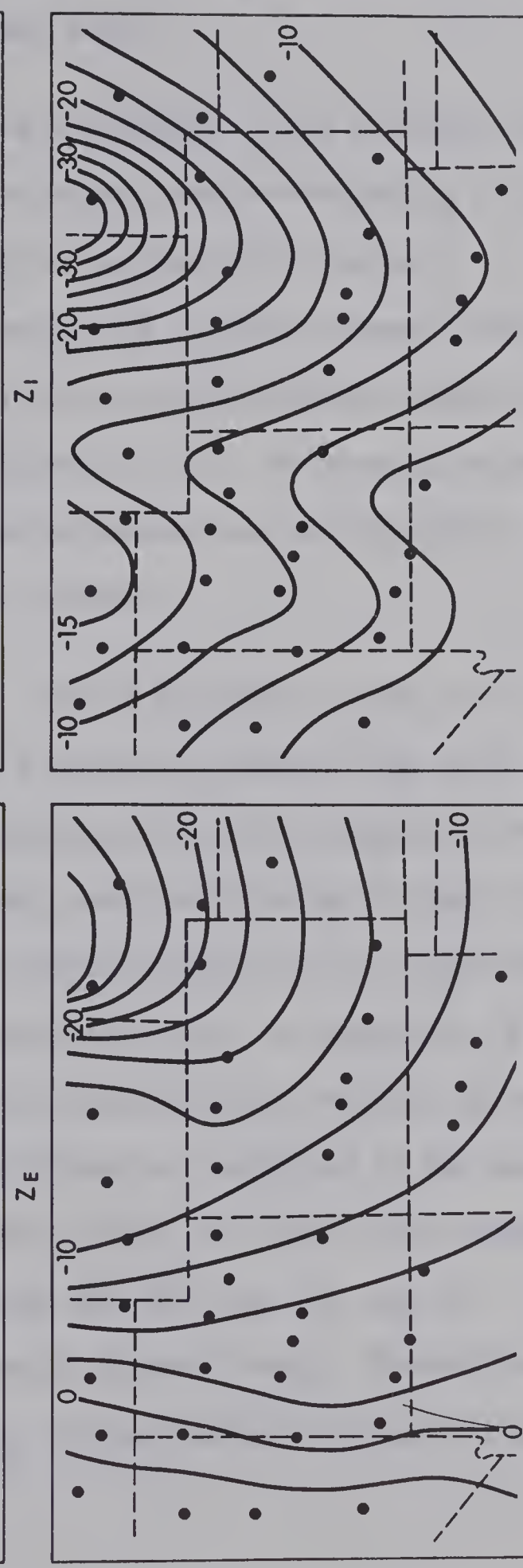
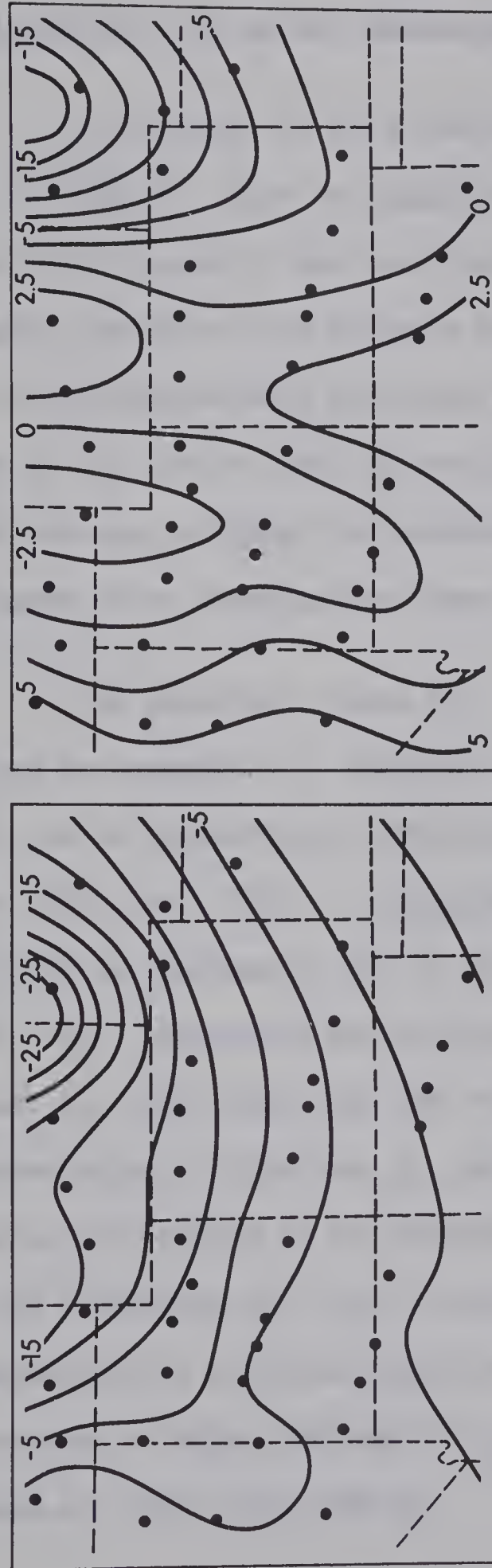


Fig. 4.6

CRW area in the north-east. Again the line of $Y_E = 0$ may or may not be associated with the actual demarcation line.

In contrast to the relative smoothness of the external fields, both Z_I and Y_I have two negative maxima, one corresponding to the Wasatch Front anomaly, and the other to the East Front anomaly. If one again considers line currents as sources for the internal field, then these currents must flow from north to south directly under the maxima of Y_I and to west of the maxima of Z_I . By visually superposing the maps of these two components one can see qualitatively that they agree as to location for these currents.

The separated fields for 0715 UT are shown in Fig.(4.7). Although the external Z field has a positive gradient from north to south, and is negative over the whole map, it is more irregular than Z_E at 0630 and 0645. A possible cause for this may be that the separation is inadequate, but it is more probable that the complicated Z_E at 0715 represents the true external field. A comparison of the Z_E and Z_I maps shows that the two components have entirely different characteristics. Since the Z_I map shows two anomalies in the same locations as observed in the separated fields at 0630, this suggests that the separation at 0715 is valid and that the Z_E map is representative of an actual complicated external field. Except for the reversal of sign, the map of Y_E is very similar to the corresponding maps at 0630 and 0645 UT.

SEPARATED FIELD COMPONENTS AT 0715 U.T.

CONTOUR INTERVAL 2.5 GAMMAS

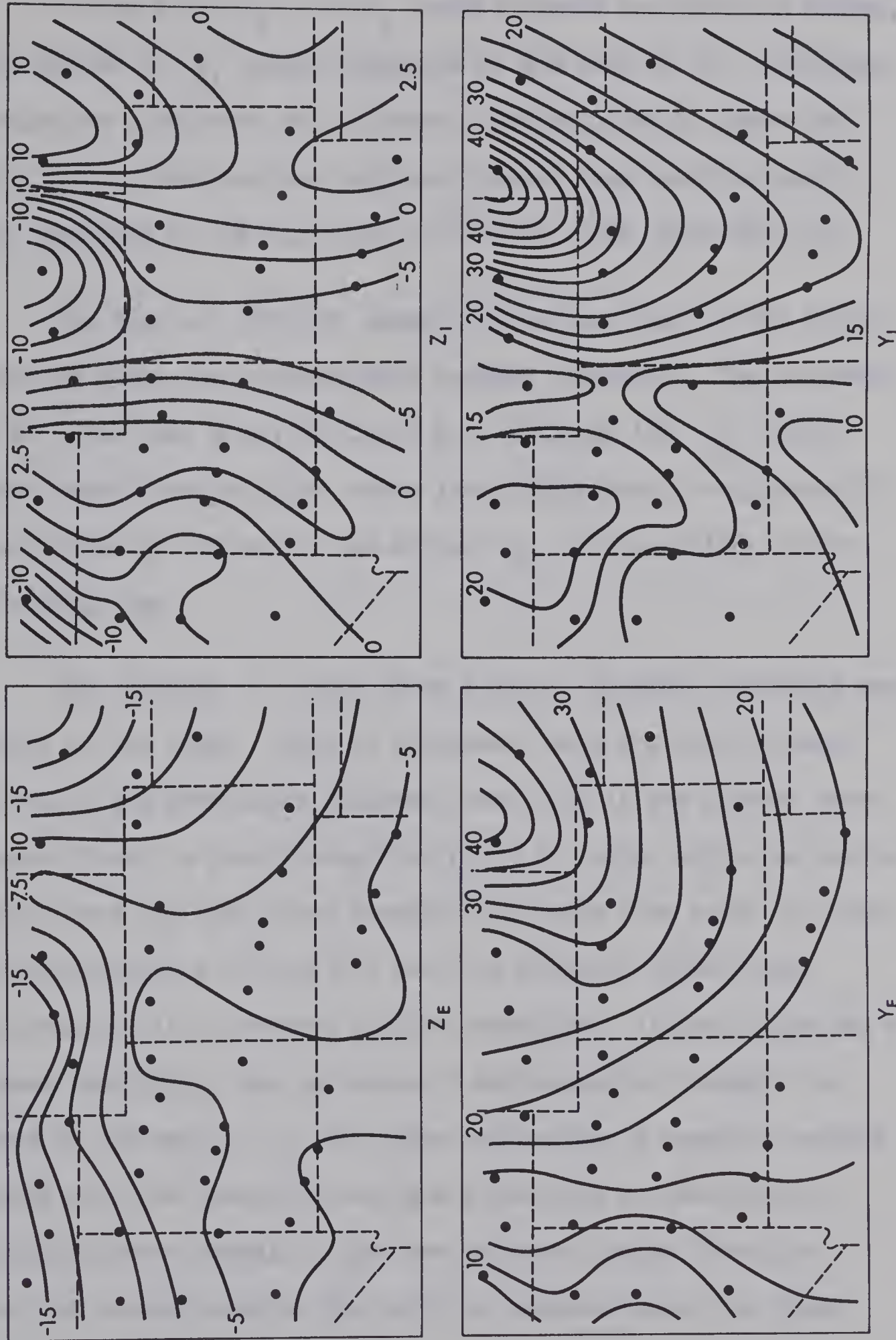


Fig. 4.7

The maps of Y_I and Z_I each indicate two positive maxima, with the maxima of Z_I again displaced to the east of Y_I . Although these maps are consistent with currents flowing directly under the maxima of Y_I , these currents are now flowing from south to north, that is, opposite to the direction of flow at 0630 and 0645 UT.

The time of 0700 UT. appears to be very near to the transition time at which the currents have changed direction. The separated fields at 0700 are shown in Fig.(4.8). Although the Z_E field indicates some irregularities, there is a difference of only about 8γ from the bottom to the top of the array. Y_E is also quite uniform over the whole map.

The internal Z field shows only one minimum, occurring near the center of the array. This is consistent with the line currents postulated at the previously analysed times only if the current under the Wasatch Front is now flowing from north to south, while the current associated with the East Front anomaly is flowing from south to north. With these directions of flow the two line currents produce one negative maximum in Z_I between the two anomalies. Although this may at first seem improbable, the existence of anti-parallel currents is confirmed by the map of Y_I which has two maxima; a negative maximum associated with the Wasatch Front, and a positive one associated with the East Front anomaly. That the currents change direction first at the eastern edge of the array is expected since the phase

SEPARATED FIELD COMPONENTS AT 0700 U.T.
CONTOUR INTERVAL 2.5 GAMMAS

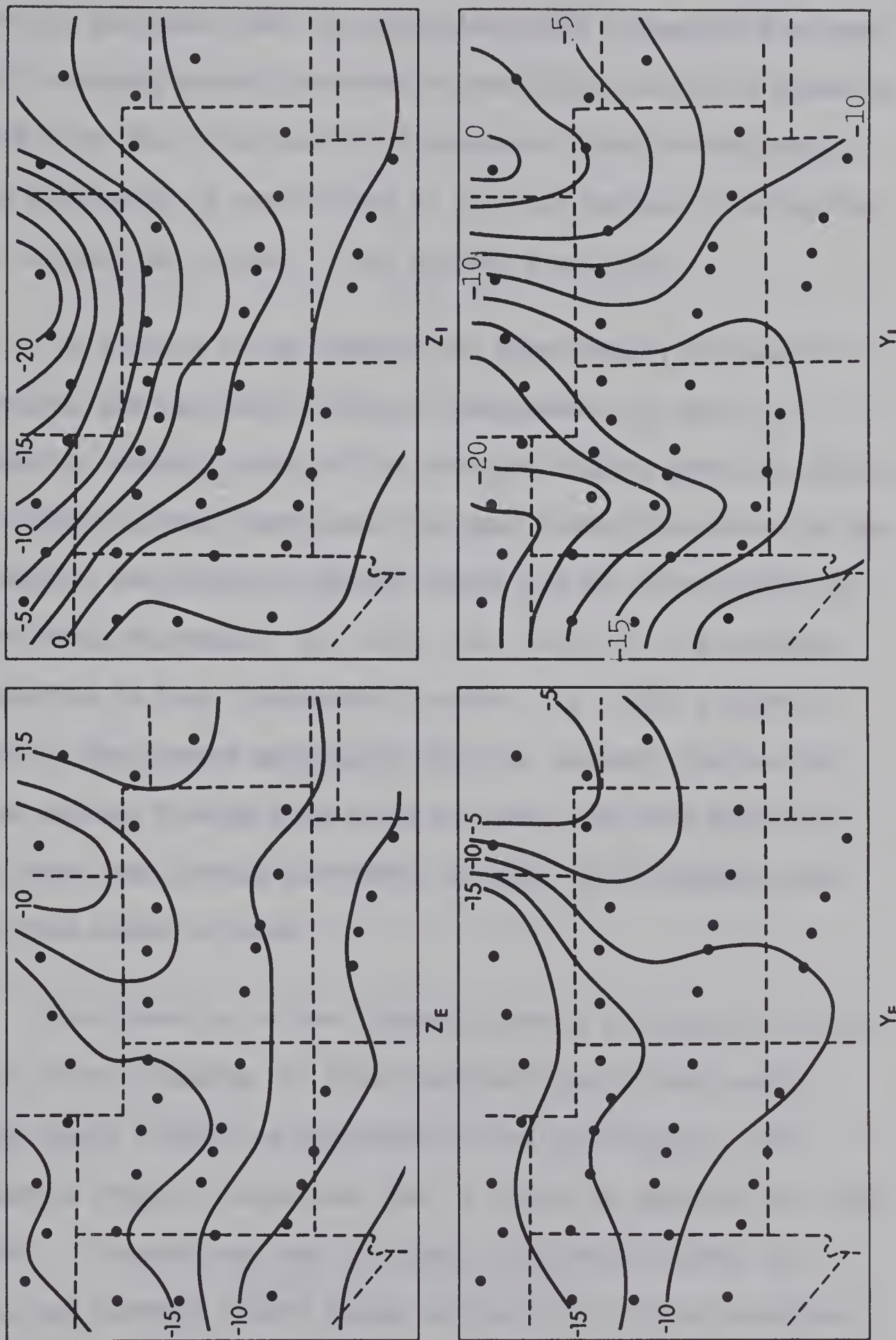


Fig. 4.8

of the external Y component (Section 4.6) and an argument given in Chapter VI, indicates that the variation field propagates from east to west, sweeping across the array at our latitudes with a velocity of about 2 km./sec. Section 4.7 discusses a possible explanation of this phenomenon by associating it with the westward lengthening of the intensified current in the auroral electrojet.

In summary of the work in the time domain, the maps of the vertical and eastward horizontal components, Z_I and Y_I , representing internal parts of the substorm fields, show the effects of two roughly linear, north-south aligned electric currents in the upper mantle, one under the Wasatch Front and the other under the Southern Rocky Mountains. At 0630 and 0645 UT. the currents were observed to flow from north to south. At 0700, a time of transition, the current associated with the Southern Rockies had reversed and was flowing from south to north, and that under the Wasatch Front was flowing southward. At 0715 both currents were flowing from south to north.

The direction of the induced currents is consistent with the sign of the inducing Y field incident upon a north-south striking highly conductive structure in the upper mantle. The magnetograms (Fig.4.1) show that the Y field is negative at 0630 and 0645. Considering that the phase difference between the internal and external fields should be small for a good conductor, the direction of flow of the currents at these times (from Lenz's Law)

should be from north to south. At 0715, with a positive (easterly) Y , the currents must flow from south to north. The variograms also show that Y changes from negative to positive at all stations within a few minutes of 0700, thus indicating a time of transition for the currents.

The external fields, though showing characteristics associated with isolated polar magnetic substorms at 0630 and 0645, are quite complex at 0700 and 0715 UT. This complexity indicates the affect of additional current sources other than the simplified line current model discussed in Chapter VI. The interpretation of such external fields into their causative sources is therefore quite difficult.

4.2. Scale Length of the External Field

Since the induction phenomenon depends critically upon the scale length ($\lambda=2\pi/v$) of the field, as shown in Chapter I, it is important to attempt an estimate of the parameter v from the maps of the separated external field.

Let F_E represent the total horizontal external field. i.e. $F_E = \sqrt{X_E^2 + Y_E^2}$. The parameter v is given (Schmucker 1964) by

$$v = 1/F_E (\partial F_E / \partial r) \approx 1/F_E (\Delta F_E / \Delta r) \quad (4.3)$$

where r is a distance in the direction of maximum gradient of F .

An estimate for v was found for each of the four separated times.

In some cases upper and lower-bound estimates were calculated.

TIME	0630	0645	0700	0715
$v(x10^{-8} \text{cm}^{-1})$	1.25	0.55-0.85	0.9	1.1
F_I/F_E	1.2	0.8	1.1	1.1

As mentioned in Chapter II, slowly varying fields such as the normal internal and external fields cannot be separated, for upon application of the separation procedure such fields are divided into internal and external parts. The large values of F_I/F_E are indicative of such a division of the normal fields. In (4.3) the absolute value of F_E affects the estimate of v . The anti-symmetric separation integrals show that a Z component with zero gradient in the direction of integration, causes the normal field to be divided equally between F_E and F_I , that is, the normal field is actually $2F_E$. However, for this case, $\Delta F_E/\Delta r$ will also be increased by a factor of two. The estimates of v are therefore probably not greatly affected by the inability to separate the normal fields, and values of v for this substorm are

$$0.55x10^{-8} \text{cm}^{-1} \leq v \leq 1.2x10^{-8} \text{cm}^{-1} \quad (4.4)$$

or

$$5000 \text{ km} \leq \lambda \leq 11,500 \text{ km}$$

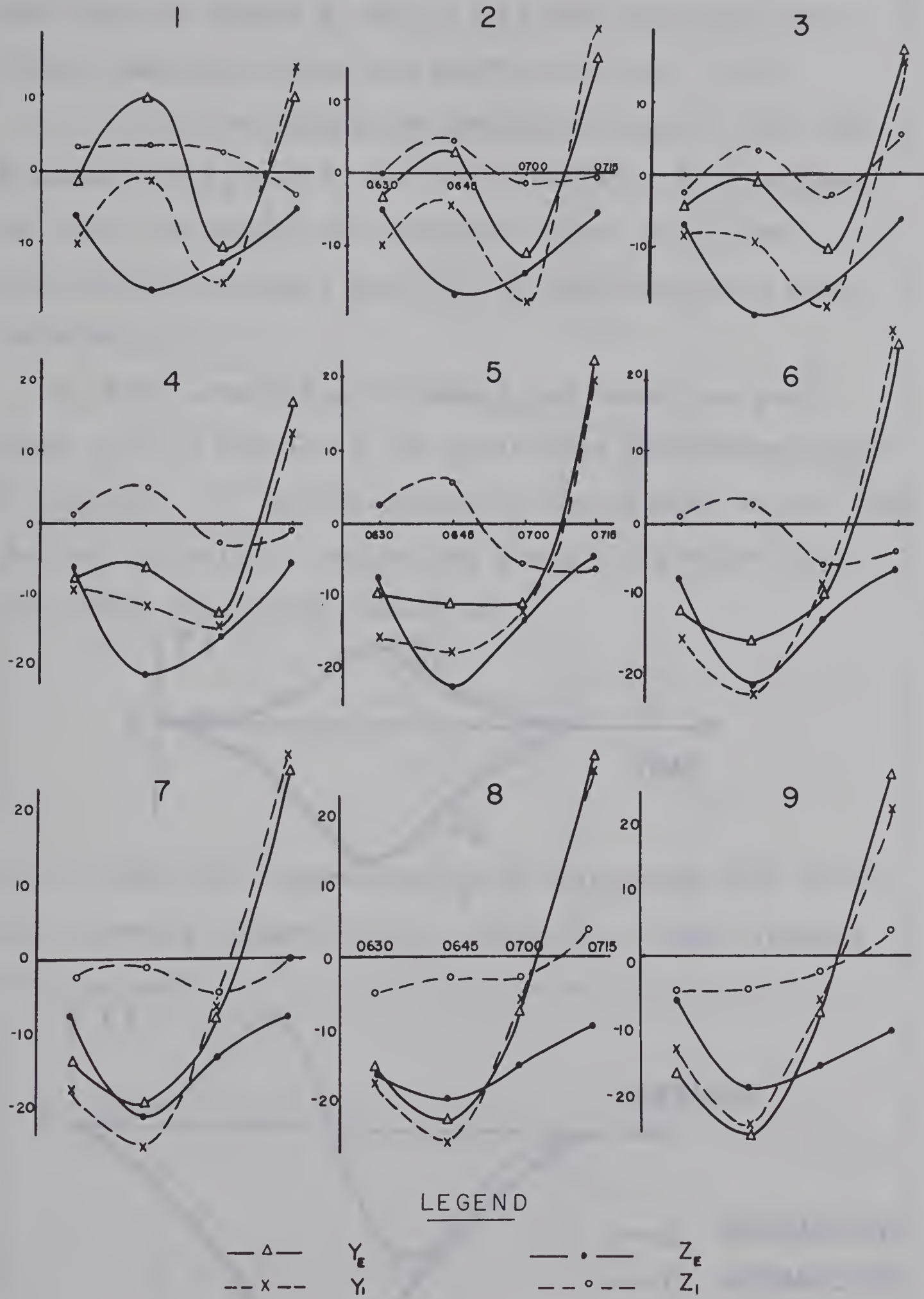
The most probable value of v is the average of all estimates and is $v \approx 0.9 \times 10^{-8} \text{ cm.}^{-1}$ corresponding to $\lambda \approx 7000 \text{ km.}$

It can be seen that the scale length of the external field is much larger than the dimensions of the array (800 x 1300 km.). The limits of v in (4.4) are larger than the value of $v = 0.4 \times 10^{-8} \text{ cm.}^{-1}$ used by Schmucker in analysis of mid-latitude bays. A possible reason for this is that our array is closer to the current system in the auroral zone and hence is more affected by the higher frequency components. The center of our array was about 600 km. north of Schmucker's line, while the auroral current was farther south than usual (63°N geomagnetic latitude). These values for λ are however, still an order of magnitude larger than values 600 to 800 km. used by Caner et. al. (1966).

4.3. Separated Magnetic Components in the Time Domain

In Fig.(4.9) the instantaneous values of the magnetic components Y_E , Y_I , Z_E , and Z_I , at the four times 0630, 0645, 0700, and 0715 UT., are plotted for nine points along a central east-west profile through the array. These graphs, though consisting only of four points, give general information about the induction process and about the phase difference between the induced and inducing field. The points of the profile as well as the locations of the current, represented by a line describing the average of the positions of the maxima of Y_I at the four times of separation, are

MAGNETIC COMPONENTS Y_E , Y_I , Z_E AND Z_I
AT FOUR TIMES



LEGEND

— Δ —
--- \times ---

Y_E
 Y_I

— \bullet —
--- \circ ---

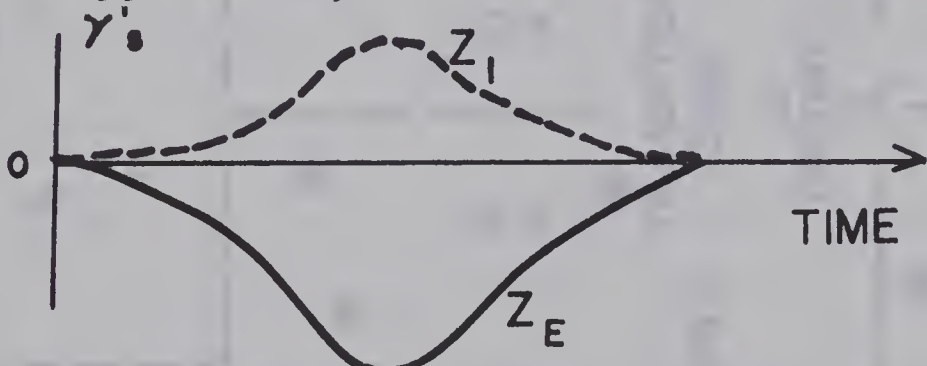
Z_E
 Z_I

Fig. 4.9

shown in Fig. (4.10). The numbers (1) to (9) used in labelling the graphs in Fig. (4.9) also represent the station locations along the profile in Fig. (4.10).

At all points along the profile it can be seen that the graphs of Y_E and Y_I are very similar. This suggests that both the normal and anomalous parts of Y_I are approximately in-phase with Y_E , as expected for a good conductor.

Z_I also consists of a normal and anomalous part. Normal Z_I is a result of the world-wide conductive "core" of the Earth. It is induced by Z_E and opposes it, so that a typical situation, neglecting a small departure from exact phase opposition, would be



On the other hand, anomalous Z_I is associated with north-south currents induced by Y_E . Since Y_I is also induced by Y_E , we have

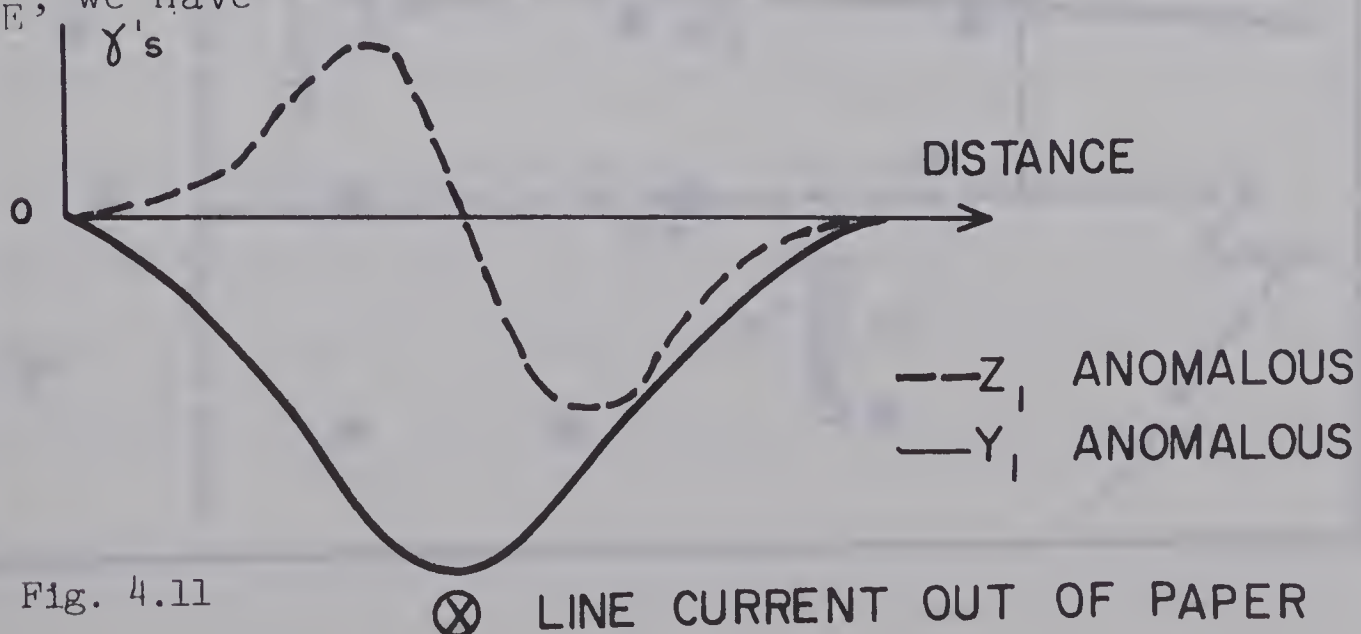


Fig. 4.11

LINE CURRENT OUT OF PAPER

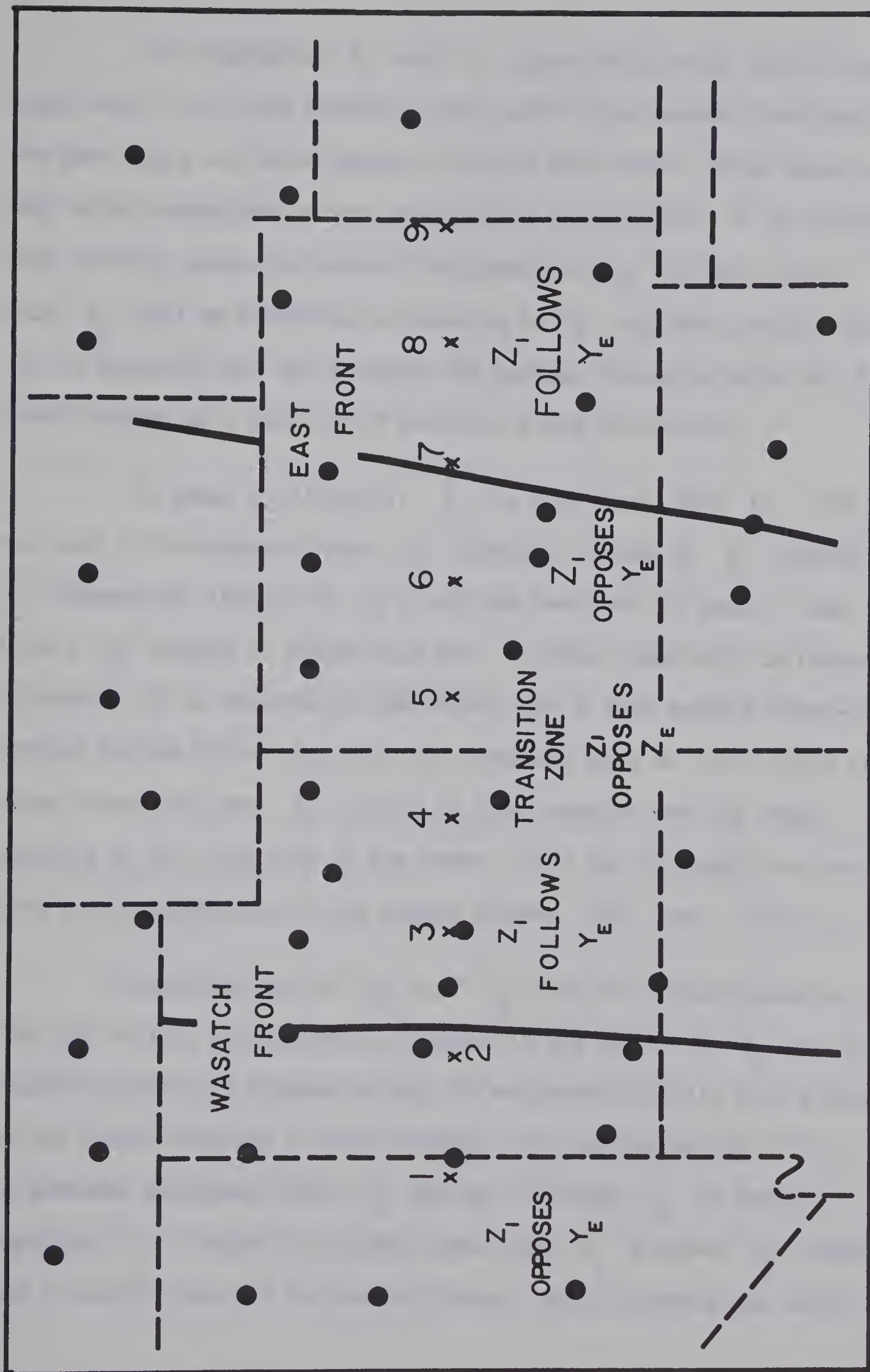


Fig. 4.10

The components Y_I and Z_I oppose each other (are of opposite sign) west of the line current, while east of the current they have the same sign, and hence appear to follow each other. This relationship holds regardless of the direction of the current. It is evident that directly above the current the anomalous Z_I is zero, thus only Z_E will be effective in inducing a Z_I component there. Fig. (4.10) indicates the way in which the general characteristics of Z_I should change as a function of position along the profile.

In graph (1) (Fig. 4.9) Z_I is flat from 0630 to 0700 UT., for west of the Wasatch Front Z_I (normal) induced by Z_E opposes Z_I (anomalous) induced by Y_E , and the resultant is small. Near 0700, Y_E begins to change sign and Z drops negatively in response to this. (It is believed by the writer that a more serious "base-line" problem exists in the Z_E and Z_I component maps at 0715 than at other times, and that Z_I should be more negative and Z_E more positive at all locations in the array. This may be taken into consideration in interpretation of the graphs between 0700 and 0715 UT.).

Since the form of Z_E and Y_E does not change appreciably from (2) to (5), characteristic changes in the graphs of Z_I can be related directly to movement along the east-west profile, with respect to the fixed locations of the currents. The interpretation of (2) is somewhat ambiguous since Z_I may be following Y_E or merely opposing Z_E . Graph (3) clearly shows that Z_I follows Y_E indicating a location east of the Wasatch Front. This following can still

be seen to a certain extent in (4). In (5) however, the currents associated with the two anomalies give opposite and nearly equal contributions to Z_I , leaving a Z_I component induced mainly by Z_E . The change of character of Z_I from (6) to (7) results from a reduction in Z_I (anomalous) as the East Front anomaly is approached. In (8) and (9) a strong following of Y_E by Z_I is indicated. Therefore the graphs of Fig. (4.9) again qualitatively show that the resultant induction affects are consistent with those expected from the postulated currents under the Wasatch Front and the Southern Rockies.

The induction of Z_I (anomalous) by Y_E at the Southern Rockies was more obvious on profiles north of that in Fig.(4.10) i.e. nearer to CRW. However, only the central profile has been discussed here, since the separations should be most reliable in the center of the array.

Although the graphs indicate only a small phase difference between the internal and external fields, it must be remembered that the observed phase difference will be an underestimate of the actual value since the normal internal field and the smoothly varying external field will have been divided nearly equally into the internal and external parts, thus causing an apparent reduction in the phase difference. To obtain a better estimate of the phase difference, it is necessary to separate the magnetic field at more times and also to make a correction for the smoothly varying fields.

In Fig.(4.12) are shown the graphs of the X_E , and X_I components. In graphs (1) to (4) X_E and X_I follow each other very closely, but a consistent change in the characteristics of X_I then occurs in graphs (5) through (9). This change is most noticeable at 0645 UT., a time corresponding to a positive maximum in X_E and a negative maximum in Z_E . Also an anomaly in X_I , large compared to that occurring at 0630, 0700, or 0715 UT., can be seen at this time, (Fig.4.3). Such an effect could be obtained by a general rising from south to north of the highly conducting medium in the area of the East Front anomaly, causing X_I (anomalous) to follow Z_E . It has been mentioned previously that Z_I (anomalous) closely follows Y_E near CRW, and this may also be indicative of the conductivity structure rising towards the north end of the array. In a north-south profile comparing X_E , X_I , and Z_E (not shown) it is evident that X_I follows X_E closely at the southern part of the array, but is more influenced by Z_E as the CRW area is approached. It therefore is probable that superposed upon a north-south striking conductivity structure we have a general rising of a highly conducting stratum as one goes northeast from the center of the array.

4.4. Separation in the Geomagnetic Coordinate System

The geographic coordinate system (x, y, z) may be artificial in the sense that it may not be physically related to the coordinate system of the currents originating in the auroral zone. It was thought that separation of the observed magnetic field in the geomagnetic

COMPONENTS X_E AND X_I AT FOUR TIMES

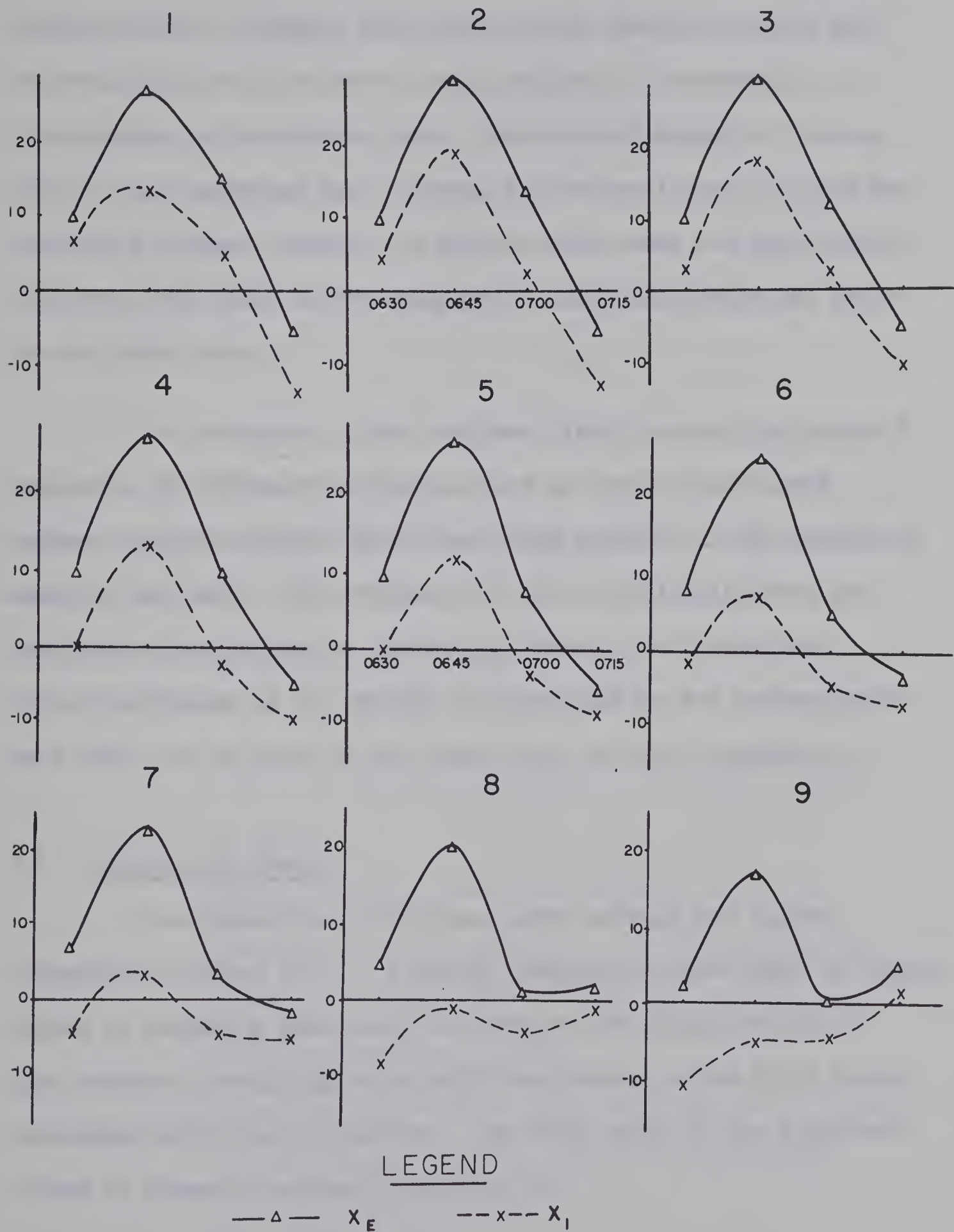


Fig. 4.12

coordinate system, resulting from fitting the observed field to the eccentric dipole (Hakawa, 1965) might yield results in which the external field could be more closely related to ionospheric disturbances in the auroral zone. The observed magnetic field at 0645 UT. was separated into internal and external parts in this new coordinate system; however, the final results were not significantly different from those in the geographic coordinate system and hence are not shown here.

In retrospect, since the same field is merely expressed by components in different orthogonal axes in the two coordinate systems, similar results should have been expected if the separation analysis was valid. The existence of such a similarity from two independent separations is reassuring since it indicates that errors introduced by our methods of interpolation and extrapolation were small, or at least of the same type, for both separations.

4.5. Analysis of Errors

The resolution of the data after editing and digital conversion is about 1.5γ . Although precautions were taken to reduce errors in timing, a time error as large as one minute may still have occurred, resulting in an additional error in the field values comparable with this resolution. The total error of the digitized values is however, believed less than 2γ .

Errors in the values of the surface integrals arising from interpolation of the data between recording stations will be small, especially for the X and Y components, where the contours have been adjusted with aid of the curl-free condition. Since no such constraint could be applied to Z, the interpolation errors for this component are greater than for the horizontal components. However, only a small error is added to the surface integral since the errors in interpolation tend to be random.

The effects of three different techniques used to interpolate the horizontal field components has been made upon the separation of the sine transform coefficients of Z at T = 50 minutes. (Porath, Oldenburg, and Gough, 1969). Contour maps of the sine transforms of X and Y at this period were prepared in three ways:

1. by linear interpolation between variometer stations.
2. by drawing a grid of squares 100 x 100 km. on the linearly interpolated maps; computing the line integrals along the boundaries of the squares; and relaxing the residual line integrals by the method of Price and Wilkins (1963).
3. by graphical adjustment of the contours of X and Y to approximate a curl-free field, in the manner discussed in Section 3.5.

External and internal parts of the sine transforms of Z , separated by the use of the X and Y maps prepared in these three ways, are shown in Fig.(4.13) for one centrally-located east-west profile. It can be seen that these three techniques yield very similar results. Hence it is the accuracy of both the measured field, and not the interpolation, which determines the final accuracy of the surface integrations.

The most serious source of error in the separation analysis is the limited size of the variometer array. Fields of scale lengths large compared with the array dimensions contain most of the energy of the substorm variation and cannot be separated. It is therefore customary to remove from the data, before separation, a "normal" horizontal field, H_n , which is assumed to be the sum of the external part, H_{en} , and an internal part H_{in} . In essence, the removal of H_n leaves zero fields over the rest of the infinite plane over which the surface integrations are to be performed. The removal of H_n leaves an anomalous internal field H_{ia} to be separated from the inhomogeneous external field H_{ea} . The procedure followed in the present work has been to make the separation analysis first. For model studies an estimated normal internal field was deducted from the separated internal field, thus permitting isolation and normalization of the internal anomalous fields. The point required for the present discussion is that separation with an array of dimensions less than the largest wavelengths in the field results

SIN Z T=50 MIN.

- LINEAR INTERPOLATION
- ✗ RELAXATION OF RESIDUALS
- ADJUSTED CONTOURS

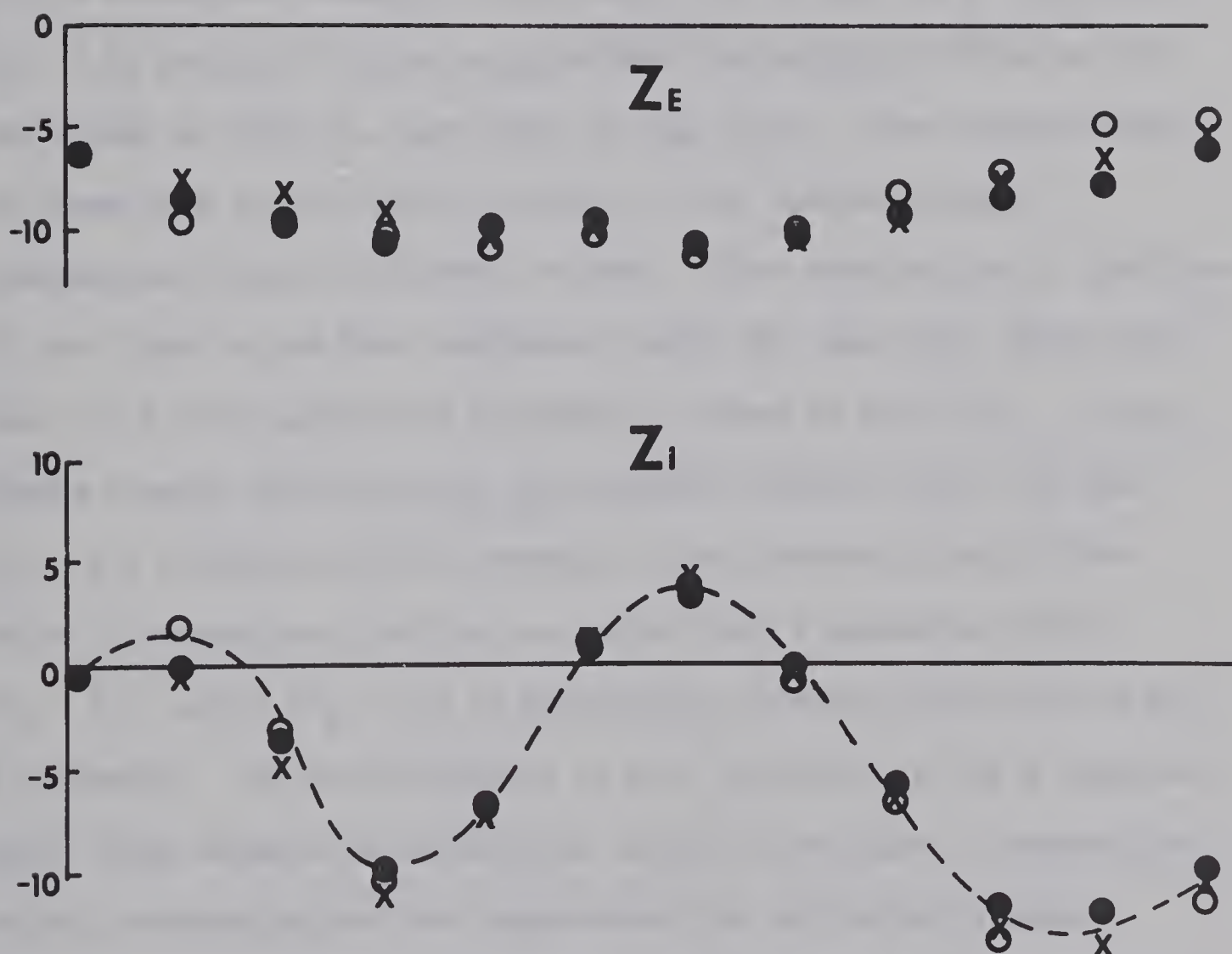


Fig. 4.13

in division of the long-wavelength fields between external and internal parts. However, this in no way invalidates the separation of fields of wavelengths less than the array dimensions, such as those of anomalous structures within the array.

The convergence of the surface integrals has been studied by means of computations in polar coordinates. The contributions of six successive rings ($\Delta r \sim 100$ km.) to the values $(X_E - X_I)$, $(Y_E - Y_I)$, and $(Z_E - Z_I)$ at a point near the center of the array for the fields at 0645 UT., are shown in Fig.(4.14). The nonconvergence of these ring contributions, because of the long-wavelength inseparable fields, is clearly evident. The contributions of portions of the rings in the four quadrants: north (N), east (E), south (S), west (W) to the separation integrals is shown in Fig.(4.15). These graphs clearly indicate that the resultant value of $(X_E - X_I)$ and $(Y_E - Y_I)$ depends upon the symmetry of the observed field at the point of separation, that is, only the E and W quadrants affect $(Y_E - Y_I)$, while $(X_E - X_I)$ is appreciably affected only by the N and S quadrants. The nonconvergence is most prominent in the X component where large negative contributions north of the point of separation do not converge and are not compensated for by similarly large positive contributions to the south. It was found that the convergence characteristics of the surface integrals at other points in the array were similar to those shown in Fig.(4.14) and Fig.(4.15).

CONVERGENCE OF SURFACE INTEGRALS

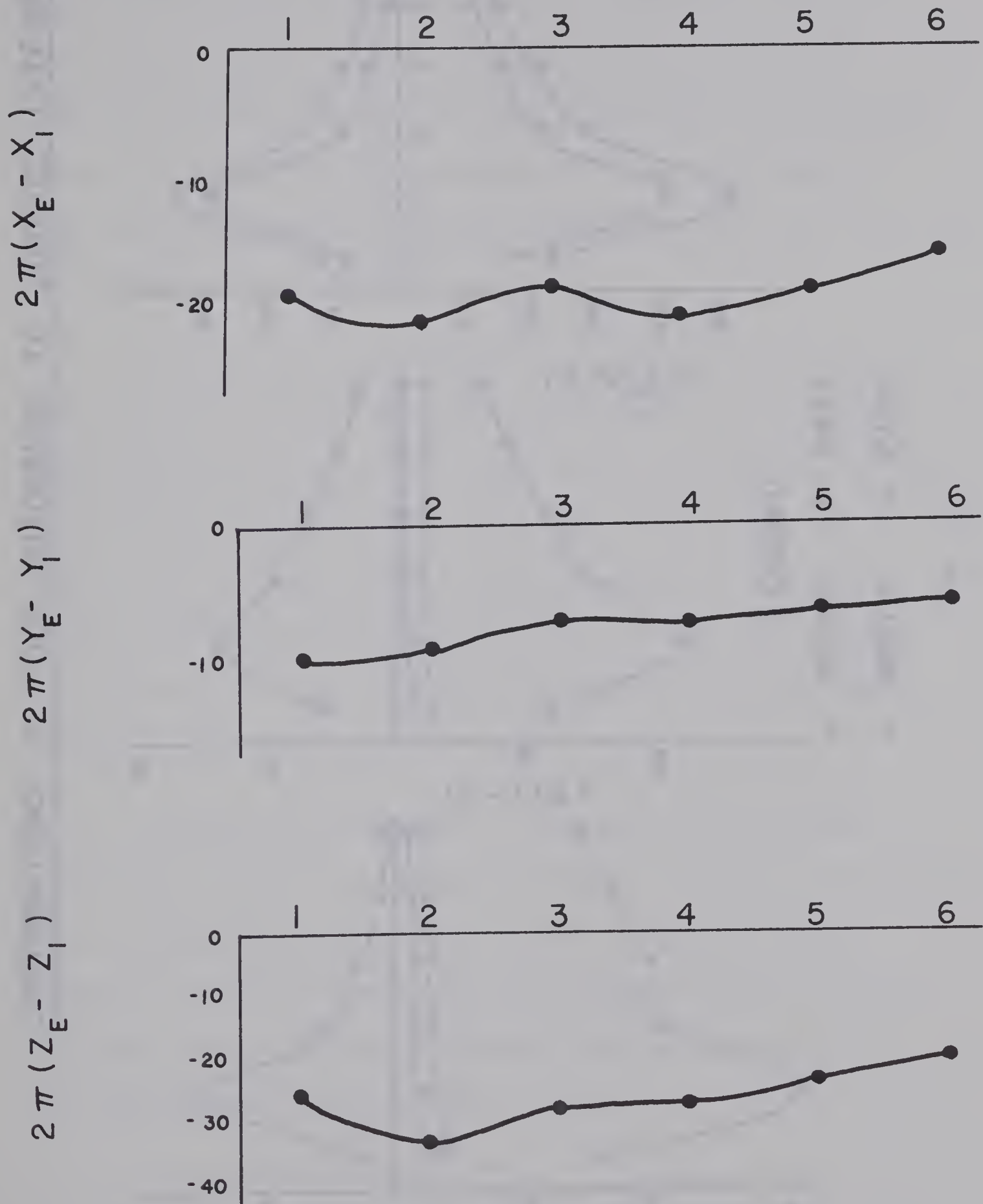


Fig. 4.14

CONTRIBUTIONS OF FOUR QUADRANTS TO SURFACE INTEGRAL

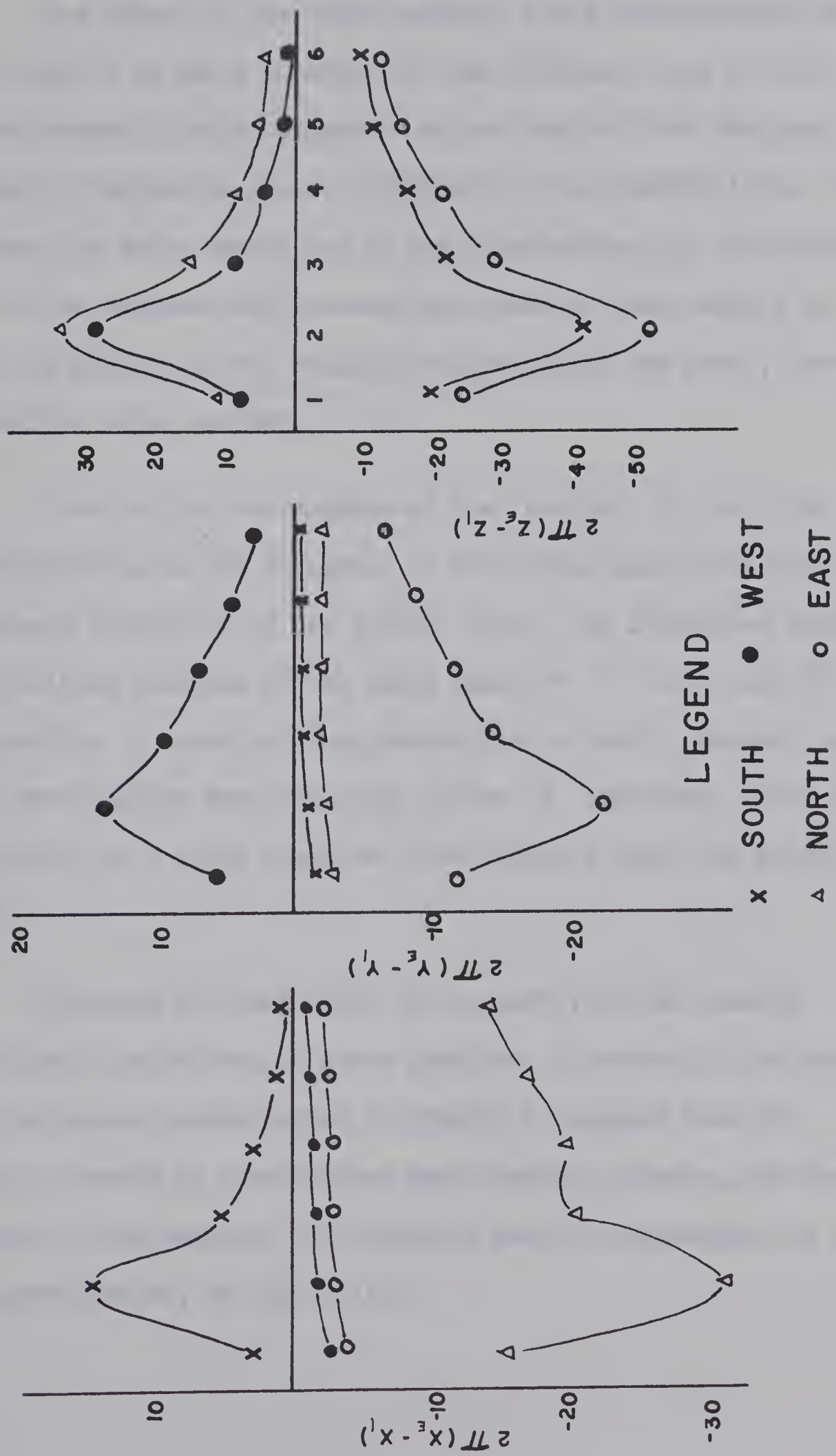


Fig. 4.15

The effect of the large magnetic field perturbations in the auroral zone is to add a constant or near constant value to the separated magnetic field components at our mid-latitude stations. These large inseparable fields contribute to the general level of the field over the whole array, and to the indeterminacy of the absolute values of the external and internal parts and of their ratio; but they do not greatly affect relative values within the array, that is, the anomalies being studied.

Consider the convergence of the integrals in the light of the contributions to the integrals of the fields associated with the westward electrojet in the auroral zone. The integrated effect at mid-latitude stations of the large negative Z south, and the large positive Z north of this electrojet is small. However, a similar cancellation does not occur in the H component, which is characterized by a large negative value directly under the auroral current.

Ignoring the sphericity of the earth, we can examine qualitatively the effects of large negative X values in the auroral zone. Analysis of magnetograms in Chapter VI suggest that the electrojet current is concentrated near Meanook, Alberta, and that the extent of the negative X influence may be represented, to a first approximation, by Fig.(4.16).

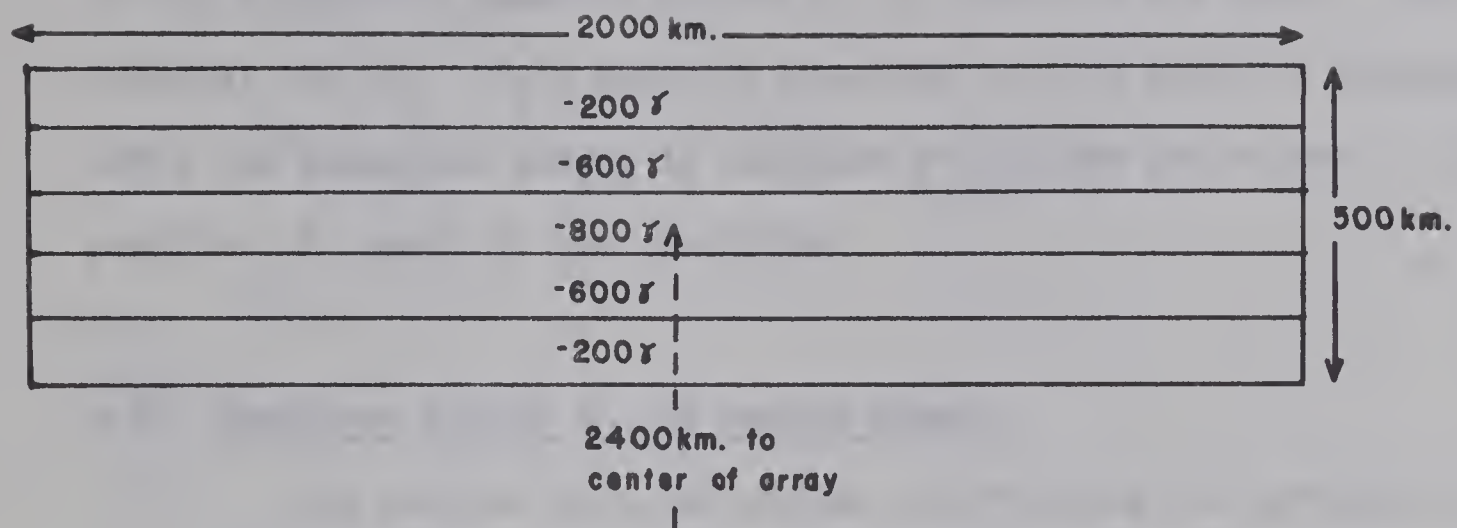


Fig. 4.16

The contribution of the X field to the value $(Z_E - Z_I)$, from equation (2.21), is $\frac{1}{2}\pi \int_S xX/r^3 ds$. The effect of the field shown in Fig. (4.16) upon the integral, evaluated at points 2100, 2400, and 2700 km. directly south of this field, is respectively $\approx -17.6\gamma$, $\approx -13.5\gamma$, and $\approx -10.6\gamma$. For such a field configuration a value of Z_E near the northern edge of the array would then be in error by -8.8γ , since this inseparable field is divided nearly equally between Z_E and Z_I , while the error at a southern station would be approximately -5.3γ . Field values in the auroral zone thus have the effect of adding a negative value ($\approx -5\gamma$) to Z_E for the whole map, plus introducing an additional north-south gradient of the Z component.

The nonconvergence of X (Fig.4.15) is primarily a result of the increasing negative values of Z north of the array. The integral for $(X_E - X_I)$, given by equation (2.19), will not converge until the summation window is extended to include the effect of the positive Z north of the electrojet.

4.6. Separated Fields in the Period Domain

The Fourier sine and cosine coefficients for periods 30.1 and 60.2 minutes have been separated into internal and external parts. The cosine transforms of Z_E , Z_I , Y_E , and Y_I at 60.2 minutes are shown in Fig.(4.17), while the sine transforms of these components are shown in Fig.(4.18).

A priori one would expect the maps of separated Fourier transforms to show the same general features as the maps of separated instantaneous fields in the time domain. For the understanding of maps of transformed components, however, one must consider certain properties of spectral estimates from a finite time series.

The signs of the cosine and sine transforms will have no physical significance, since they simply reflect the sign of the spectral component concerned at the start of the time interval, ΔT , transformed. A change in the starting time introduces changes in the relative magnitudes and signs of the cosine and sine transforms, thus determining whether a given spectral term appears

COSINE TRANSFORM OF MAGNETIC FIELD COMPONENTS

$T = 60.2$ MINUTES CONTOUR INTERVAL = 0.5 GAMMAS

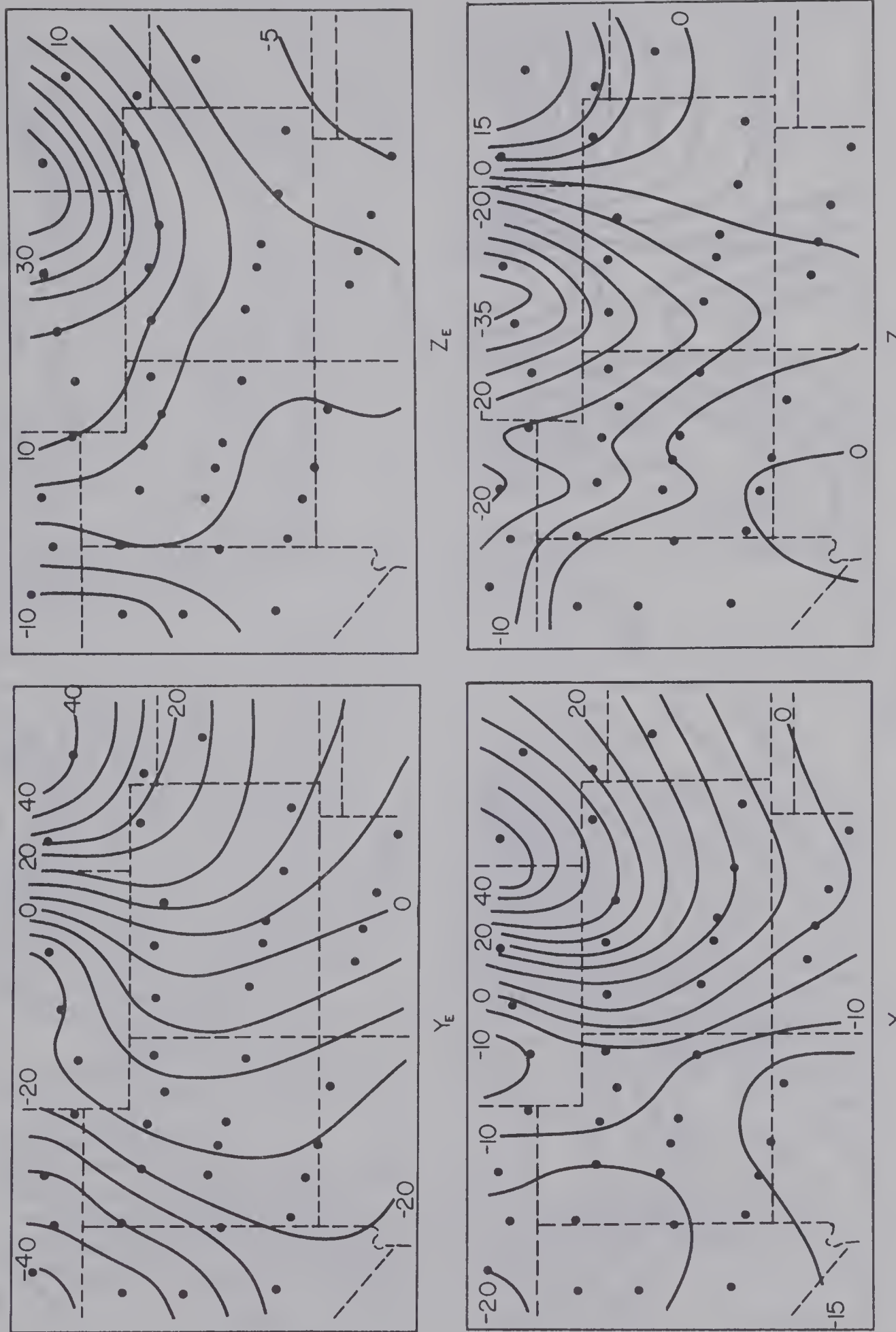


Fig. 4.17

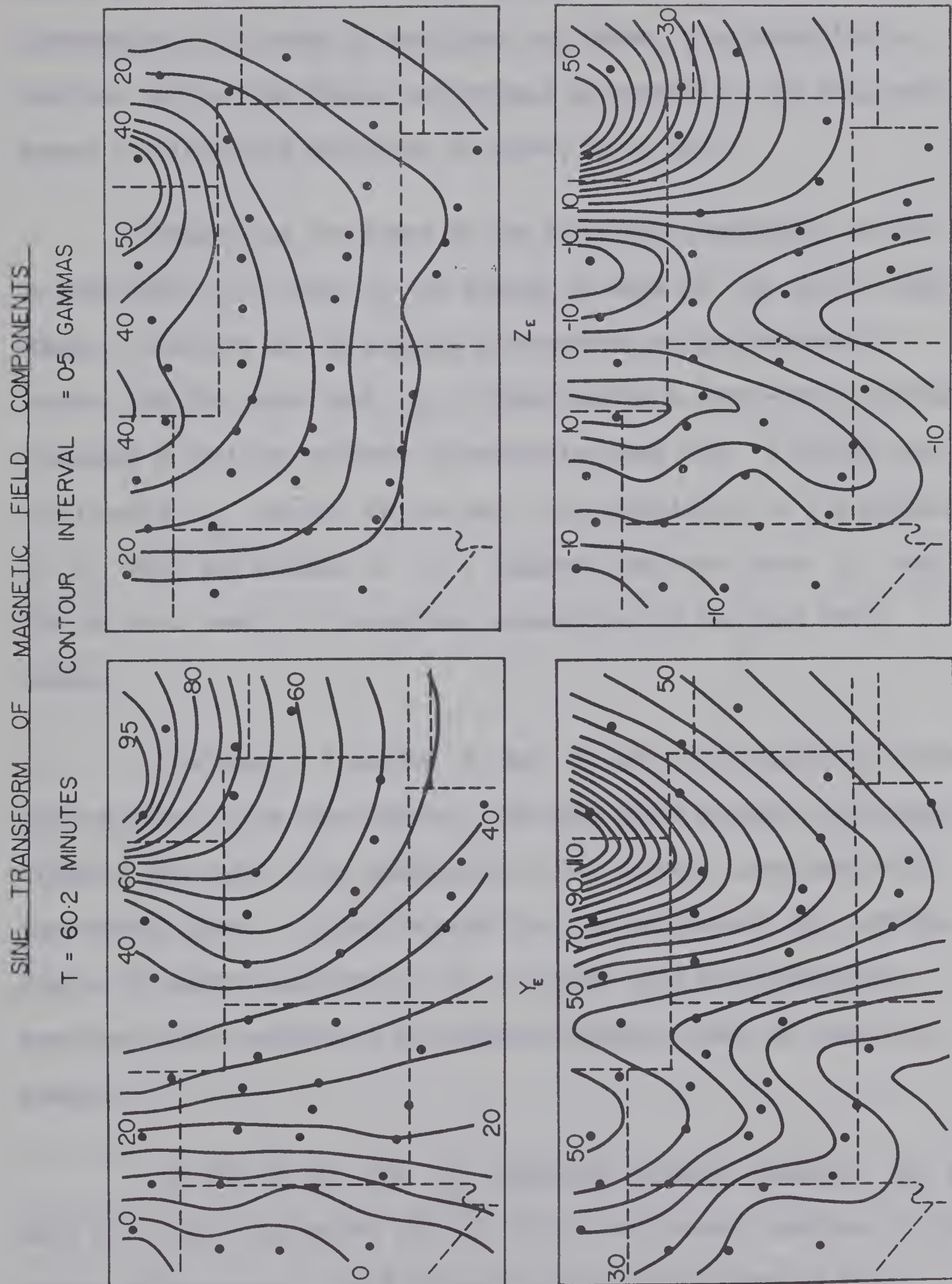


Fig. 4.18

mainly in the cosine transform, in the sine transform, or in both. Alternatively, in terms of amplitude and phase, this means that a spectral term of the field, and perhaps an anomaly on the map, may appear in either the amplitude or phase, or in both.

Neglecting the signs of the transform components, it can be seen (Fig.4.17) that Y_E is similar to maps of Y_E in the time domain. Contours are in general north-south and are reasonably smooth. On the other hand Z_E , though having a north-south gradient, indicates a positive maximum concentrating near CRW. Although this complicated Z_E pattern may be real, the coincidence of the maximum of Z_E with the maximum of Y_I , suggests that the large Z_E near CRW may be a result of incomplete separation for the East Front anomaly.

The maps of internal Z and Y are very similar to corresponding maps in the time domain. The East Front anomaly is strongly evident, but there is no indication of the anomaly associated with the Wasatch Front. It can be seen that the maximum of Y_I and the region of maximum gradient of Z_I coincide with the postulated position of the current of the Southern Rockies found in the time domain.

In Fig.(4.18), the Z_E component closely resembles Z_E at 0645 UT., for it is smooth and has only a north-south gradient in the center of the array. The increased east-west gradients of this

field near the eastern and western borders may be a result of inadequate extrapolation. If the sign is again neglected, it can be seen that Y_E has characteristics nearly identical with maps of Y_E in the time domain.

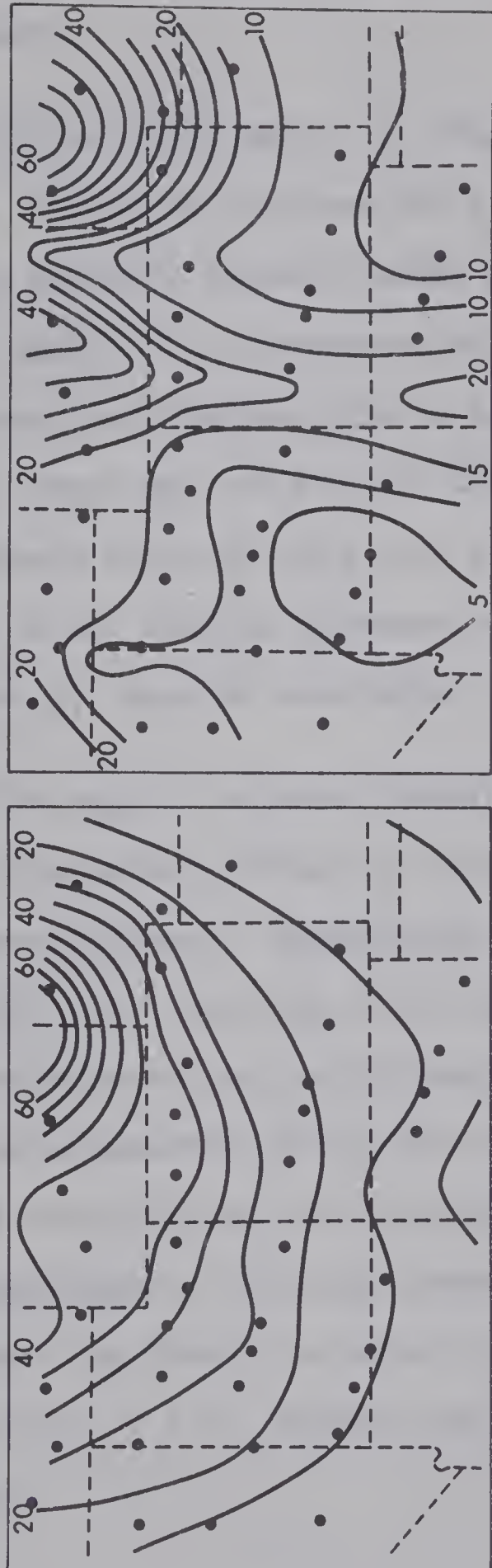
Y_I and Z_I each have two positive maxima indicating the two anomalies. The locations of maxima of Y_I are the same as those found in the time domain. The appearance of the Wasatch Front is evident in these maps, whereas it was not seen in maps of the cosine transform.

The maps for the amplitude and phase of Z_E and Z_I at 60.2 minutes are shown in Fig.(4.19). Both the amplitude and phase of Z_E are smooth. The East Front anomaly, though not seen in the phase, is the dominant feature in the amplitude map of Z_I . Conversely, the Wasatch Front anomaly is not evident in the amplitude map, but is represented by an outstanding anomaly in the phase. The large number of contours corresponding to the Wasatch Front is a result of both the sine and cosine transforms having values near zero, so that a slight change in either transform produces a large change in phase. Such large phase changes between stations made contouring difficult since this led to ambiguity in the actual values of the phase, i.e. a phase of 25° may actually be 385° . In such ambiguous cases, phase values were chosen which resulted in the least number of contours to be drawn. From the maps of Fig.(4.19) it is evident that one cannot make an interpretation of the anomalies by considering either the amplitude map or the phase

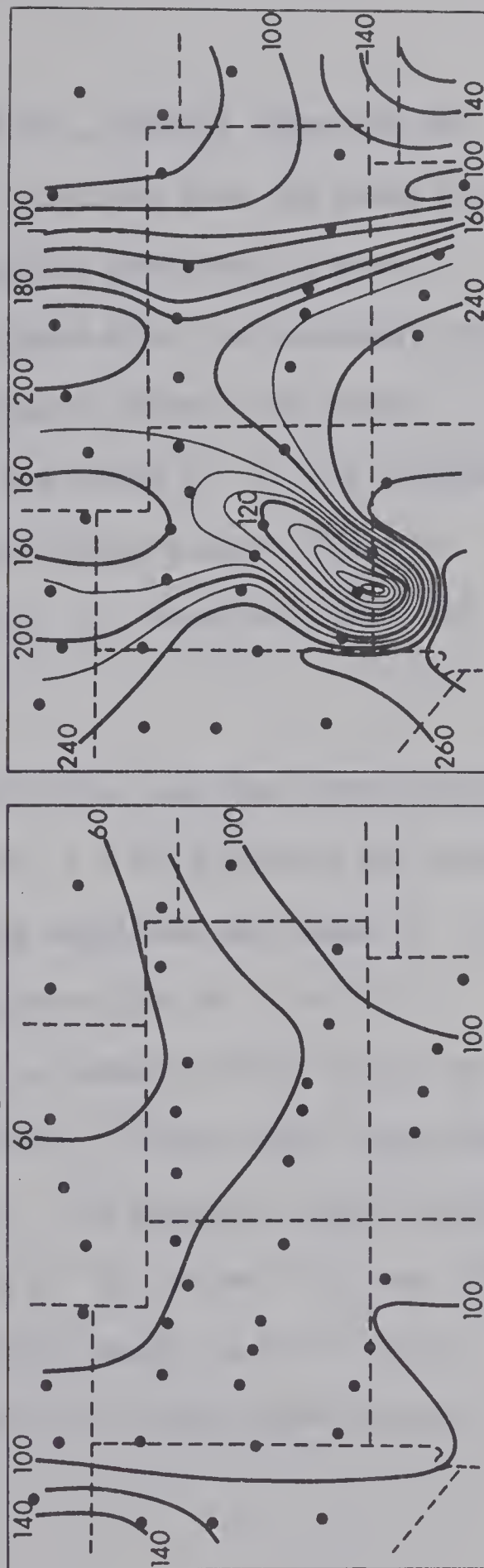
AMPLITUDE AND PHASE OF SEPARATED COMPONENT

VERTICAL FIELD

$T = 60.2$ MINUTES CONTOUR INTERVALS 0.5 GAMMAS AND 20 DEGREES



AMPLITUDE Z_E



PHASE Z_E

Fig. 4.19

map alone, but must consider the information in these two maps simultaneously.

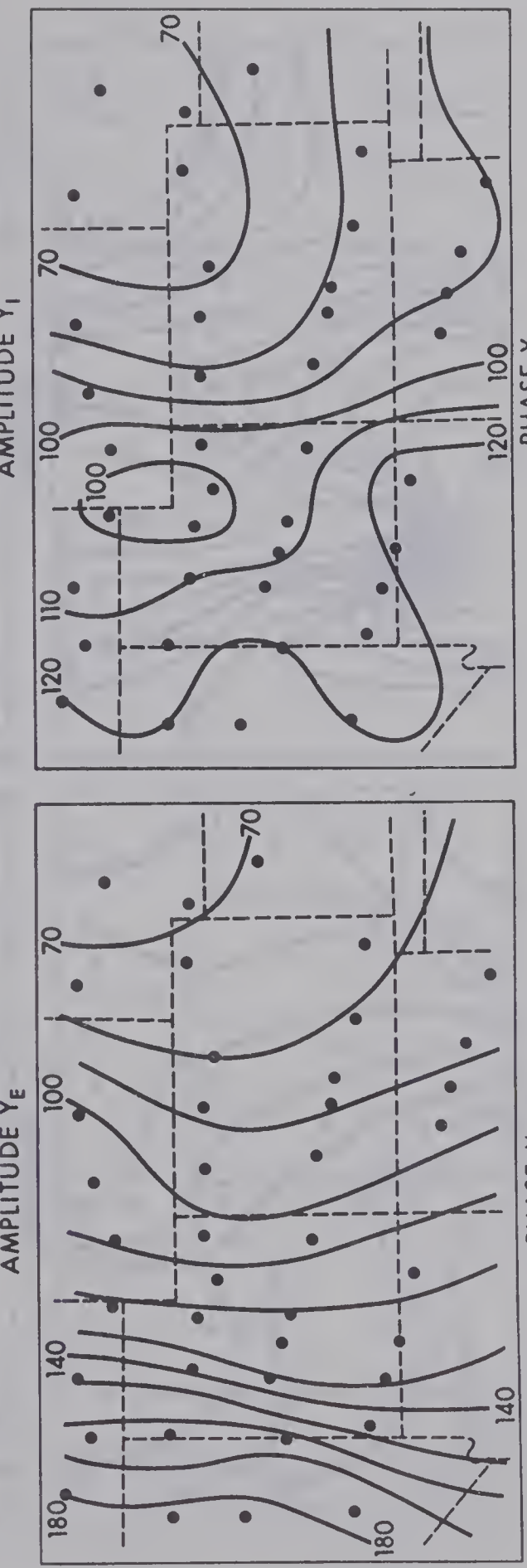
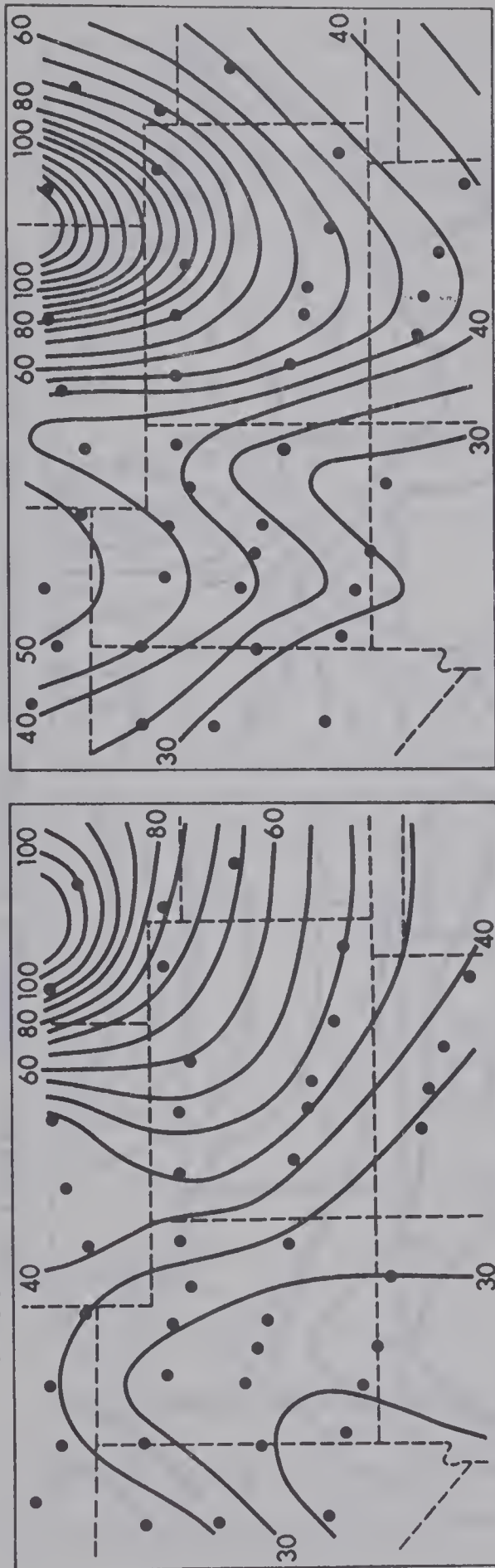
The amplitude map of Y_I (Fig.4.20), clearly shows the two anomalies. The map of the phase of Y_E indicates that the phase change of 110° (or nearly 18 minutes) varies smoothly from east to west across the array. This phenomenon, associated with the east-west motion of the external disturbance, will be discussed later. The rather smooth Z_E phase map, and the fact that the phase of Y_E is consistent with a westward motion of the field, gives strong support to one's confidence in the validity of separation of Z , especially when the complicated Z_I maps are considered.

The maps of separated transform cosine and sine coefficients at 30.1 minutes were similar to those at $T = 60.2$ minutes and hence are not presented here. Comparison of the amplitude and phase of Z_I , shown in Fig.(4.21), with Fig.(4.19) indicates that at $T = 30.1$ minutes the Wasatch Front, while keeping an anomaly in the phase, has a more intense amplitude than at 60.2 minutes. Only a small amplitude anomaly is associated with the East Front. The physical significance for the convergence of the phase contours of Z_E below CUB and ESP is not known. As there is relatively little energy in the field of the substorm at $T = 30$ minutes, the reality of this effect cannot be assumed.

AMPLITUDE AND PHASE OF SEPARATED COMPONENT

EASTWARD HORIZONTAL FIELD

$T = 60.2$ MINUTES CONTOUR INTERVALS 0.5 GAMMAS AND 10 DEGREES



PHASE Y_E

Fig. 4.20

AMPLITUDE AND PHASE OF SEPARATED COMPONENT

VERTICAL FIELD

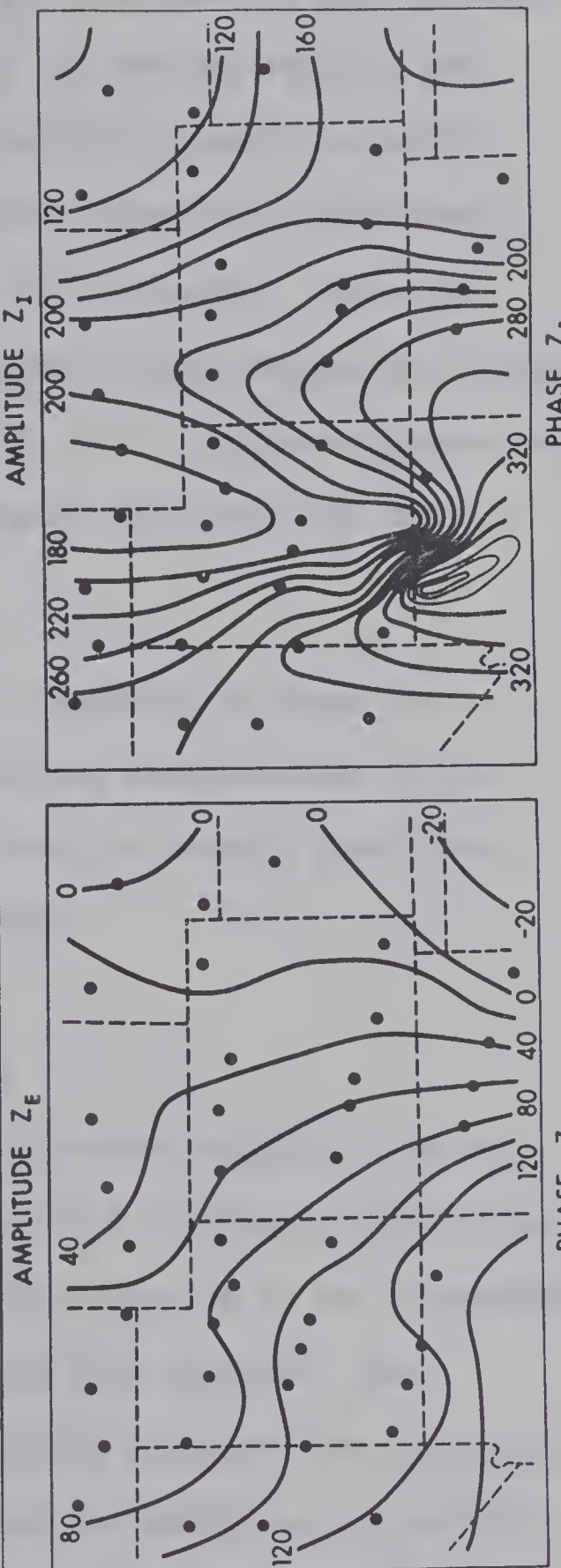
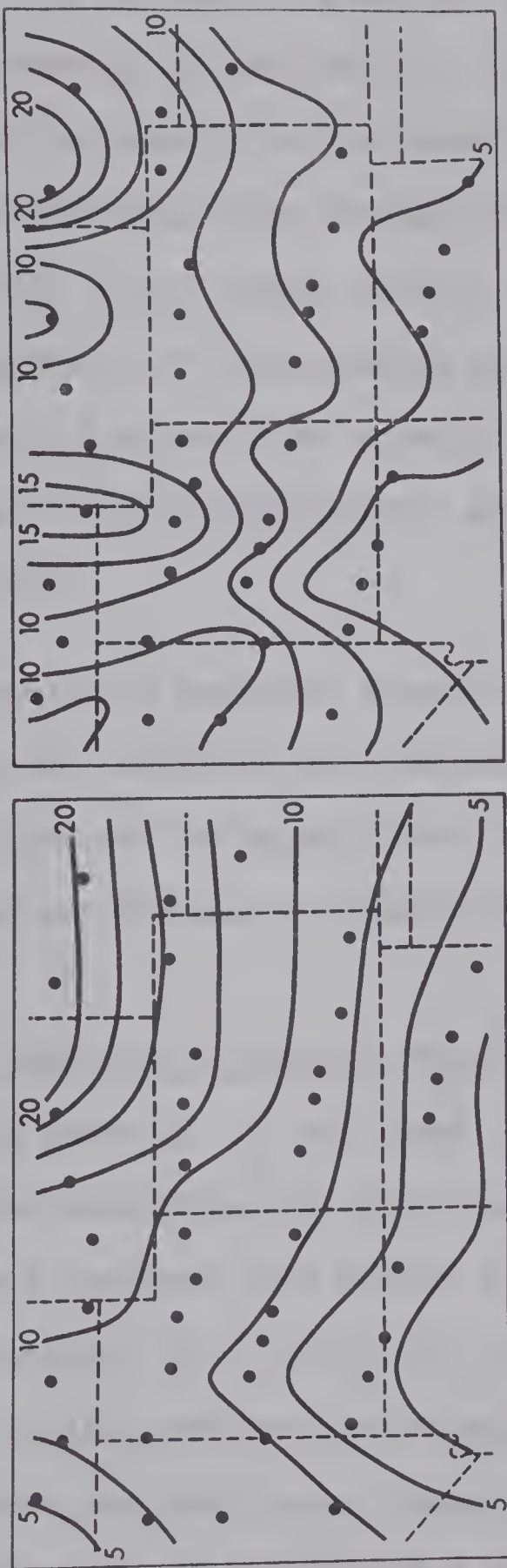
 $T = 30.1$ MINUTES CONTOUR INTERVALS 0.5 GAMMAS AND 20 DEGREES

Fig. 4.21

The Y component maps for $T = 30.1$ minutes are shown in Fig.(4.22). The increase of phase of Y_E from east to west is again evident. Comparing the amplitude of Y_I at the two periods, one can see that the intensity of the Wasatch Front anomaly is nearly the same in both maps, while the East Front anomaly is considerably more intense at 60.2 minutes than at 30.1 minutes. Since the depth of penetration of the inducing magnetic field depends upon period, the weakness of the East Front anomaly at 30.1 minutes suggests that this structure is at a significantly greater depth than the Wasatch Front structure.

Results of separated internal components at these two periods thus are consistent with the previous analysis made in the time domain, as both the Wasatch Front, and the anomaly associated with the Southern Rockies are clearly shown.

4.7. Phase Variation of External Fields

The phase of Y_E was found to increase smoothly from east to west in the separations at 30.1 and 60.2 minutes. Maps of the phase of the D-component from Fourier transformation of the unseparated fields, for periods 32.5, 50.0, 60.2, and 89.0 minutes, also indicated a similar east-west phase variation of about 9 to 12 minutes. If the constant east-west phase change can be related to the motion of the substorm current system then a velocity of the substorm field as it moves westward across the station network may be calculated.

AMPLITUDE AND PHASE OF SEPARATED COMPONENT
EASTWARD HORIZONTAL FIELD

T = 30.1 MINUTES CONTOUR INTERVALS 0.25 GAMMAS AND 10 DEGREES

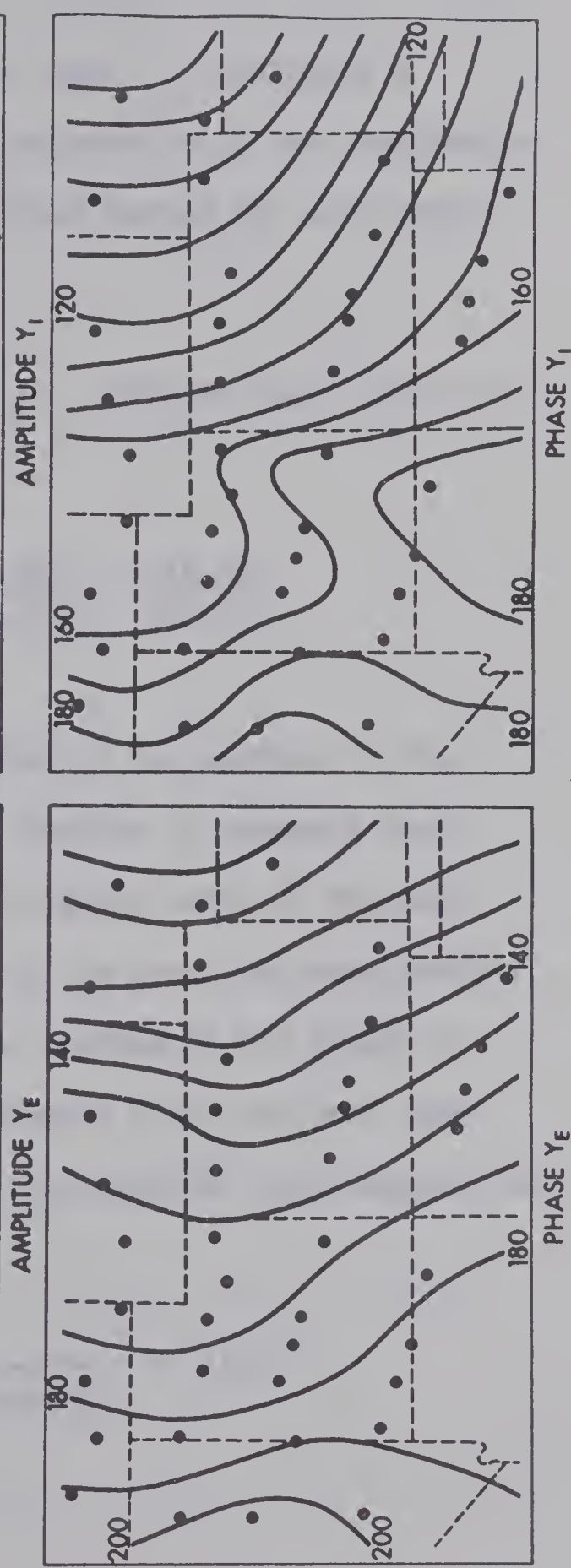
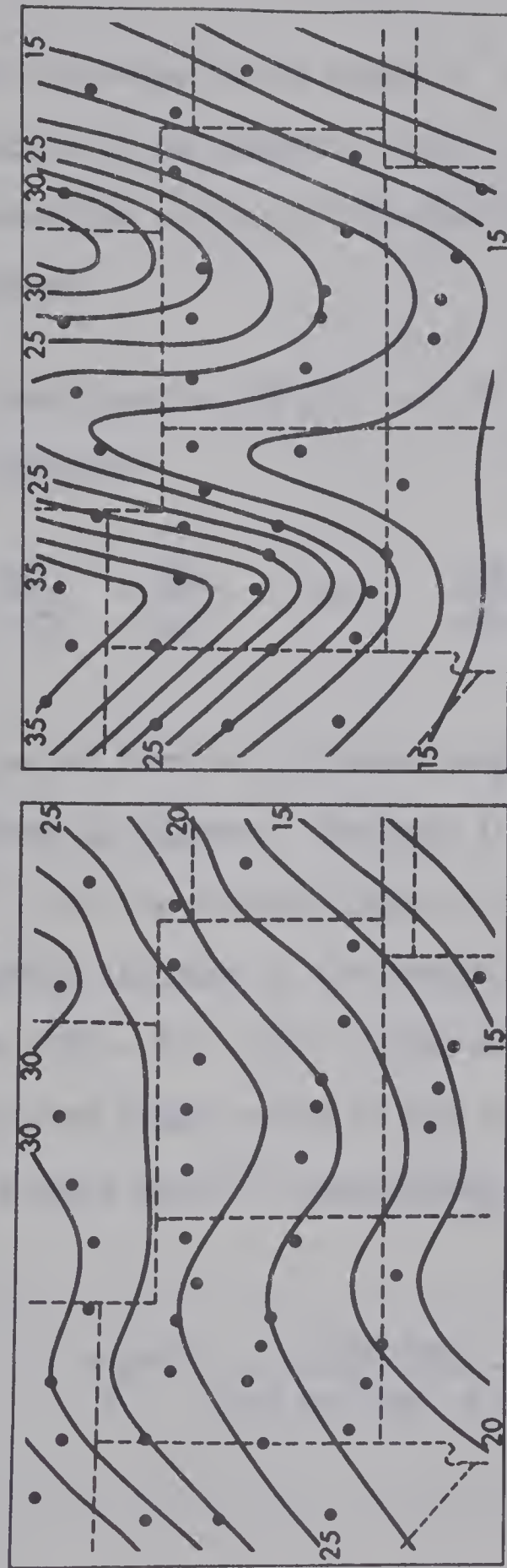


Fig. 4.22

viz.

$$\text{Vel} \approx \frac{1200 \text{ km.}}{12 \times 60 \text{ sec.}} \approx 1.7 \text{ km./sec.}$$

The westward increase in the phase of D and $\frac{Y}{E}$ indicates a westward motion of the magnetic field consistent with the lengthening of the intensified portion of the electrojet during the development of the substorm.

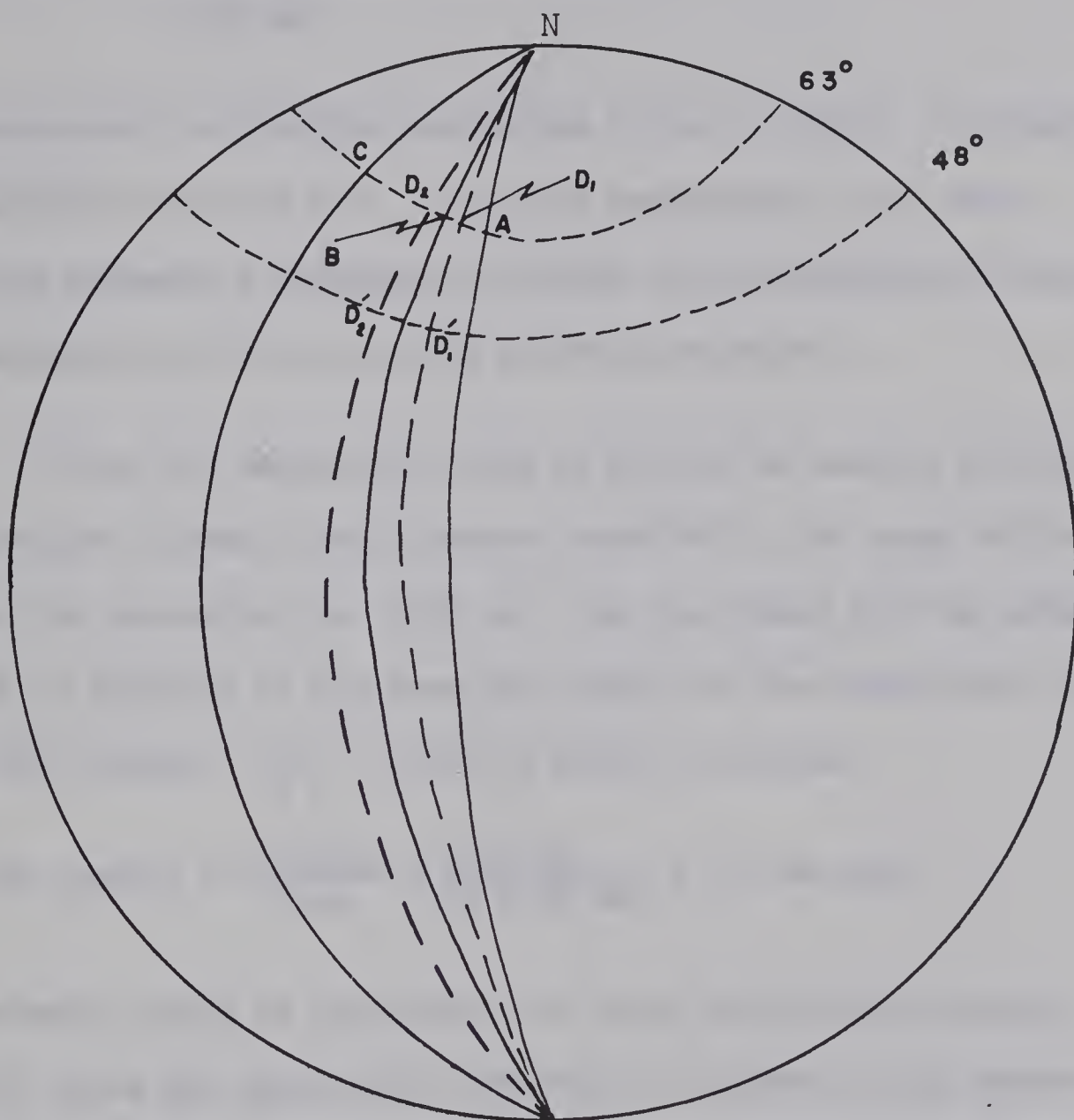
The triangles $ND_2'D_1'$ and ND_2D_1 shown in Fig. (4.23) are similar. Therefore

$$\frac{ND_2'}{D_2'D_1'} = \frac{ND_2}{D_2D_1} \quad \text{and} \quad \frac{\sin ND_2'}{\sin D_2'D_1'} = \frac{\sin ND_2}{\sin D_2D_1}$$

where the second formula indicates lengths on the surface of the earth measured in degrees. Analysis in Chapter VI suggests that $ND_2 \approx 27^\circ$ (i.e. the current system is slightly north of Meanook). The geomagnetic latitude of the center of the array is approximately $48^\circ N$, hence $ND_2' \approx 42^\circ$. $D_2'D_1' = 1200 \text{ km.}$ represents the length of array, since the phase change of the external field has been taken across this whole array. Transforming this distance into degrees, we have

$$D_2'D_1'^\circ = \frac{1200 \text{ km.}}{111 \text{ km./deg.} \times \cos 48^\circ} = 16.1^\circ$$

GEOMETRY OF SYSTEM ILLUSTRATING THE
SPATICAL MOTION OF DEMARCACTION LINE



AB - length of intensified electrojet just after onset of substorm

AC - length of intensified electrojet later in the substorm

$D_1 D_1'$ - position of D-component demarcation line just after onset of substorm

$D_2 D_2'$ - position of D-component demarcation line later in the substorm

Fig. 4.23

$$\sin D_{21} = \frac{\sin 27^\circ \times \sin 16.1^\circ}{\sin 42^\circ} = 0.188$$

$$\text{Therefore } D_{21} = 10.8^\circ \times 111 \text{ km./deg} \times \cos 63^\circ \\ = 545 \text{ km.}$$

It is convenient to describe the motion of the D-field in terms of the demarcation line ($D = 0$). Thus the demarcation line, while travelling westward a distance of 1200 km. at the latitude of our array, has travelled only 545 km. at the auroral electrojet.

Since the demarcation line is defined as exactly dividing the electrojet current, the distance travelled by the surge at the front of the electrojet is 1090 km. The time taken for the surge to travel this distance is the same time taken for the demarcation line to travel the distance D_{21}' , that is, about 12 minutes.

$$\text{Vel. (surge)} = \frac{\text{distance}}{\text{time}} = \frac{1090 \text{ km.}}{12 \times 60 \text{ sec.}} = 1.5 \text{ km./sec.}$$

This estimate should be regarded as an upper limit for the surge velocity, since any appreciable break-up of current in the eastern sector will result in a reduction of the calculated surge velocity. This calculated velocity of the westward surge is consistent with that of 1 km./sec. measured by Akasofu et al. (1965).

Eventhough Y and D are closely related, this relationship is not exact, and therefore, in the separated Y_E maps there is a contribution from the external X component. This, plus the fact

that the larger phase changes near the edges of the array may in part be due to inaccurate extrapolation, may explain why the external phase varies by 18 minutes across the array at $T = 60.2$ minutes, while this phase, at $T = 30.1$ minutes, varies only by 9 minutes (thus giving estimates to the velocity of the westward surge as 1 and 2 km./sec. respectively).

Whatever the meaning of the variation with period in the westward velocity of the external Y field, the striking fact remains that westward velocities of the same order of magnitude are found in the two Y_E phase maps as well as in the phase of the unseparated D component, and that the field velocities are consistent with the hypothesis that they result from the westward extension of the auroral-zone electrojet in the substorm development.

CHAPTER VMODEL STUDIES5.1. Isolation and Normalization of Anomalous Fields

Each internal field component given by our separation procedure, F_{is} , includes the anomalous internal field F_{ia} and also some fraction β of the inseparable normal field:

$$F_{is} = F_{ia} + \beta F \quad (5.1)$$

The normal field F_n is that field which would exist in the absence of conductive structures. It is the sum (for X and Y) and the difference (for Z) of the field of the external currents (F_e), and the normal internal field F_{in} . The external field component found by separation is

$$F_{es} = (1-\beta) F_n \quad (5.2)$$

In the plane approximation the conductive mantle at depth becomes a half-space. At a distance outside its plane boundary small compared with the scale-length of the external field, F_{in} will be independent of this distance, that is, of the depth.

Thus the normal field, F_n , at the surface will be the inducing field at a conductive structure. From (5.2)

$$F_n = F_{es}/(1-\beta) \quad (5.3)$$

and the inducing field can be found if β is known. The anomalous internal field, F_{ia} , may then be normalized with respect to the inducing fields F_n .

The normal variation fields X and Y are to a first approximation represented by a curl-free plane. For such a plane, equation (2.21) shows that Z_n appears in unequal parts in Z_{es} and Z_{is} , such that

$$(Z_n)_{es} - (Z_n)_{is} = \frac{A}{\pi} \left(\frac{\partial X}{\partial x} + \frac{\partial Y}{\partial y} \right) \ln \left(\frac{\sqrt{2+1}}{\sqrt{2-1}} \right) \quad (5.4)$$

where A represents the length of a side of the summation window used to evaluate the integral. Therefore from equations (5.3) and (5.4) we have

$$(Z_n)_{es} - (Z_n)_{is} = (1-2\beta)Z_n \quad (5.5)$$

and $Z_{es} - Z_{is} = (1-2\beta)Z_n - Z_{ia}$ (5.6)

The normal and anomalous components are found by combining (5.4), (5.5) and (5.6).

$$Z_{ia} = Z_{is} - Z_{es} + \frac{A}{\pi} \left(\frac{\partial X}{\partial x} + \frac{\partial Y}{\partial y} \right) \ln \left(\frac{\sqrt{2+1}}{\sqrt{2-1}} \right) \quad (5.7)$$

$$Z_n = Z - Z_{ia}$$

The normal and anomalous Y components were found in two ways:

(i) Z_{es} showed only small east-west gradients over the center of the array. From (2.20) it is evident that a field with zero east-west gradient does not contribute to the integral for Y , and that Y is thus equally divided between Y_{es} and Y_{is} , that is, $\beta = 0.5$. Therefore

$$Y_n = 2 Y_{es}$$

$$Y_{ia} = Y_{is} - Y_{es} \quad (5.8)$$

(ii) A first approximation to a normal Z component, obtained by fitting the observed Z values to a plane by least squares, was used in the separation formula (2.20). The resultant values, $(Y_n)_{es} - (Y_n)_{is}$, were combined with values of $Y_n = (Y_n)_{es} + (Y_n)_{is}$ obtained from fitting X and Y to a curl-free plane. Since better defined anomalies in Y_{ia} and smoother Y_n fields were found, it is believed that this method may be preferable to that of (i), which is used by Porath, Oldenburg and Gough (1969).

It is evident from the anomalous Y and Z components at 0630 and 0700, shown in Fig.(5.1), that this method of removing the normal field eliminates the "level" problem seen on maps of previous separations. In other words, removal of the normal field greatly reduces systematic effects due to the inability to apply the surface integrations over the rest of an infinite plane. Thus the Z_{ia} component appears with nearly equal positive and negative values, while the

ANOMALOUS EASTWARD AND VERTICAL FIELDS AT 06.30 AND 07.00 UT.

CONTOUR INTERVAL = 2.5 GAMMAS

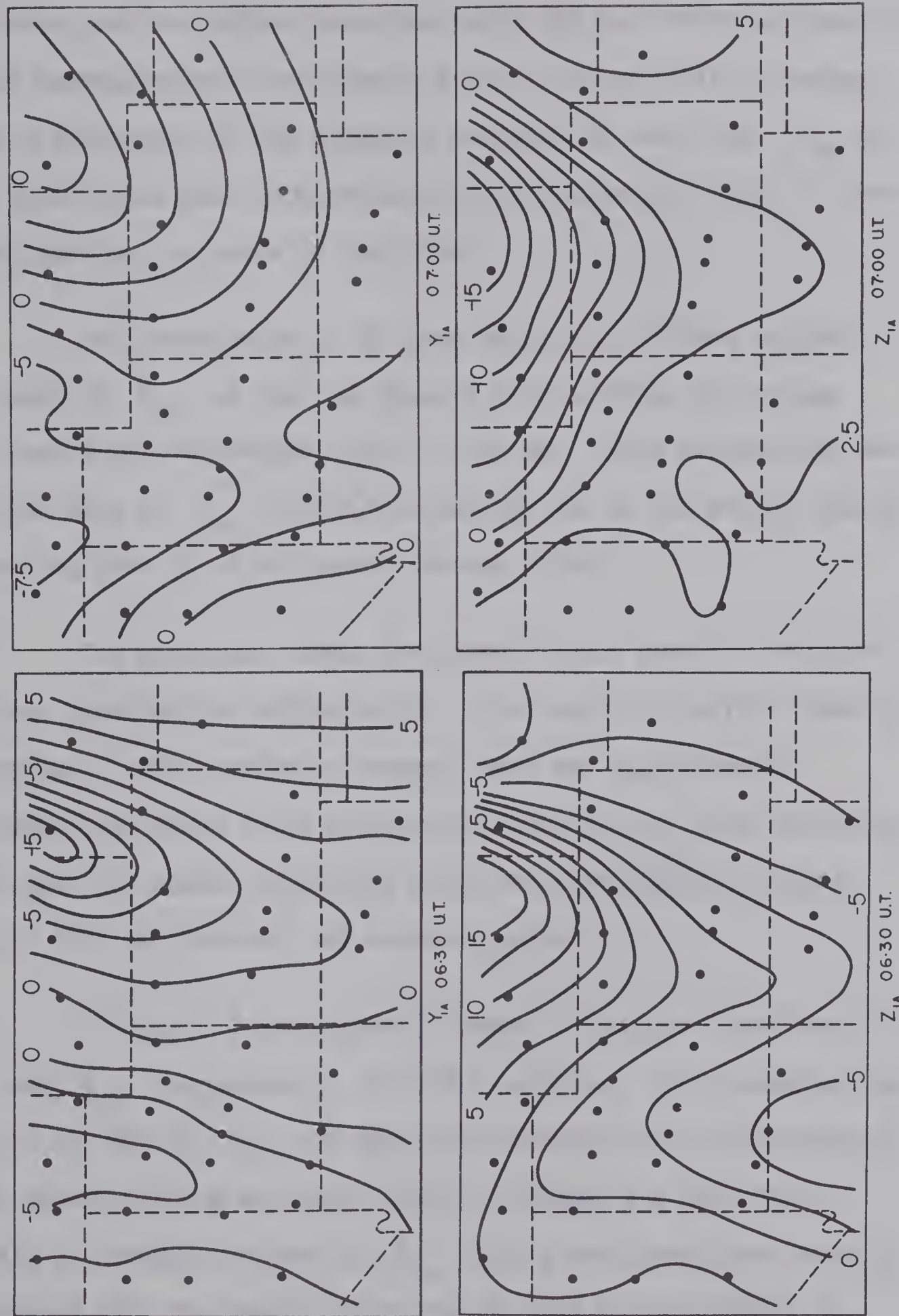


Fig. 5.1

baseline for Y_{ia} at 0630 UT. is near zero. Y_{ia} at 0700 UT. indicates positive values associated with the East Front and negative values associated with the Wasatch Front, thus explicitly showing the two directions of the anomalous currents at this time. Z_{ia} at 0700 again shows that interpretation of the anomalous field in terms of antiparallel currents is justified.

One characteristic of these maps which differs slightly from maps of F_{is} is that the Wasatch Front anomaly now swings more toward the south-west corner of the map. This feature was seen on other maps of Y_{ia} in the time domain, and in the period domain, suggesting that it is not due to an edge effect.

The separated normal horizontal field, found to be quite uniform, provided new estimates of v for each of the four times of separation. These estimates however, were not significantly different from those found previously (Section 4.2), thus indicating again that the normal horizontal field was approximately divided equally into the internal and external parts.

In Fig.(5.2) are shown the maps of the sine transform of the Y_{ia} and Z_{ia} components at $T = 60.2$ minutes. Both anomalies can be seen on the map of Y_{ia} but again the southern part of the Wasatch Front shows a strong east-west trend. Although the East Front anomaly is strongly evident in Z_{ia} only a small amplitude anomaly associated with the Wasatch Front can be seen in the complex Z_{ia}

SINE TRANSFORM OF ANOMALOUS
HORIZONTAL AND VERTICAL FIELDS

$T = 60.2$ MINUTES CONTOUR INTERVAL = 0.5 GAMMAS

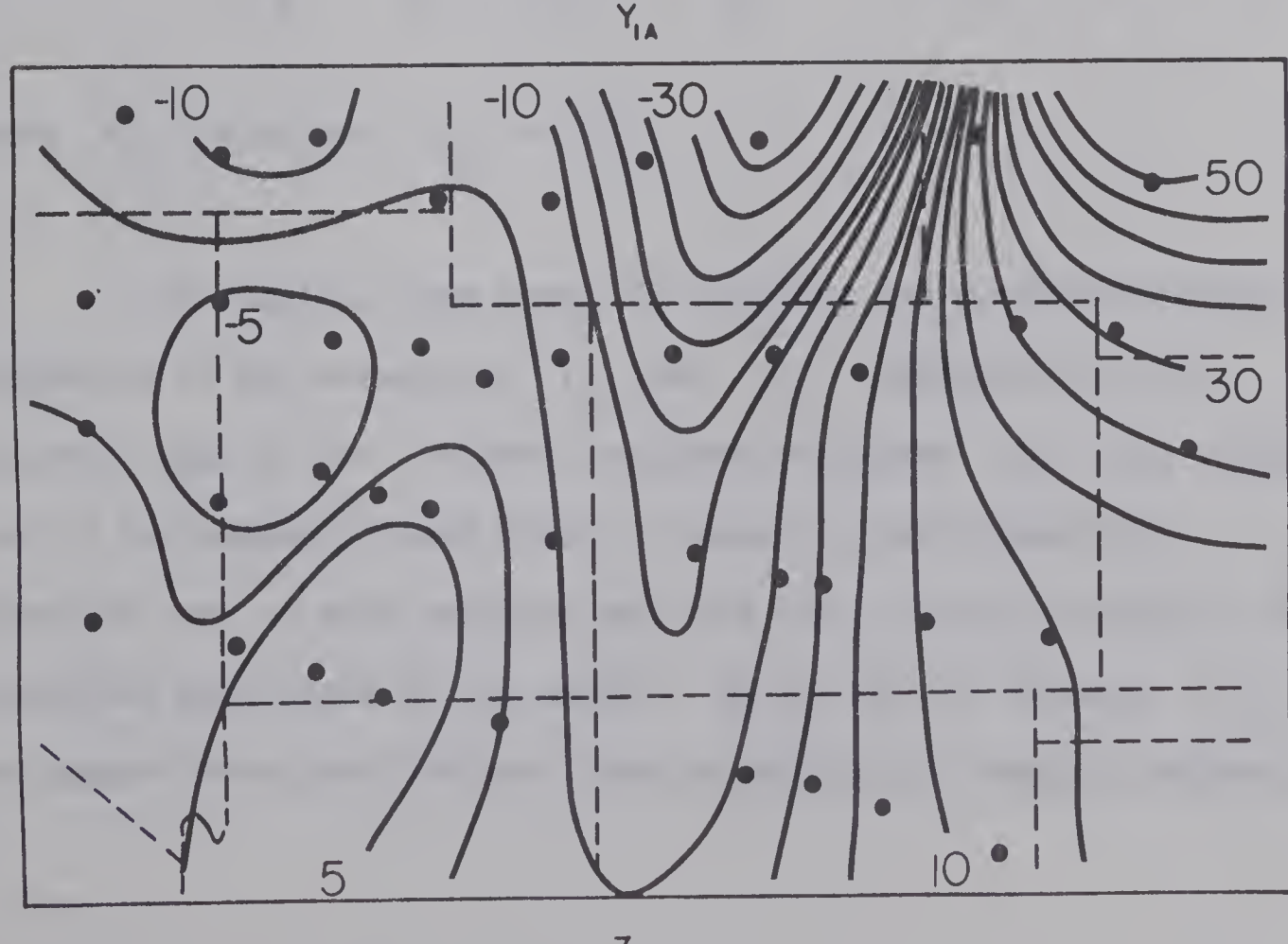
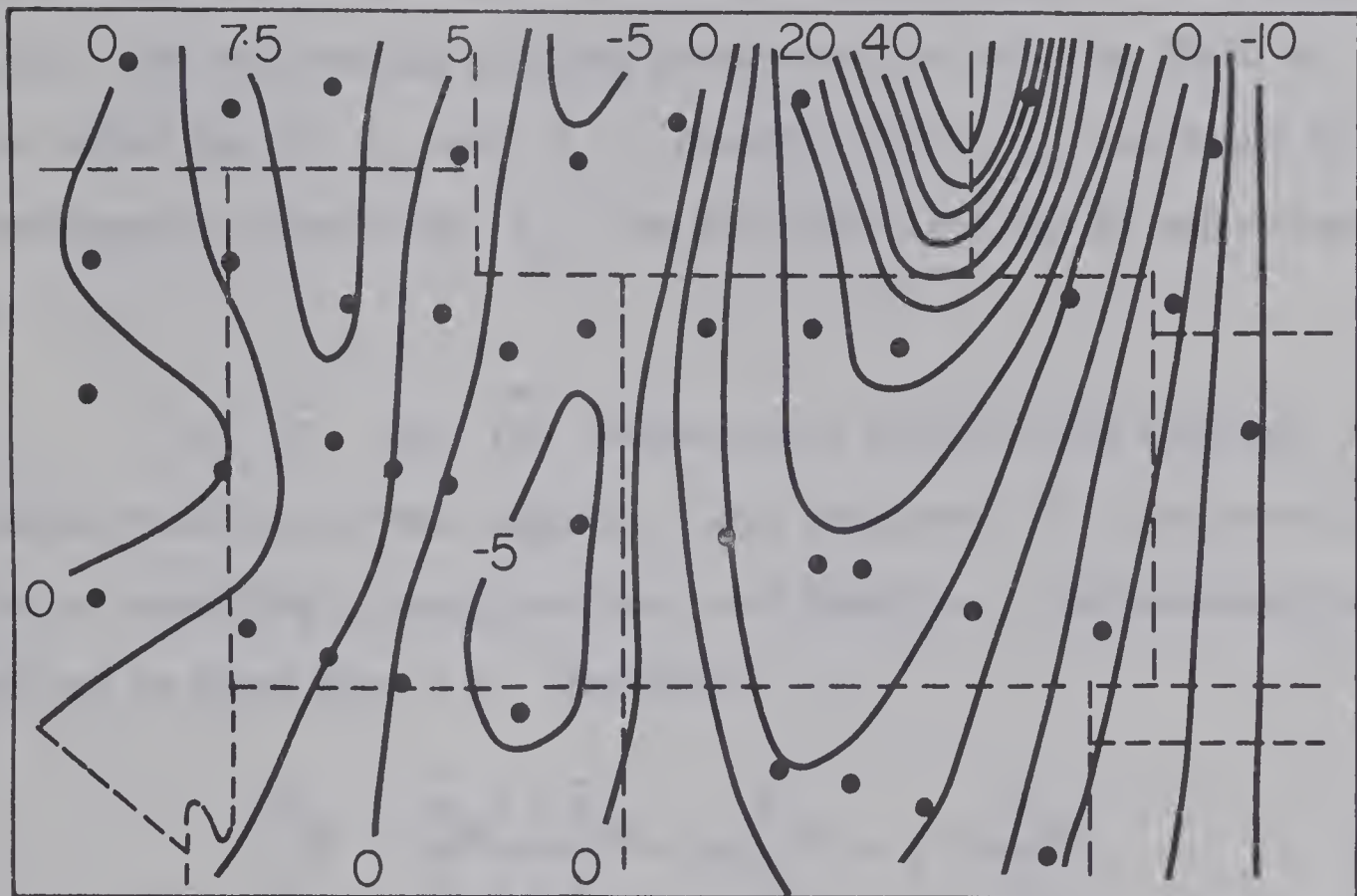


Fig. 5.2

component in that region.

Maps of type shown in Fig.(5.2) are more informative when the anomalous fields have been normalized with respect to the inducing field. For north-south striking conductors the inducing field is the vector sum of Z_n and Y_n . However, since Y_n was found to be considerably larger than Z_n , the inducing field may be approximated by Y_n .

Let $\bar{(F)}$ and $\bar{\bar{(F)}}$ respectively indicate the sine and cosine transforms of any magnetic field component F . The normalized fields consisting of real(in-phase) and imaginary (quadrature-phase) parts and can be found from 5.8. Therefore

$$\frac{F_{ia}}{Y_n} = \frac{\bar{\bar{F}}_{ia} + i \bar{F}_{ia}}{\bar{\bar{Y}}_n + i \bar{Y}_n} = \text{Re}\left(\frac{F_{ia}}{Y_n}\right) + i \text{Im}\left(\frac{F_{ia}}{Y_n}\right) \quad (5.8)$$

where F_{ia} is either Y_{ia} or Z_{ia} .

In Fig.(5.3) are shown the in-phase and quadrature-phase components of the normalized Y_{ia} and Z_{ia} fields at $T = 60.2$ minutes. Maps of the in-phase component represent only that contribution to the magnetic field which is caused by self-induction. Anomalies seen on such in-phase maps are then probably related to deep conductive structures in the mantle. In the map of in-phase Y_{ia} , the Wasatch Front and the East Front anomalies are sharply defined as

NORMALIZED ANOMALOUS INTERNAL FIELDS
 $T = 60.2$ MINUTES CONTOUR INTERVAL = 0.05

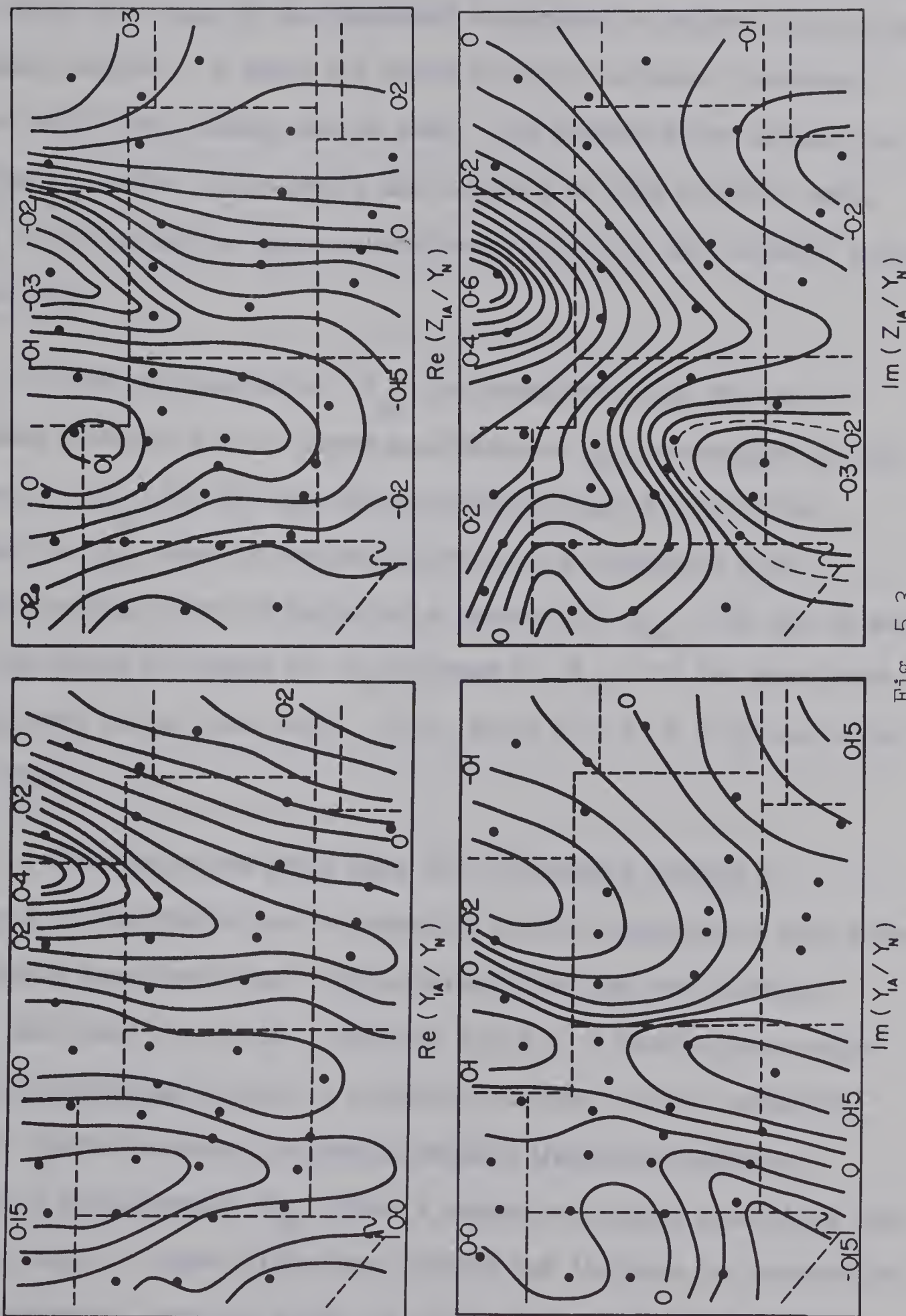


Fig. 5.3

two positive maxima. The resolution of these anomalies is much greater than found from maps of the separated components in either the time or frequency domains. A small but quite distinct east-west component of the East Front anomaly can be seen. The Wasatch Front anomaly is observed to strike north-south, and contrary to some previous maps, there is no indication that the southern portion of this anomaly swings to the west.

The in-phase map of Z_{ia} is consistent with the map of anomalous eastward field. Large gradients in Z_{ia} correspond to the maximum of Y_{ia} for the East Front anomaly, while the positive maximum in Z_{ia} west of the Wasatch Front, is consistent with a current flowing under the region of a maximum of Y_{ia} . It can be seen that the ratios of (range of Y_{ia})/(range of Z_{ia}) for the East Front anomaly give values near unity. (i.e. about 0.75 to 1.0 in the center of the map.)

The quadrature-phase maps will in general contain a component of the fields due to induction in the upper-mantle structures, since these structures have finite conductivity and the anomalous fields must lead the normal (inducing) field by a finite phase angle. In addition they may contain a contribution from crustal conductors at small depths in which resistance exceeds inductive reactance. The map of out-of-phase Y_{ia} shows a resistive anomaly associated with the East Front. Phase differences between the in-phase and quadrature-phase components computed along the crest of the East Front anomaly

near the center of the map vary from about 21° to 35° . A representative phase difference between the anomalous and normal fields is thus found to be about 30° .

The situation is less obvious for the Wasatch Front. However in the south-west quadrant of the map the quadrature-phase shows a positive and negative maximum on the east and west sides respectively of the Wasatch Front. Part of this quadrature-phase anomaly could represent a current, perhaps near the surface, flowing under the maxima of these peaks, though such an interpretation is highly speculative. Nevertheless the observed quadrature-phase induction in this region of the map is responsible for the observed westward trend of the southern portion of the Wasatch Front seen on previous maps, and of the general complication of its characteristics.

This very qualitative explanation is verified by the negative maximum in the quadrature-phase of Z_{ia} concentrating near the southern part of the Wasatch Front. A current flowing along the 0.20 contour in this map qualitatively gives the observed patterns in the quadrature-phase of both the Y_{ia} and Z_{ia} components.

5.2. Types of Anomalies

Local anomalies in geomagnetic variations can often be accounted for by one of three types of conductive structures (Schmucker 1964):

1. Superficial anomalies caused by high conductivities in near surface rocks. These may be related to deep basins of porous sediments saturated with electrolytic solutions. For such conductors ohmic resistance is usually more important than self-induction and thus large phase differences between the normal and anomalous fields are observed.

2. Intermediate anomalies associated with highly conductive bodies buried in a "non-conducting" region between the surface layers and the mantle.

3. Deep anomalies resulting from undulations in a conducting medium of large extent. Because of the relation between conductivity and temperature, this type of model is suitable for deep conductive structures in the Earth. The surfaces of equal conductivity may in fact be isothermal surfaces. For an undulation of this type to produce significant anomalous variations at the earth's surface, the shielding effect of the surface layers must be small for the frequency chosen, and the amplitude of the undulation must be comparable to the depth of the highly conducting substratum. For deep structures of large extent and high conductivity the currents are controlled by self-induction rather than resistance, and the phase difference between normal and anomalous fields will be rather small.

The general correspondence between our induction anomalies and the heat-flow distribution (Reitzel et al., 1969) and the

inability of superficial conductors to account for the small observed phase differences between the normal and anomalous fields, or for the fact that our conductive structures cause anomalies in the daily variation field (Reitzel et al., 1969), suggest that our results should be interpreted in terms of deep anomalies.

For interpretation of anomalies by means of upheavals in the mantle, it can be seen that neither a line current nor a two-dimensional dipole, resulting from induction in an isolated cylinder, are physically realistic, since the former allows for no return current, while the latter postulates two anti-parallel currents in the hump. In reality, the anomalous fields are a second order effect superposed upon the much larger normal fields. We can therefore think of the current concentration of the elevated portion of the upheaval as approximated by a line current, and the dilution of current density on either side of the upheaval as corresponding to return currents of opposite polarity. These current reductions can be regarded as equivalent to a return current along their geometrical center, under the forward current. In the particular case of a semi-cylindrical upheaval of infinite conductivity, the effective return currents are equivalent to an image of the forward current in the upheaval (Rikitake and Whitham 1964), so that the half-cylinder has the same induction response as a conducting cylinder embedded in an insulator and so produces the field of a two-dimensional dipole Fig.(5.4).

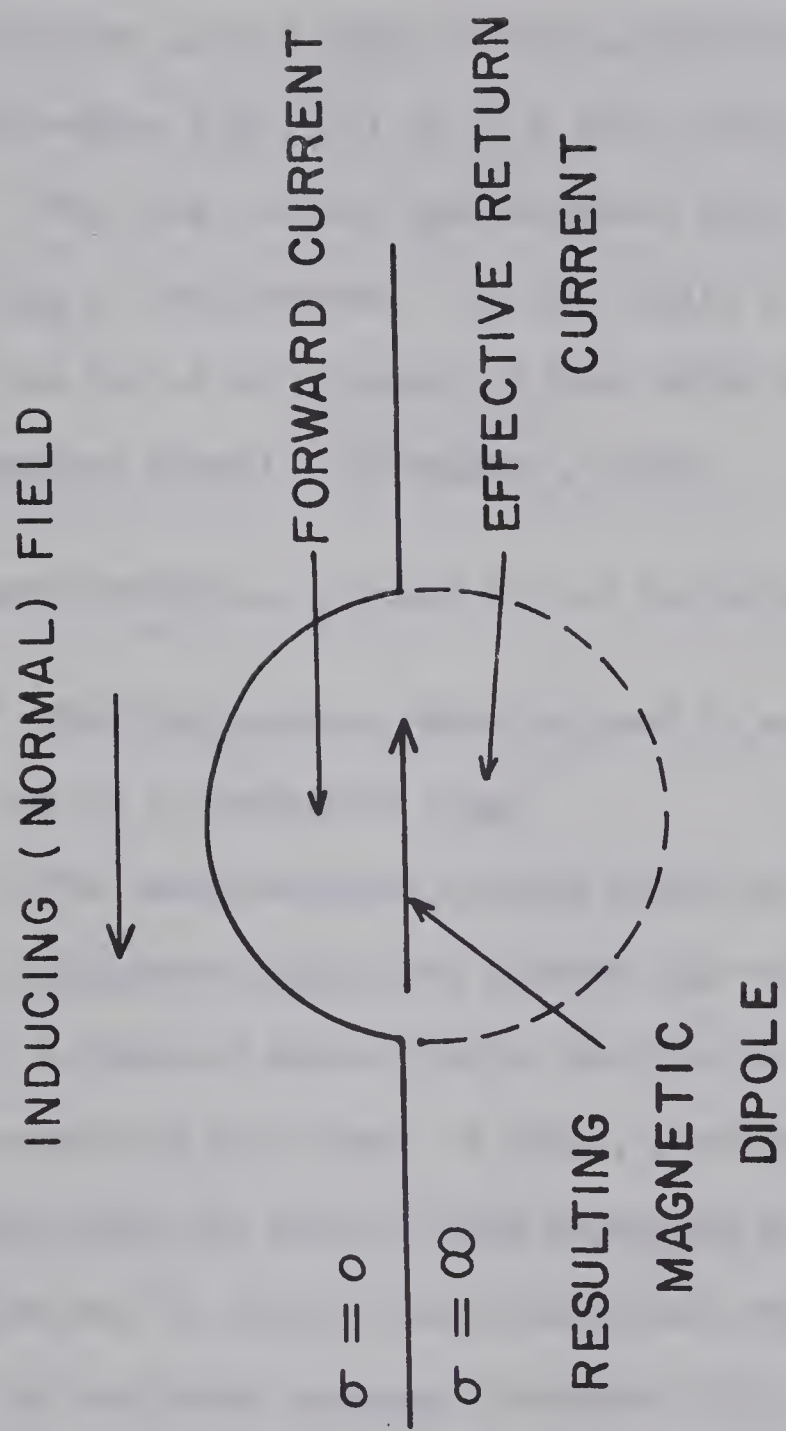


Fig. 5.4

If a real structure approximates a semi-cylinder on the surface of a perfect conductor, its field can be approximated either by a line of dipoles at the depth of the undisturbed surface of the conducting half-space Fig.(5.4) or by a line current near the top of the upheaval. The line current approximation thus gives a maximum depth to the top of the upheaval. In the limit, a line current will appear along the top of an upheaval of zero width and infinite height (edge of a vertical sheet). (Schmucker, 1959).

A model study may proceed in the following steps:

- (i) The line current model is used to estimate maximum depth to the top of a conductive ridge.
- (ii) The two-dimensional dipole model is used to estimate depth to the undisturbed conductive surface near the ridge.
- (iii) A ridge of semi-circular section on the surface of a perfectly conducting half-space is tried, starting with depth and radius estimated from (i) and (ii) and adjusting either to improve the fit. Fields due to such a half-cylindrical ridge can be computed by the method of conformal mapping (Schmucker 1964).
- (iv) Asymmetrical anomalies can be fitted by a step in the surface of the half-space, if necessary combined with a half-cylinder.
- (v) Once the dimensions of the required conducting ridge are established, the phase difference between the normal and anomalous field can be used to estimate the true, finite conductivity.

These five steps are followed in the paper by Porath, Oldenburg and Gough (1969).

Although in this thesis the results of the whole process are reported, only steps (i), (ii) and (v) are considered in detail, since the writer did not contribute to steps (iii) and (iv).

LINE CURRENT

The line current model is shown in Fig.(5.5(a)). The magnetic components are

$$H_x = \frac{Iz}{2\pi R^2} \quad H_z = \frac{Ix}{2\pi R^2} \quad (5.9)$$

Depth estimates to the line current are found by solving the two equations $H_x = \frac{1}{2} H_x \text{ max}$ and $\partial H_z / \partial x = 0$
Both equations are solved when $x = \pm z$.

CONDUCTING CYLINDER IN A HARMONICALLY VARYING FIELD

The model for induction within an isolated cylinder by a harmonically varying field is shown in Fig.(5.5(b)). The anomalous induced fields (Ward, 1967; and Kertz, Upper Mantle Symposium, 1964) are

$$H_x = \left[\frac{L}{r^2} (\cos^2 \phi - \sin^2 \phi) \right] e^{-i\omega t}$$

$$H_z = \left[\frac{2L}{r^2} \sin \phi \cos \phi \right] e^{-i\omega t}$$

$$L = -R^2 (M+iN) H_0 \quad (5.10)$$

LINE CURRENT MODEL

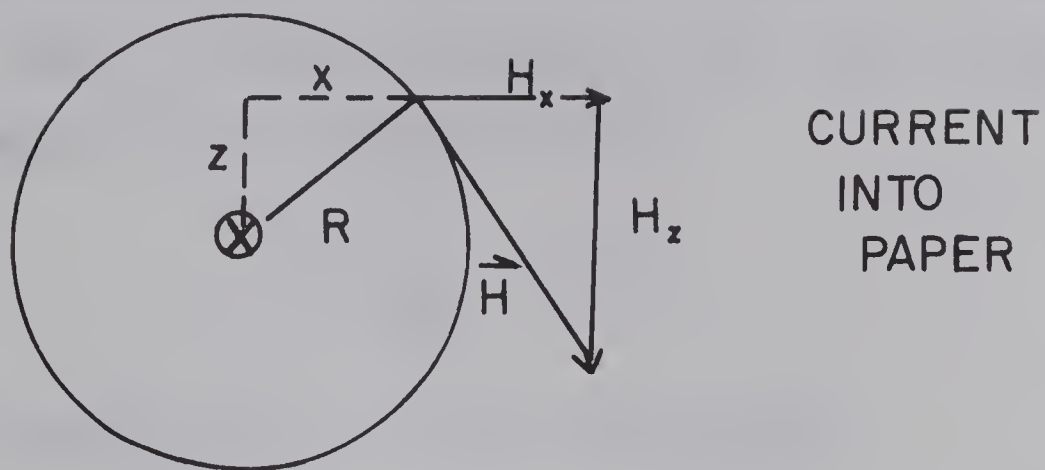


Fig. 5.5(a).

CYLINDER MODEL

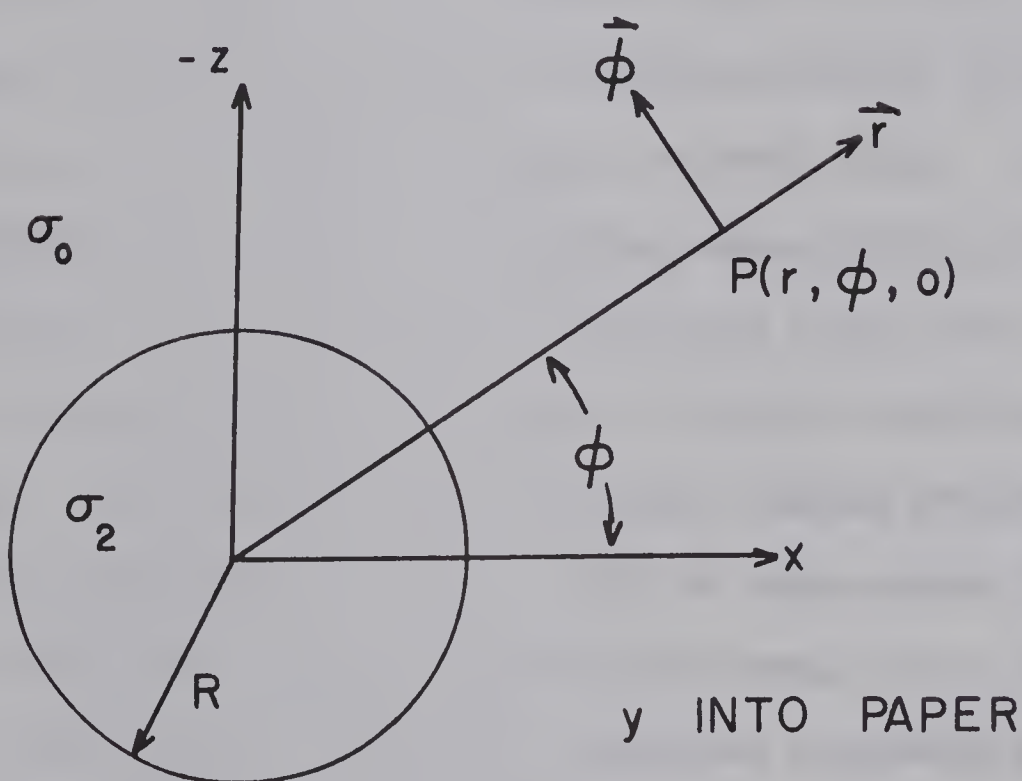


Fig. 5.5(b)

where L is the dipole momentum of the two-dimensional dipole. M and N are respectively the in-phase and quadrature phase of the anomalous field. A plot of the induction parameter, $\theta = \sqrt{4\pi\sigma\omega} R$, versus M and N is found in Rikitake, p.200. From (5.10) the depth relation from the horizontal field is

$$z = \frac{\pm x}{\sqrt{\sqrt{5}-2}} \approx 2.04 x$$

while the relation from the vertical field becomes

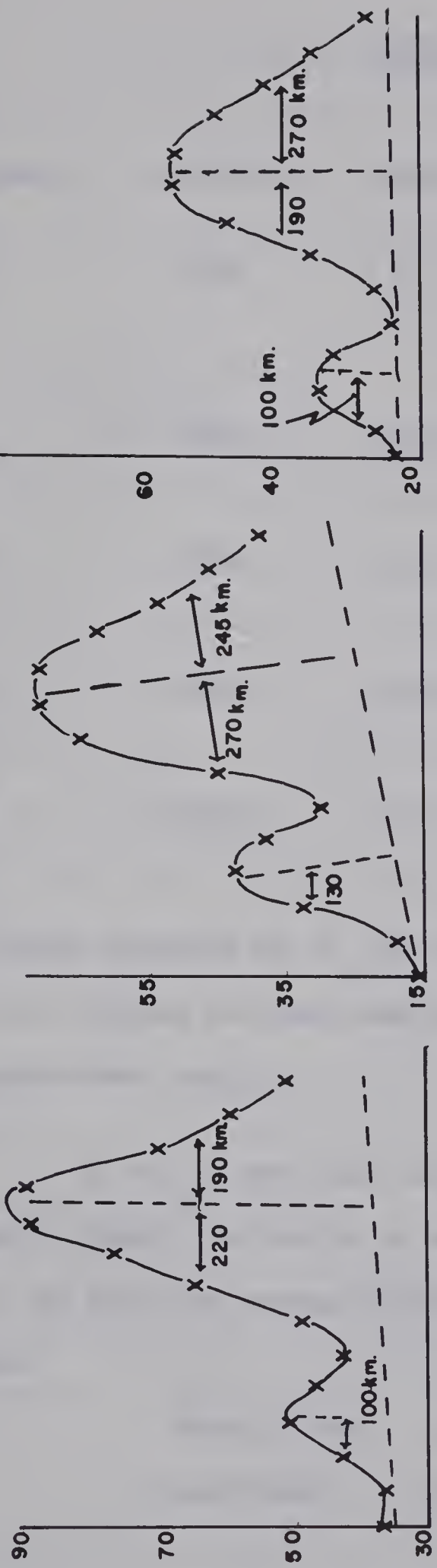
$$z = \pm\sqrt{3} x$$

Since the separation procedure gave average values for the internal components over a square, it was believed that the anomalies could be made more distinct by subtracting smoothed external values of the field at each station from the original recorded values. See Fig.(4.4). Depth estimates were obtained from graphs, shown in Fig.(5.6), of the separated unnormalized magnetic variations along three centrally located east-west profiles on the maps of the sine transform of Y_I and Z_I at 60.2 minutes. The north-south spacing between these profiles was approximately 175 km. Since in these graphs the anomalous fields were not isolated from the normal field, depth estimates were obtained only after a baseline, representing some portion of the normal field, was drawn.

Depth estimates of the line currents associated with the East Front and Wasatch Front anomalies are given in Table 5.1.

DEPTH ESTIMATES FROM UNNORMALIZED FIELDS

HORIZONTAL COMPONENT



VERTICAL COMPONENT

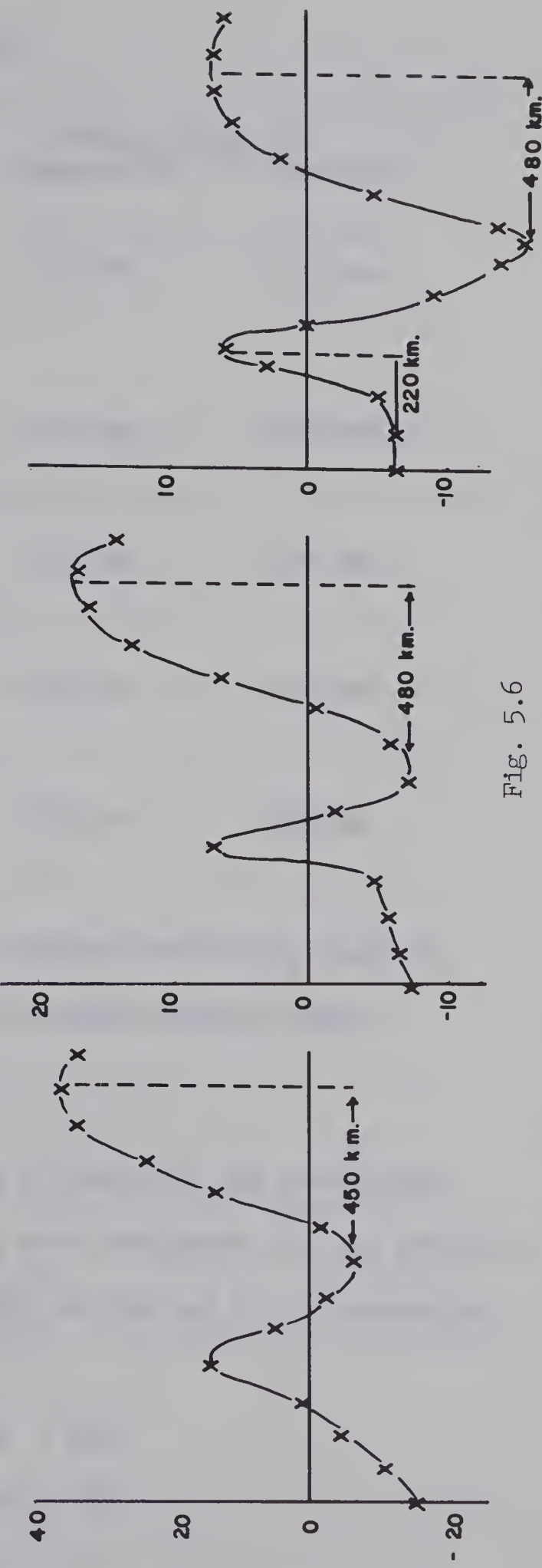


Fig. 5.6

TABLE (5.1)

Component	Transform	Period	Average Depth To Wasatch Fr. East Fr.	
Y_I	SINE	60.2	115 km.	225 km.
Z_I	SINE	60.2	125 km.	230 km.
Y_I	SINE	30.1	90 km.	240 km.
Z_I	SINE	30.1	110 km.	215 km.
Y_I	COSINE	60.2	105 km.	230 km.

The cosine transform of Z_I at 30.1 minutes and of Y_I and Z_I at 60.2 minutes were not used since the amplitudes of these components were small.

It can be seen that estimates of depth of the postulated currents, though qualitative in nature, are consistent for all profiles taken, and that the average maximum depth to the top of the anomalies becomes

Wasatch Front 110 km. \pm 20%

East Front 230 km. \pm 20%

It was found that depth estimates from similar profiles on maps of the sine and cosine transforms of Z_{ia} and Y_{ia} and on maps of $\text{Re}(Z_{ia}/Y_n)$ and $\text{Re}(Y_{ia}/Y_n)$ also gave maximum depths of the line current which were within the limits of the previous estimates.

5.3 . Conductivity Models:

Modelling of the upper mantle conductivity structure was carried out by fitting the observed anomalous fields to the responses of perfectly conducting upheavals and step structures of various dimensions. (Porath et al. 1969). Once the dimensions of the upheaval have been found, the conductivity can be estimated from the maximum amplitude of the normalized anomalous field, and the phase difference between this field and the normal field. Although quantitative model studies were not carried out in this thesis, the dimensions of a model used by Porath (Porath, Oldenburg and Gough, 1969) in analysis of separation of the transform components at $T = 89$ minutes, will be used to estimate the conductivity. It was found that profiles over the East Front anomaly of the in-phase normalized Y_{ia} component at $T = 60.2$ minutes closely resembled that of Y_{ia} obtained by Porath et al. at $T = 89$ min. Dimensions of the East Front anomaly should therefore be approximately valid for results at $T = 60.2$ minutes.

In Fig.(5.7) the calculated Y_{ia} field at $T = 89$ minutes from the model is shown to be in good agreement with the observed

T=89 MINUTES

Y_{1a}

x CYLINDER SOUTHERN ROCKIES
 • CYLINDER WASATCH FRONT
 o STEP WASATCH FRONT

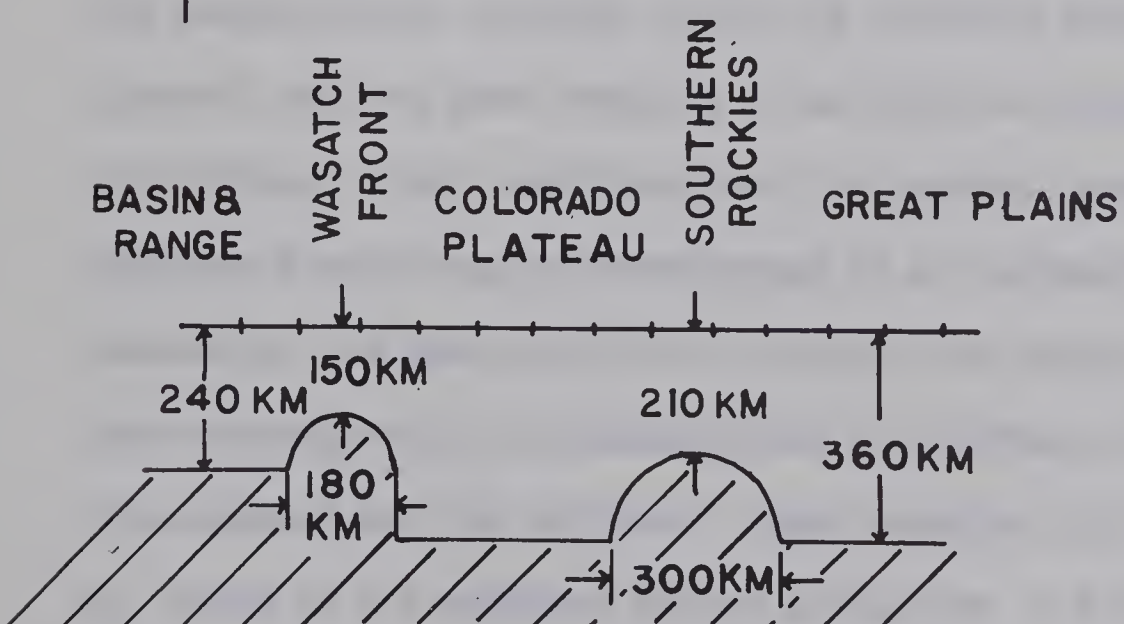
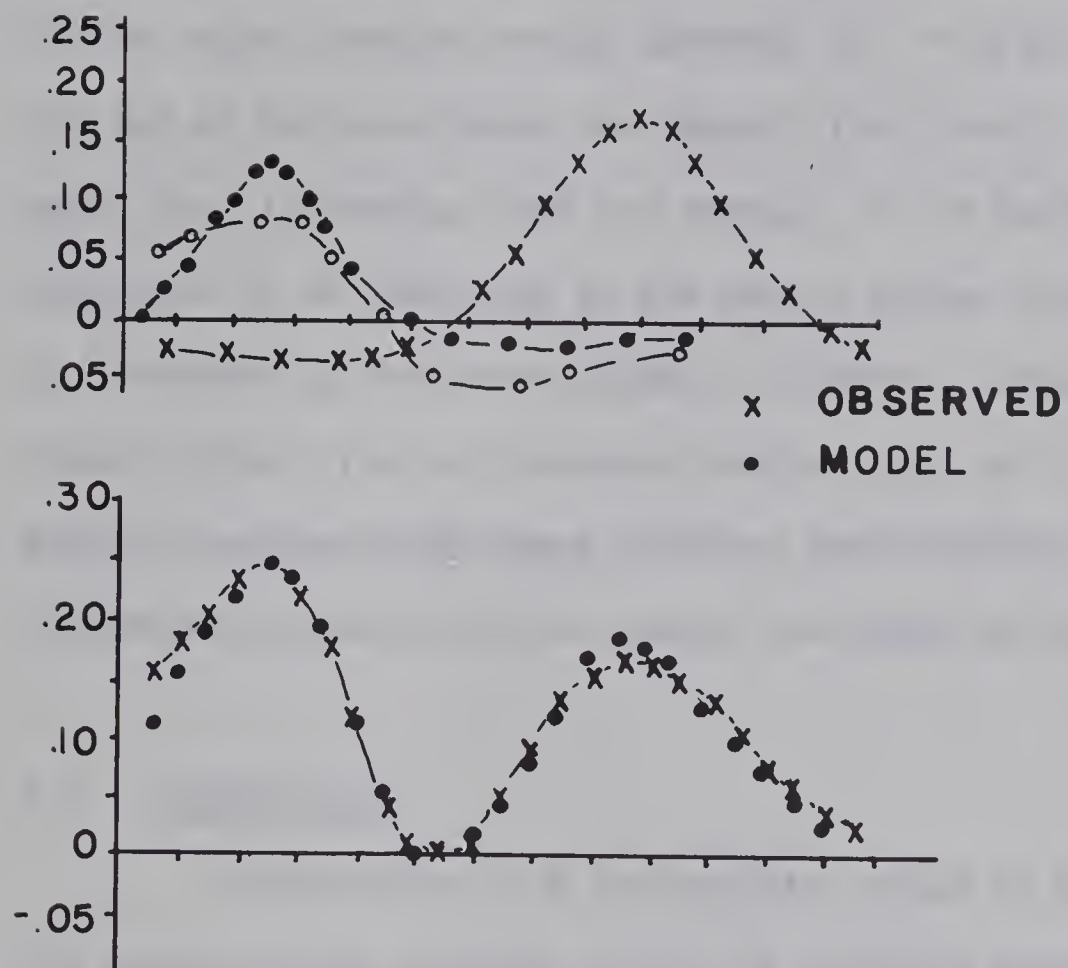


Fig. 5.7

field. The model consists of a semi-circular upheaval $R_1 = 150$ km. and $z = 360$ km. associated with the Southern Rockies, while the anomalous field over the Wasatch Front was approximated by a step of 120 km. with a semi-circular upheaval ($R_2 = 90$ km., $a = 240$ km.) on the top of the step under the Wasatch fault belt. The fit is quite good, thus indicating that the anomaly of the Southern Rockies can be explained by an upwelling in the mantle rather than a step as supposed by Schmucker in the Texas anomaly. However, Schmucker's Texas anomaly should differ from our Southern Rockies one, as it is at the eastern edge of the Basin and Range Province and therefore may well resemble the Wasatch Front structure rather than that of the Southern Rockies.

5.4. Conductivity

Calculation of a conductivity value is most convenient for the semi-circular upheaval under the Southern Rockies. Such an upheaval has the same response as an isolated cylinder (Rikitake and Whitham, 1964), and therefore the magnetic response of the Southern Rockies can be represented by an "effective" cylinder located at the same depth ($z = 360$ km.) and having a radius R , such that the magnetic field measured at the surface is the same from both the upheaval and the cylinder. From equation (5.9) the normalized H_x field of the cylinder at the surface at $\phi = 90^\circ$ is

$$\frac{H_x}{H_0} = \frac{R^2}{z^2} (M + iN) \quad (5.11)$$

and this must be the same as the measured anomalous field

$$W_{ia} = Y_{ia}/Y_n$$

$$W_{ia} = \frac{R^2}{z^2} (M + iN) \quad (5.12)$$

The radius of the cylinder is then found by using only the real part of (5.12), i.e.

$$R = z\sqrt{W_{ia}/M}$$

Consider a phase difference of 30° . Then $M/N = 1.73$, and the induction parameter $\theta = 3.6$ e.m.u. For the Southern Rockies $M = 0.6$, $z = 360$ km. and $W_{ia} = 0.175$ (Fig. 5.6). Therefore

$$R = 195 \text{ km.}$$

$$\sigma \sim 2 \times 10^{-12} \text{ e.m.u.}$$

Experimental data on the relation between electrical conductivity and temperature in upper-mantle materials show considerable dependence on the composition assumed, and require extrapolation to reach the conductivity estimate just given. For reasonable fayalite concentrations the temperature will lie in the vicinity of 1500°C . (Hamilton 1965). Clarke and Ringwood (1964) give this temperature at depth 350 km. under a continental shield. This is consistent with the depth to the unperturbed conductor under the Great Plains in our model. Further discussion of the relations between temperature, conductivity, and geothermal and geomagnetic deep sounding anomalies,

is given by Reitzel, Gough, Porath and Anderson (1969) and by Porath, Oldenburg and Gough (1969).

CHAPTER VI

MORPHOLOGY OF THE SUBSTORM

The mid-latitude magnetograms shown in Fig. (4.1) represent a complex variational field which is composed of a superposition of the effects of individual magnetic substorms occurring in the auroral zone. If these magnetograms are decomposed, so that the effects of individual magnetic substorms are isolated, then the characteristics of the individual substorms can be compared with characteristics of the external magnetic field found previously by the separation of the surface field into internal and external parts.

The magnetic perturbations associated with auroral substorms are caused by intense currents flowing mainly in the auroral zone in the region of magnetic midnight. Bonnevier et al. (1969) have suggested that the currents associated with a polar magnetic substorm may be represented by a three-dimensional current model shown in Fig.(6.1). The currents (labelled 1, 2, 3 in the diagram) are respectively: a current flowing downward along a geomagnetic field line into the ionosphere, an intense westward electrojet, and a return field-aligned current. The closed loops extending outward from the westward electrojet are parallel to the earth's surface, and represent magnetic equipotentials. The gradient of this is the horizontal magnetic variation field on the surface below. Although

MAGNETIC SUBSTORM

POSSIBLE CURRENTS ASSOCIATED WITH POLAR

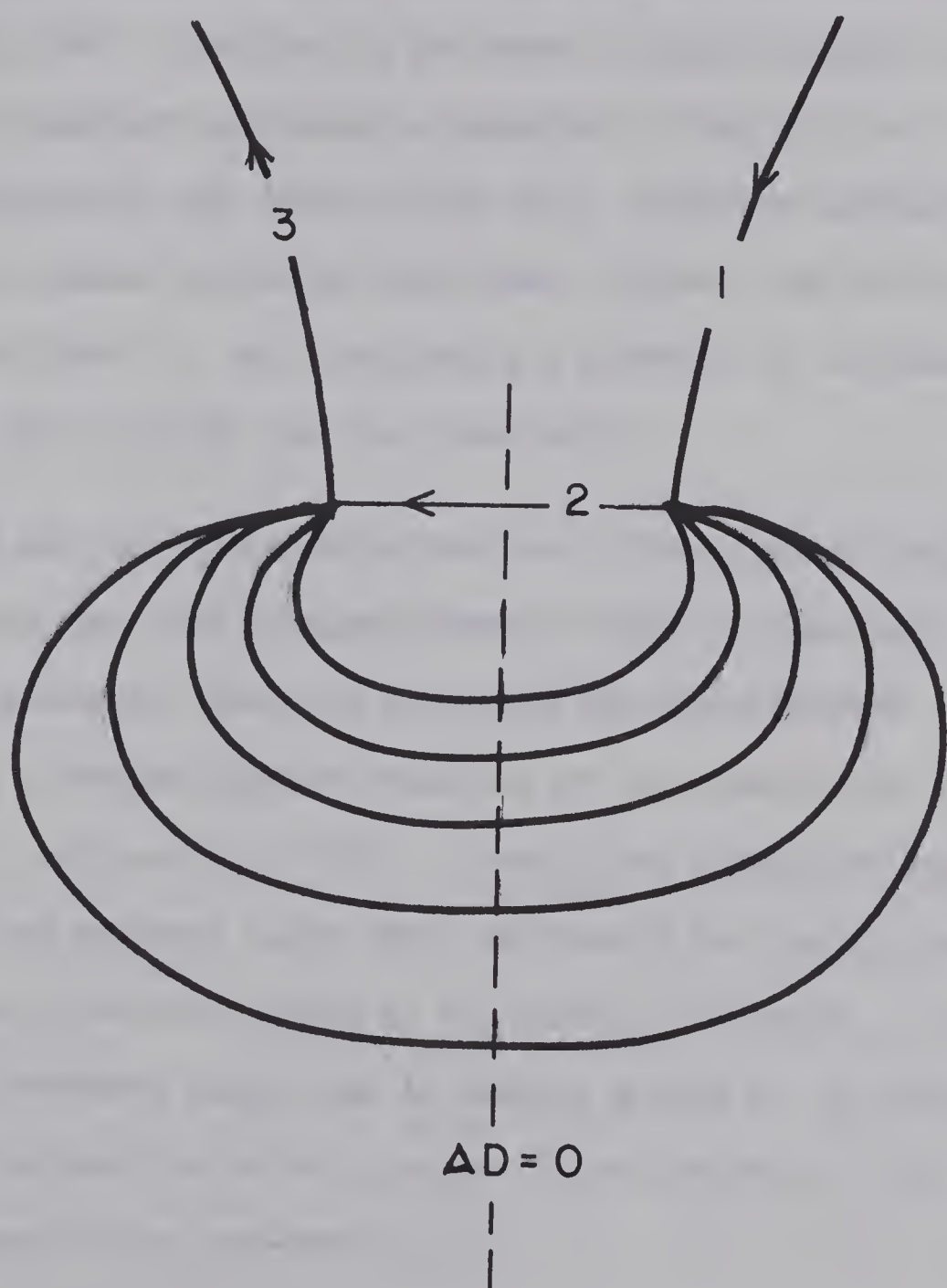


Fig. 6.1

the current model in Fig.(6.1) is an obvious simplification of the real physical situation, it has been shown by Bonnevier et al. that this model satisfies the gross characteristics of the observed magnetic perturbation field of an individual polar magnetic substorm.

The line $\Delta D = 0$ in Fig.(6.1) is known as the demarcation line (Rostoker, 1966). Stations to the west of this line will observe a positive D component bay, while a negative D bay will be observed by stations to the east of this line. Rostoker has shown that due to the spatial motion of the current system, some stations exhibit a transitional D bay, indicating a movement of the demarcation line from east to west over the observatory.

There are two contributing factors to this type of transition bay. The auroral oval is approximately fixed in space with respect to the sun-earth line, and therefore the earth rotates under this oval giving an apparent velocity of the demarcation line of about 0.4 km. per second at 45°N . In addition, transition bays are related to the westward surge which represents the leading edge of the ionospheric current flowing in the auroral electrojet. The velocity of the westward surge that is usually quoted (~ 1 km./sec.) is the sum of the rotation effect plus the actual velocity of the surge with respect to the sun-earth line.

The characteristics of a magnetic substorm vary with geomagnetic latitude. Magnetic perturbations in the auroral zone,

where the effects of the electrojet are dominant, are characterized by large negative H bays, and by positive Z bays to the north and negative Z bays to the south of the electrojet.

In mid-latitudes, the nearly vertical field-aligned currents contribute greatly to the horizontal perturbation field, causing a positive peak in the ΔH perturbation to the south of the intense negative peak associated with the electrojet. At mid-latitudes one may therefore expect positive H bays and negative Z perturbations (since the Z perturbation is caused only by the auroral electrojet).

Rostoker (1968) has claimed that the onset of a polar magnetic substorm is always accompanied by at least two distinct Pi 2 micropulsations. Onset times for such a substorm may then be obtained from either the rapid run or field magnetograms which clearly display these micropulsations.

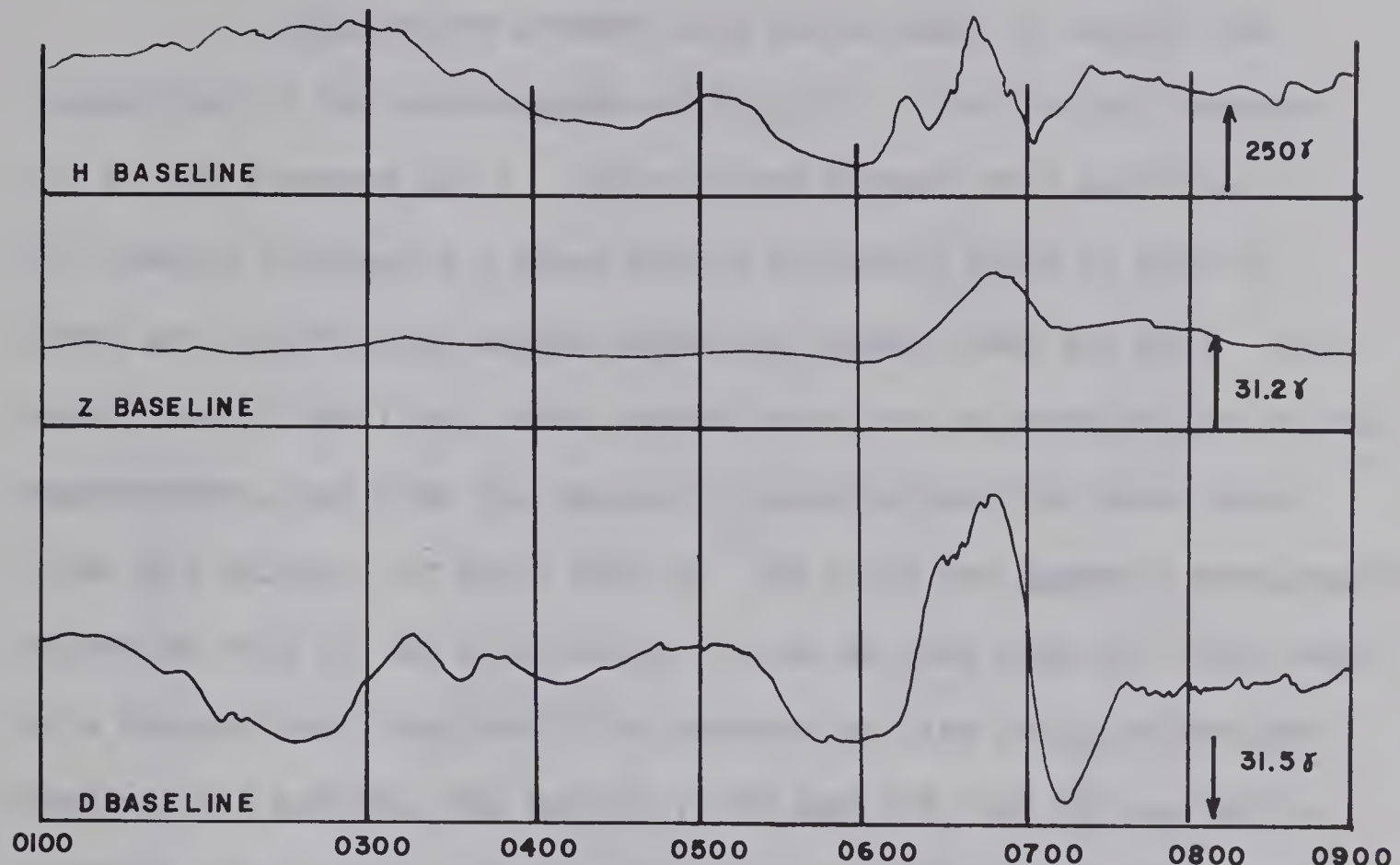
Table (6.1) is a listing of stations, with their geographic and geomagnetic coordinates, used to study the morphology of the substorm of September 1. The magnetogram from BOU, an observatory very close to LYO in our array, is shown in Fig. (6.2). Unfortunately the substorm which was analysed only from 0500 - 0830 UT, started about 0115 UT with a relatively large component of Dst. This storm time variation continued until about 0715 at which time the magnetic traces began to recover to an undisturbed position. Superposed upon

TABLE (6.1)

STATION	ABBREV	GEOGRAPHIC				GEOMAGNETIC	
		LAT		LONG		LAT	LONG
BARROW	BAR	71°	18'	W	156° 45'	69.7°	247.0°
COLLEGE	COL	64°	52'	W	147° 50'	64.9°	260.3°
SITKA	SIT	57°	04'	W	135° 19'	59.8°	276.6°
BAKEK LAKE	BAK	64°	18'	W	96° 00'	75.1°	320.4°
FORT CHURCHILL	FTC	58°	30'	W	94° 12'	70.0°	326.0°
GT. WHALE	GTW	55°	17'	W	77° 46'	68.2°	353.8°
MEANOOK	MEA	54°	37'	W	113° 20'	62.5°	301.2°
VICTORIA	VIC	48°	31'	W	123° 25'	53.9°	292.6°
NEWPORT	NEW	48°	30'		117° 14'	53.7°	298.7
AGINCOURT	AGI	43°	47'	W	79° 18'	57.2°	350.1°
BOULDER	BOU	40°	02'	W	105° 15'	49.3°	315.6°
TUCSON	TUC	32°	15'	W	110° 50'	39.7°	311.4°
DALLAS	DAL	32°	47'	W	96° 48'	43.4°	326.9°
LEIRVOGWER	LEI	64°	11'	W	21° 42'	66.6°	71.2°

MAGNETIC COMPONENT H, D AND Z

BOULDER, COLORADO SEPT. 1, 1967



H COMPONENT LEIRVOGUE

SEPT 1, 1967

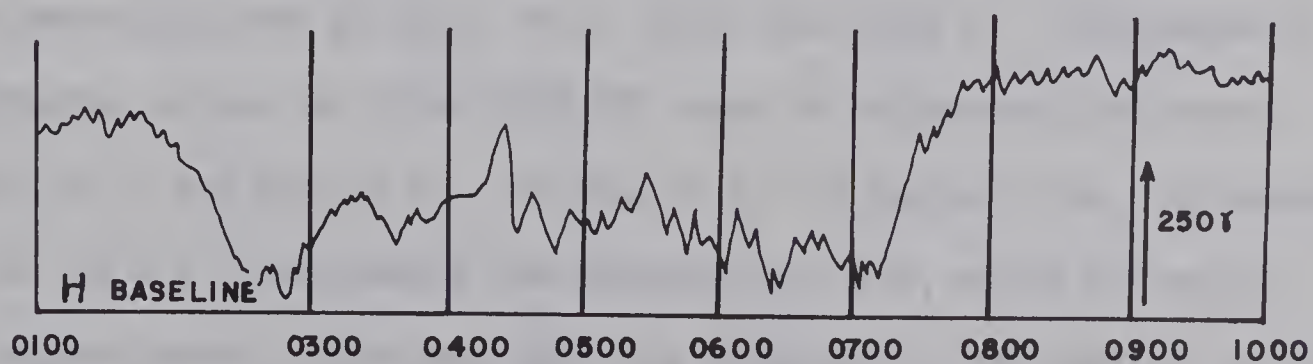


Fig. 6.2

the Dst. variations are separate substorms exhibiting characteristics associated with the current model in Fig.(6.1).

A qualitative attempt will now be made to explain the composition of the magnetograms of Fig.(4.1). The initial decrease in H and increase in D, which occurs between 0500 and 0600 on all traces, represents a decay from a disturbed state at 0500 UT. There are two separate events occurring between 0600 and 0645. The onset time of the first event, established from micropulsations on the magnetograms, and from the rapid-run magnetograms from Great Whale River and Ralston, is about 0605 UT. By using the magnetic perturbation values at 0600 UT. as a reference, it can be seen that the first event is a transitional D-bay with the demarcation line lying between the stations CAS and SWE, WAL and CRA, MOA and CIM, and KAY and GCC on profiles one to four respectively. The D variation begins negatively east of this line, and positively at stations to the west.

The magnetograms from stations listed in Table (6.1) were hand-digitized at 0600, 0615, 0622, and 0630 UT. The magnetic variations, ΔD and ΔH (with 0600 UT. used as reference) are shown in Fig.(6.3) and Fig.(6.4). In Fig.(6.3) the dashed line, corresponding to $\Delta D = 0$, represents the demarcation line, while the solid line approximately coincides with the location of the current in the auroral zone. Values of ΔD at SWE and CAS have also been plotted on the map at 0615 to show that the demarcation line does lie

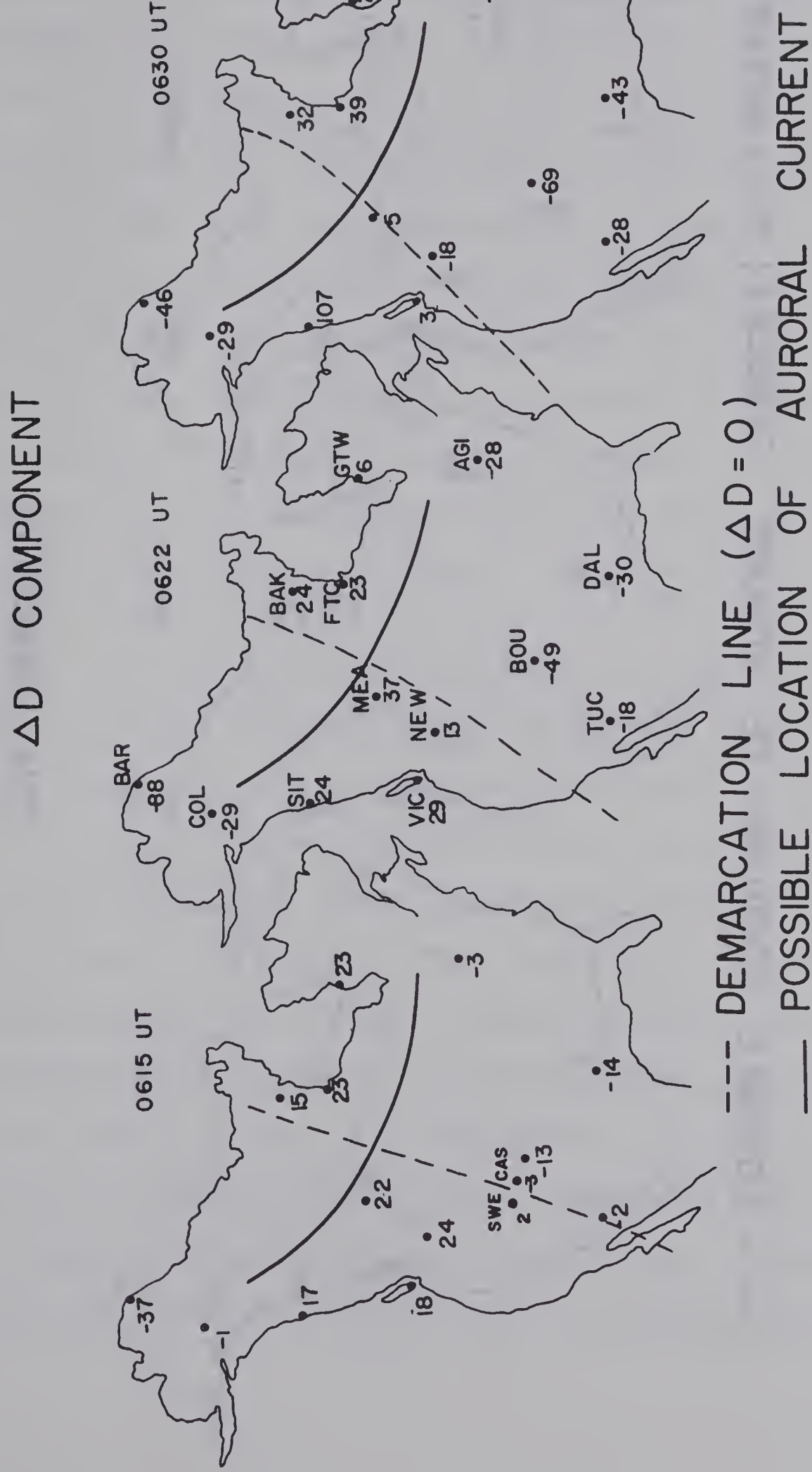
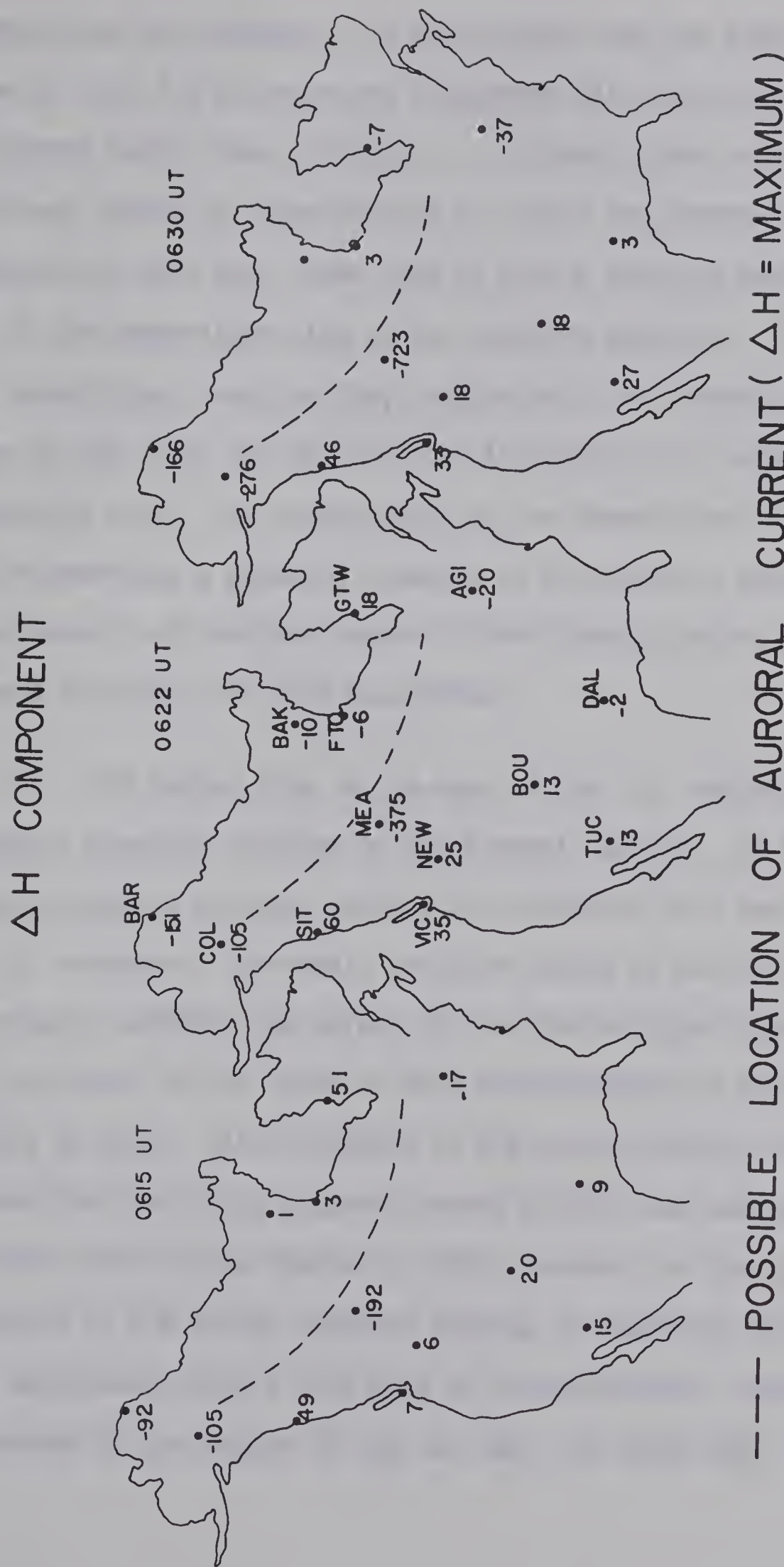


Fig. 6.3



between these two stations. It can be seen that the signs of the values of ΔD for all maps are consistent with those expected from the current model shown in Fig.(6.1). Although there is not a sufficient number of observatories to locate the demarcation line accurately on each map, these maps do show a definite westward movement of the demarcation line as the substorm develops. The development of a transitional D-bay at NEW, coupled with the increasing negative values at BOU, TUC, and DAL are also indicative of a westward moving demarcation line. The intersection of the demarcation line and the line representing a probable location of the current, which should approximately indicate the center of the current system, also shows a westward movement with time toward MEA.

The dashed line on the maps of the ΔH variations (Fig.6.4) indicate a possible location of the auroral current. It can be seen that the location for this current is consistent with that given by the ΔD component. The small positive values at BAK, FTC, VIC, and NEW probably indicate the effect of the field-aligned currents. The large positive ΔH at GTW at 0615 has decreased by 0622 and is negative at 0630. With reference to the current model, this may indicate that the field aligned current at 0615 was east of GTW and has moved west of this station by 0630; however, in view of the complexity of the actual currents causing the magnetic perturbation, a large uncertainty exists with such an interpretation. Nevertheless an increase in the values of ΔH at MEA at 0622 and 0630

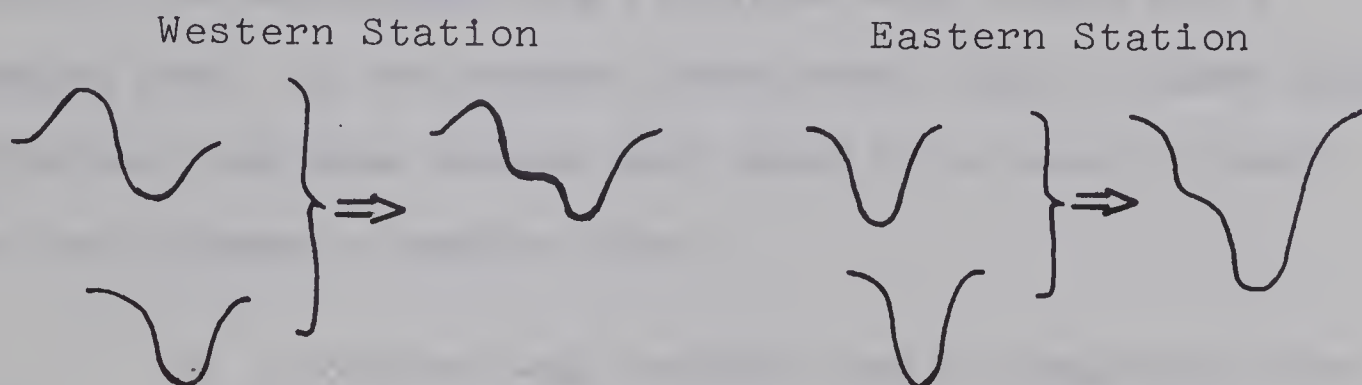
indicates an intensification of the current relative to its magnitude at 0615, but in spite of this large intensification and a probable northward movement of the auroral electrojet (Akasofu and Chapman, 1962), the ΔH component at BAK and FTC attains only a small negative value at 0622 and has a small positive value at 0630. These results are again qualitatively consistent with a westward movement of the eastern field-aligned current plus a possible intensification of such a current, thus cancelling the effect of the intensification of the electrojet at these stations.

The ΔZ perturbations of the field were also obtained for these times. After the initial phase of the substorm it was found that the ΔZ variations were positive to the north, and negative to the south of the electrojet. Thus each of the observed ΔH , ΔD , ΔZ variations are qualitatively consistent with the magnetic perturbations of the proposed current model.

The onset time of the second auroral substorm is about 0626 UT. The perturbation is entirely negative across our array. Since the demarcation line appears slightly to the west of the array, the recorded negative D-bays have a progressively larger amplitude as the array is traversed from west to east. (The amplitude of the D-bay is zero at the demarcation line, increases to a maximum, and falls slowly to zero as one moves east, or west, in a direction perpendicular to the demarcation line.) The H-component also substantiates this,

for at mid-latitudes the horizontal external field is quite uniform, hence the increase in ΔD at the eastern stations should correspond to a decrease in the ΔH component at these stations. This is observed in the magnetograms.

The smooth change of characteristics of the D-component from 0600 UT. to 0645 UT. from west to east across the array may be explained by the addition of a small negative D-bay and a transitional D-bay at the western stations; while at the eastern stations, one has the addition of two large negative D bays.



In an analogous situation to ΔD , the character of the H component results from the addition of two small positive H-bays at the eastern stations, and two large positive bays at the western stations.

In both the H and D magnetograms a particular peak occurs earlier at a station on the east side of the array than at a station on the west side. A possible explanation of this peak shift is the westward movement of the demarcation line. It is this peak shift which is associated with the shift in phase of the horizontal

components seen in Chapter IV.

Although there appears to be another bay-like event occurring about 0700 UT., it is possible that the perturbation fields of the second bay decay back to a disturbed baseline caused by a storm-time perturbation. This decay continues until about 0715 UT., at which time a sharp recovery of the Dst. occurs. A number of reasons suggest that this is a recovery of the storm time component as opposed to a separate event.

1. Considering this to be a substorm beginning about 0700 UT., the magnetograms show a positive D-bay coupled with a negative H-bay. If the proposed current model (Fig.6.1) causes this deflection, then these currents must indeed be far south in order for one to observe a negative H-bay.
2. A positive D-bay indicates that the demarcation line has jumped from west to east of the array. Such a motion of the demarcation line has not been observed in the past, suggesting that this type of situation is highly unlikely.
3. Stations not anomalous in Z, eg. CIM, SAG, KAY, and SWE show a gradual rise in Z back to the initial value at 0500, i.e. there is no indication of an additional negative Z which should have been recorded if this was a substorm.
4. The magnetogram from Leirvoguer, shown in Fig.(6.5),

shows a sharp recovery about 0715 from a depressed H component. Other observatories, including those in equatorial regions, also indicated an event at 0715 which could be interpreted as a recovery of Dst.

BIBLIOGRAPHY

Akasofu, S.I., D.S. Kimball, and C.I. Meng. Dynamics of the aurora: II Westward travelling surges, *J. Atmosph. Terrest. Phys.*, 27, (1965) 173.

Akasofu, S.I., S. Chapman, and C.I. Meng. The polar electrojet. *J. Atmosph. Terrest. Phys.* 27, (1965) 1275.

Akasofu, S.I., C.I. Meng, and D.S. Kimball. Dynamics of the aurora: IV Polar magnetic substorms and westward travelling surges, *J. Atmosph. Terrest. Phys.* 28 (1966) 489.

Bonnevier, B., R. Boström, and G. Rostoker. A three Dimensional Model Current System for Polar Magnetic Substorms (submitted for publication).

Bullard, E.C., 1967. Electromagnetic Induction in the Earth. *Quart. J. RAS* 8, 143-160.

Cagniard, I., 1953. Basic theory of the magneto-telluric method of geophysical prospecting. *Geophysics*, 18: 605-635.

Caner, B., W.H. Cannon and C.E. Livingstone. Geomagnetic depth sounding and upper mantle structure in the Cordillera Region of Western North America, *J. Geophys. Res.*, 72, 6335-6351, 1967.

Chapman, S., 1919. The solar and lunar diurnal variation of the earth's magnetism. *Phil. Trans. Roy. Soc. London, Ser. A.* 218: 1-118.

Chapman, S. and Whitehead, T.T., 1923. The influence of electrically conducting material within the earth on various phenomena of terrestrial magnetism. *Trans. Cambridge Phil. Soc.*, 22: 463-482.

Chapman, S. and J. Bartels, 1940. *Geomagnetism*, Oxford University Press, London, 1049 pp.

Clark, S.P. and A.E. Ringwood, 1964. Density distribution and constitution of mantle, *Rev. Geophys.*, 2, 35-88.

Gough, D.I. and J.S. Reitzel, 1967. A portable three-component magnetic variometer, *J. Geomag. Geoelect.*, 19, 203-215.

Gough, D.I. and J.S. Reitzel. Magnetic deep sounding and local conductivity anomalies, in *The Application of Modern Physics to the Earth and Planetary Interiors*. Edited by S.K. Runcorn, Interscience Publishers (1969, in press).

Hakura, Y., 1966. Tables and Maps of Geomagnetic Coordinates corrected by the higher order spherical harmonic terms, Radio Research Laboratories, Kokubunjo, Tokyo. 121-146.

Hamilton, R.M., 1965. Temperature variation at constant pressure of the electrical conductivity of periclose and olivine, *J. Geophys. Res.*, 70, 5679-5692.

Hartmann, A., 1963. Behandlung lokaler erdmagnetischer Felder als Randwertaufgabe der Potential theorie, *Abhandl. Akad. Wiss. Göttingen, Math Phys. Kl.*, Bertr. I.G.J., 9, 1-50.

Hyndman, R.D. Electrical Conductivity Inhomogeneities in the Earth's Upper Mantle. M.Sc. Thesis, University of British Columbia (1963).

Jackson, J.D., 1962. *Classical Electrodynamics*, John Wiley and Sons, Inc., New York.

Kertz, W., 1964. The conductivity anomaly in the upper mantle found in Europe. *J. Geomagnetism Geoch.*, 15: 185-192.

Lahiri, B.N. and Price, A.T., 1939. Electromagnetic induction in non-uniform conductors, and the determination of the conductivity of the earth from terrestrial magnetic variations. *Phil Trans. Roy. Soc. London, Ser. A.* 237: 509-540.

Matsushita, S., W.H. Campbell, 1967. *Physics of Geomagnetic Phenomena* Vol. I. Academic Press, New York and London.

Pakiser, L.C., 1963. Structure of the Crust and Upper Mantle in the Western United States. *J. Geophys. Res.*, 68: 5747-5756.

Parkinson, W.D., 1962a. The influence of continents and oceans on geomagnetic variations. *Geophys. J.*, 4: 441-449.

Parkinson, W.D., 1959. Directions of rapid geomagnetic fluctuations *Geophys. J.*, 2: 1-14.

Sierbert, M. und Kertz, W., 1957. Zur Zerlegung eines lokalen erdmagnetischen Feldes in aussern and innern Anteil. *Nachr. Akad. Wiss. Göttingen, II. Math-Physik. Kl.*, 1957: 87-112.

Siebert, M., 1958. Die Zerlegung eines zweidimensionalen Magnetfeldes in äussern und innern Anteil mit Hilfe des zweidimensionalen Fourier-Theorems. *Abhandl. Akad. Wiss. Gottingen, Math. Physik. Kl. Beitr. I.G.J.*, 4: 33-38.

Siebert, M., 1962. Die Zerlegung eines zweidimensionalen Magnetfeldes in äussern und innern Anteil mit Hilfe des Cauchyschen Integralformel. *Z. Geophysics.*, 28: 231-236.

Swift, C.M., A Magnetotelluric Investigation of an Electrical Conductivity Anomaly in the Southwestern United States, Ph. D. Thesis, Massachusetts Institute of Technology, 1967.

Taylor, J.H., 1944. On the determinations of magnetic vertical intensity Z, by means of surface integrals. *Terrest. Magnetism Atmospheric Elec.*, 49: 223-237.

Tozer, D.C., 1959. The electrical properties of the earth's interior. In: L.H. Ahrens, F. Press, K. Rankama and S.K. Runcorn (Editors), *Physics and Chemistry of the Earth*. Pergamon, London, 3: 414-436.

Upper Mantle Project, (1964), Symposium, IAGA-IUGG, Berkely Journal of Geomag. and Geoelect. Vol. XV, No. 4, 179-293.

Vestine, E.H., 1941. On the analysis of surface magnetic fields by integrals. 1. *Terrest. Magnetism Atmospheric Elec.*, 46: 27-41.

Vestine, E.H. and Davids, N., 1945. Analysis and interpretation of geomagnetic anomalies. *Terrest. Magnetism Atmospheric Elec.*, 50: 1-36.

Wait, J.R., 1951. The magnetic dipole over the horizontally stratified earth. *Can. J. Phys.*, 29: 577-592.

Wait, J.R., 1960. Some solutions for electromagnetic problems involving spheroidal, spherical, and cylindrical bodies. *J. Res. Natl. Bur. Std. B.*, 64: 15-32.

Ward, S.H., Mining Geophysics Vol. II., The Society of Exploration Geophysicists, Tulsa, Oklahoma.

Weaver, J.T., 1963. On the separation of local geomagnetic fields into external and internal parts. *J. Geophys.*, 29, 29-36.

Whitham, K., 1963. An anomaly in geomagnetic variations at Mould Bay in the Arctic archipelago of Canada. *Geophys. J.*, 8: 26-43.

Whitham, K., and Andersen, F., 1962. The anomaly in geomagnetic variations at Alert in the Arctic archipelago of Canada. *Geophys. J.* 220-243.

Whitham, K., 1964. Anomalies in geomagnetic variations in the Arctic archipelago of Canada. *J. Geomagnetism Geoelec.*, 15: 227-240.

Wiese, H., 1965. *Geomagnetische Tiefentellurik*, Deutsche Akad. Wiss. Berlin, Geomagn. Inst. Potsdam, Abh. 36, 1-146.

APPENDIX

Maxwell's equations in m.k.s. units are:

$$\nabla \times E = - \frac{\partial B}{\partial t} \quad (1)$$

$$\nabla \times H = 4\pi J + \frac{\partial D}{\partial t} \quad (2)$$

$$\nabla \cdot B = 0 \quad (3)$$

$$\nabla \cdot D = 4\pi \rho \quad (4)$$

where $D = \epsilon E$, $B = \mu H$, and $J = \sigma E$

E = electric field intensity (volts/meter)

B = magnetic induction (Weber/m²)

D = dielectric displacement (coulombs/m²)

H = magnetic field intensity (ampere-turn/m)

In general ϵ , μ , and σ are spatial dependent functions.

Since $\nabla \cdot (\nabla \times F) = 0$ for any vector F

$$\nabla \cdot (4\pi J + \frac{\partial D}{\partial t}) = 0$$

or $\nabla \cdot J = \frac{\partial \rho}{\partial t}$ (Equation of continuity.)

$$\nabla \cdot \sigma E = \sigma \nabla \cdot E + E \cdot \nabla \sigma = - \rho \quad (5)$$

Expanding (4) we have

$$\nabla \cdot E = \frac{1}{\epsilon} (4\pi \rho - E \cdot \nabla \epsilon) \quad (6)$$

APPENDIX (cont'd.)

Putting (6) into (5) and recognizing $\nabla(\epsilon/\sigma) = \sigma\nabla\epsilon - \epsilon\nabla\sigma/\sigma^2$

we have

$$\rho_0 + \frac{4\pi\sigma}{\epsilon} \rho = \frac{\sigma}{\epsilon} \mathbf{J} \cdot \nabla \left(\frac{\epsilon}{\mathbf{r}} \right) \quad (7)$$

From (7) we see that if \mathbf{J} is \perp to $\nabla(\epsilon/\sigma)$ or if ϵ/σ is a constant; then

$$\rho = \rho_0 e^{-\frac{4\pi\sigma t}{\epsilon}}$$

that is, there is an exponential decay of the space charge ρ .

Thus if ρ is initially zero, it will remain so, but if not, it will decay to this state. From the equation of continuity one obtains

$$\nabla \cdot \mathbf{J} = 0$$

If the time variations of the fields are slow, the displacement current $\frac{\partial D}{\partial t}$ can be neglected compared to the conduction current J .

Let T be the period of the field. D is of the order $\frac{\epsilon E}{T}$ and $J = \sigma E$. For the displacement current to be neglected,

$$\frac{\epsilon E}{T} \ll 4\pi\sigma E$$

that is,

$$T \gg \frac{\epsilon}{4\pi\sigma} .$$

In e.m. units $\epsilon\mu = c^{-2}$. Even if σ is as small as 10^{-19} , T need only to be as large as a few seconds to satisfy this requirement. Therefore, within the conductor $\nabla \cdot \mathbf{J}$ may be taken to be zero.

APPENDIX (cont'd.)

Outside the conductor $\overset{\circ}{H} \sim \frac{E}{\mu L}$ where L is the scale length of the field. Therefore

$$\nabla \times H \sim \frac{ET}{\mu L^2}$$

Neglect of the displacement current requires that

$$\overset{\circ}{D} \ll \nabla \times H$$

and this is satisfied if $T \gg (\epsilon\mu)^{1/2}L$, that is, if T is large compared by the time taken by the e.m. wave to travel across the region. This is probably satisfied if $T \gg 0.1$ sec. Thus for both the conducting and nonconducting regions the displacement current may be neglected. In the conducting region the space charge density $\rho = 0$ and in the nonconducting region $\sigma = 0$.

Maxwell's equation reduce to:

CONDUCTING REGION

$$\nabla \times E = - \frac{\partial B}{\partial t} \quad (8)$$

$$\nabla \times H = 4\pi J \quad (9)$$

$$\nabla \cdot D = 0$$

$$\nabla \cdot B = 0$$

NON CONDUCTING REGION

$$\nabla \times E = - \frac{\partial B}{\partial t} \quad (10)$$

$$\nabla \times H = 0 \quad (11)$$

$$\nabla \cdot D = 0$$

$$\nabla \cdot B = 0$$

By assuming a time varying field of the type $e^{i\omega t}$, equations (8) and (9) can be combined into the induction or the diffusion equation.

APPENDIX (cont'd.)

$$\nabla^2 \left\{ \frac{H}{E} \right\} = 4\pi i \omega \sigma \mu \left\{ \frac{H}{E} \right\} \quad (12)$$

Outside the conductor, where $\sigma = 0$, (12) reduces to Laplace's equation,

$$\nabla^2 \left\{ \frac{H}{E} \right\} = 0 \quad (13)$$

Equation (12) and (13) are the starting equations for electromagnetic induction problems in the earth.

B29925